Infectious Disease Modelling 9 (2024) 828–874

Contents lists available at ScienceDirect

Infectious Disease Modelling

journal homepage: www.keaipublishing.com/idm

Mathematical assessment of the roles of age heterogeneity and vaccination on the dynamics and control of SARS-CoV-2

Binod Pant [a], Abba B. Gumel [a, b, *]

[a] Department of Mathematics, University of Maryland, College Park, MD, 20742, USA
[b] Department of Mathematics and Applied Mathematics, University of Pretoria, Pretoria, 0002, South Africa

ARTICLE INFO

Article history:
Received 29 September 2023
Received in revised form 10 April 2024
Accepted 11 April 2024
Handling Editor: Dr. Raluca Eftimie

Keywords:
COVID-19
SARS-CoV-2
Heterogeneous model
Reproduction number
Herd immunity

ABSTRACT

The COVID-19 pandemic, caused by SARS-CoV-2, disproportionately affected certain segments of society, particularly the elderly population (which suffered the brunt of the burden of the pandemic in terms of severity of the disease, hospitalization, and death). This study presents a generalized multigroup model, with m heterogeneous subpopulations, to assess the population-level impact of age heterogeneity and vaccination on the transmission dynamics and control of the SARS-CoV-2 pandemic in the United States. Rigorous analysis of the model for the homogeneous case (i.e., the model with $m = 1$) reveal that its disease-free equilibrium is globally-asymptotically stable for two special cases (with perfect vaccine efficacy or negligible disease-induced mortality) whenever the associated reproduction number is less than one. The model has a unique and globally-asymptotically stable endemic equilibrium, for special a case, when the associated reproduction threshold exceeds one. The homogeneous model was fitted using the observed cumulative mortality data for the United States during three distinct waves (Waves A (October 17, 2020 to April 5, 2021), B (July 9, 2021 to November 7, 2021) and C (January 1, 2022 to May 7, 2022)) chosen to align with time periods when the Alpha, Delta and Omicron were, respectively, the predominant variants in the United States. The calibrated model was used to derive a theoretical expression for achieving vaccine-derived herd immunity (needed to eliminate the disease in the United States). It was shown that, using the one-group homogeneous model, vaccine-derived herd immunity is not attainable during Wave C of the pandemic in the United States, regardless of the coverage level of the fully-vaccinated individuals. Global sensitivity analysis was carried out to determine the parameters of the model that have the most influence on the disease dynamics and burden. These analyses reveal that control and mitigation strategies that may be very effective during one wave may not be so very effective during the other wave or waves. However, strategies that target asymptomatic and pre-symptomatic infectious individuals are shown to be consistently effective across all waves. To study the impact of the disproportionate effect of COVID-19 on the elderly population, we considered the heterogeneous model for the case where the total population is subdivided into the subpopulations of individuals under 65 years of age and those that are 65 and older. The resulting two-group heterogeneous model, which was also fitted using the cumulative mortality data for wave C, was also rigorously analysed. Unlike for the case of the one-group model, it was shown, for the two-group model, that vaccine-derived herd immunity can indeed be achieved during Wave C of the pandemic if at least 61% of the populace is fully vaccinated. Thus, this study shows that adding age heterogeneity into a SARS-CoV-2

* Corresponding author. Department of Mathematics, University of Maryland, College Park, MD, 20742, USA.
E-mail address: agumel@umd.edu (A.B. Gumel).
Peer review under responsibility of KeAi Communications Co., Ltd.

https://doi.org/10.1016/j.idm.2024.04.007

vaccination model with homogeneous mixing significantly reduces the level of vaccination coverage needed to achieve vaccine-derived herd immunity (specifically, for the heterogeneous model, herd-immunity can be attained during Wave C if a moderate proportion of susceptible individuals are fully vaccinated). The consequence of this result is that vaccination models for SARS-CoV-2 that do not explicitly account for age heterogeneity may be overestimating the level of vaccine-derived herd immunity threshold needed to eliminate the SARS-CoV-2 pandemic.

1. Introduction

The novel coronavirus that emerged late in 2019 (named COVID-19), caused by SARS-COV-2, became the greatest public health and socioeconomic challenge of mankind since the 1918 influenza pandemic (Morens & Fauci, 2007; Ngonghala, Iboi, Eikenberry, et al., 2020; Samuel Faust et al., 2020). As of October 20, 2022, the COVID-19 pandemic accounted for over 623 million confirmed cases and 6.5 million deaths globally (World Health Organization). The control and mitigation strategies against COVID-19 were mostly limited to the use of nonpharmaceutical interventions (NPIs), such as social-distancing, community lockdown, the use of face covering (e.g., fabric and N-95 masks), quarantine, isolation and contact-tracing (Bo et al., 2021; Flaxman et al., 2020; Ngonghala, Iboi, Eikenberry, et al., 2020), until safe and effective anti-COVID vaccines (notably the Pfizer and Moderna vaccines) received Emergency Use Authorization (EUA) by the United States Food and Drugs Administration (FDA) in December of 2020 (Pfizer, 2020). Other safe and effective COVID-19 vaccines, such as the Johnson & Johnson and the Novavax vaccines, also received FDA-EUA during 2021 and 2022, respectively (Oliver et al., 2021; US Food and Drug Administration, 2022). Some other vaccines, such as the Astrazeneca vaccine, were also developed and used in other parts of the world (but not in United States, were only the aforementioned FDA-EUA vaccines were or are being used) (FDA, 2022). As of October 21, 2022, at least 12 billion dosages of COVID-19 vaccines have been administered globally (COVID-19 map). Despite the deployment of the aforementioned control and mitigation strategies, COVID-19 cases continued to rise until the end of 2022, and numerous SARS-COV-2 variants of concern emerged (Katella, 2022; Mancuso et al., 2021; Ngonghala et al., 2022).

Numerous mathematical models, of varying types, have been developed and used to gain insight into the transmission dynamics and control of the pandemic. For instance, models that take the form of deterministic systems of nonlinear differential equations have been used to assess the impacts of non-pharmaceutical interventions (such as face-masks usage, social-distancing, quarantine and self-isolation) (Eikenberry et al., 2020; Gumel, Iboi, Ngonghala, & Elbasha, 2021; Ngonghala et al., 2020a, 2021), pharmaceutical interventions (such as vaccination and the use of antiviral drugs) (Gumel et al., 2021a, 2021b; Iboi et al., 2020a; Ngonghala et al., 2022; Safdar et al., 2022) and human mobility between neighboring countries (Brozak et al., 2021) on the transmission dynamics and control of the COVID-19 pandemic. Similarly, agents-based (or individual-based) models have been used to study various aspects of the pandemic, such as the impact of contract tracing (Almagor & Picascia, 2020; Hinch et al., 2021) and the impact of pharmaceutical and non-pharmaceutical interventions against COVID-19 (Ferguson et al., 2020a; Hoertel et al., 2020; Kerr et al., 2021). Network models have been used to study the impact of testing and contact tracing (Karaivanov, 2020) and social-distancing etc. (Calvetti et al., 2020; Huang et al., 2020; Soures et al., 2020; Xue et al., 2020). Rahimi et al. reviewed various statistical models used to forecast the outbreak of COVID-19 (Rahimi et al., 2021).

The COVID-19 pandemic has highlighted the importance of heterogeneity in disease transmission process (i.e., not everyone is equally affected by the disease; some are more likely to acquire infection, develop severe disease and/or die of the disease than others). Specifically, heterogeneities arise in numerous forms, such as heterogeneities in mortality (where individuals with underlying health conditions, such as diabetes and hypertension, are more likely to die of COVID-19 than those without those co-morbidities (Callender et al., 2020; Djaharuddin et al., 2021; Omame et al., 2021; Sanyaolu et al., 2020; Wang et al., 2020)), age (where humans of age 65 and older are more likely to suffer severe COVID-19 infection and mortality, in comparison to those who are younger (Freed et al., 2021; Powell et al., 2020)), risk (where some humans, such as health care workers or other essential workers (e.g., grocery workers, law enforcement agents etc.) are more at risk of acquiring infection than others) (Chen et al., 2021, 2022; Ing et al., 2020; Iyengar et al., 2020; Matz et al., 2022; Mutambudzi et al., 2021) and adherence to interventions (where some individuals are more likely to adhere to interventions than others) (Haischer et al., 2020; Kricorian et al., 2022; Neely et al., 2022). Hence, it is paramount that models for the transmission dynamics of COVID-19 explicitly incorporate the impacts of some of these heterogeneities. The need for heterogeneity in COVID-19 modeling becomes even more apparent as data shows disparity in vaccination coverage by not only age, but also by race and ethnicity (Kriss et al., 2022). Very few models for the transmission dynamics of COVID-19 explicitly incorporates the impact of heterogeneities in the modeling process. Age-structured models were developed and used to study the impact of social-distancing (Singh & Adhikari, 2020) and non-pharmaceutical interventions (Richard et al., 2021) on the spread of COVID-19. Elbasha and Gumel (Elamin H Elbasha and Abba B Gumel, 2021) used a generalized multigroup vaccination model

to analyze the impact of heterogeneities on vaccine-induced herd immunity threshold. The current study focuses on extending the study in (Elamin H Elbasha and Abba B Gumel, 2021) by developing a modeling framework for assessing the impact of various (generalized) heterogeneities on the transmission dynamics of COVID-19 pandemic in a heterogeneous population that uses an FDA-EUA COVID-19 vaccine.

The paper is organized as follows. The general heterogeneous model, which stratifies the total population into m subgroups, is formulated in Section 2. The model incorporates the use of FDA-EUA administered vaccines in the United States. The basic theoretical results for the general $m-$ group model are also presented. The corresponding homogeneous version of the model (i.e., the general model with $m = 1$) is rigorously analysed in Section 3. In addition to fitting the homogeneous model to observed data, detailed global sensitivity analysis, with respect to the parameters of the model, is also carried out in this section. Another special case of the general heterogeneous model with $m = 2$ is considered and qualitatively analysed, with respect to the asymptotic stability of its associated disease-free equilibrium, in Section 4. The main conclusions of the study are presented in Section 5.

2. Formulation of the heterogeneous model

In the formulation of the COVID-19 transmission model in heterogeneous population (henceforth named *heterogeneous model*), the total population is divided into m groups with $k = \{1, 2, \cdots m\}$ distinct subgroups (with each subgroup k being homogeneous). Each subgroup k is further subdivided into the mutually-exclusive compartments of unvaccinated susceptible ($S_k(t)$), fully-vaccinated susceptible ($V_k(t)$), exposed/latent ($E_k(t)$), pre-symptomatic infectious ($P_k(t)$), symptomatic infectious ($I_k(t)$), asymptomatically-infectious ($A_k(t)$), hospitalized ($H_k(t)$), and recovered ($R_k(t)$) individuals. Hence, the total number of individuals in any of the k subgroup at time t, denoted by $N_k(t)$, is given by:

$$N_k(t) = S_k(t) + V_k(t) + E_k(t) + P_k(t) + A_k + I_k(t) + H_k(t) + R_k(t).$$

Thus, the total population (in all k subgroups) at time t, denoted by $N(t)$, is given by:

$$N(t) = \sum_{k=1}^{m} N_k(t). \tag{2.1}$$

It is assumed that the population of unvaccinated susceptible individuals in subgroup $k(S_k)$ are fully-vaccinated using an FDA-EUA vaccine with protective efficacy $\varepsilon_{v,k}$ at a *per capita* rate $\xi_{v,k}$. In keeping with the CDC definition of being "fully vaccinated" (Centers for Disease Control and Prevention (CDC), 2021), individuals in the fully-vaccinated susceptible compartment, V_k, are those that have received the single dose of the Janssen/Johnson & Johnson COVID-19 vaccine or the second dose of any of the mRNA SARS-CoV-2 vaccines at least 14 days earlier (Centers for Disease Control and Prevention (CDC), 2021) (and the vaccine has not waned yet). Additionally, the unvaccinated susceptible population is increased by the recruitment of individuals into the population (either by birth or by immigration) at a rate Π_k, and by the waning of vaccine-derived protective immunity in fully-vaccinated individuals (at a rate $\omega_{v,k}$). Individuals in the S_k class acquire COVID-19 infection at a rate λ_k (i.e., the *force of infection*), given by:

$$\lambda_k = \sum_{l=1}^{m} a_k c_{kl} \left[\frac{\mathcal{P}_{P,l} P_l(t) + \mathcal{P}_{I,l} I_l(t) + \mathcal{P}_{A,l} A_l(t) + \mathcal{P}_{H,l} H_l(t)}{N_l(t)} \right], \tag{2.2}$$

where a_k is the average number of contacts made by individuals in group k during a time period and c_{kl} is the proportion of contacts that individuals in group k have with individuals in group l (Elamin H Elbasha and Abba B Gumel, 2021). Furthermore, the parameters $\mathcal{P}_{P,l}$, $\mathcal{P}_{I,l}$, $\mathcal{P}_{A,l}$, and $\mathcal{P}_{H,l}$ represent the *per* contact transmission probability of infectious individuals (in group l) that are pre-symptomatic (P_l), symptomatic (I_l), asymptomatic (A_l), and hospitalized (H_l), respectively. Mixing should meet the closure relation $a_k c_{kl} N_k = a_l c_{lk} N_l$ (Glasser et al., 2012). In other words, the total number of contacts individuals in group k have with individuals in group l must balance the total number of contacts individuals in group l have with individuals in group k. Exposed (or latent) individuals in the kth sub-population progress to pre-symptomatic class in the kth sub-population at a rate σ_k, and a proportion r_k of these individuals progress to the I_k class (at the rate $r_k\psi_k$), while the remaining proportion, $1 - r_k$, progress to the A_k class (at the rate $(1 - r_k)\psi_k$). Symptomatic individuals in the kth sub-population are hospitalized at a rate φ_k, recover at a rate $\gamma_{I,k}$ or die due to the disease at a rate $\delta_{I,k}$. Asymptomatic infectious individuals recover naturally at a rate $\gamma_{A,k}$, and recovered individuals are assumed not to acquire reinfection while in the recovered class. It is assumed that recovered individuals lose their infection-acquired (natural) immunity at a rate $\omega_{n,k}$. Furthermore, natural death is assumed to occur in each epidemiological class at a rate μ_k.

Based on the above derivations and assumptions, the general m-group heterogeneous model for the spread of COVID-19 in a population that uses an FDA-EUA vaccine, is given by the following deterministic system of nonlinear differential equations (where a dot represents differentiation with respect to time t):

$$\begin{cases} \dot{S}_k(t) &= \Pi_k + \omega_{v,k}V_k(t) + \omega_{n,k}R_k(t) - \lambda_k(t)S_k(t) - (\xi_{v,k} + \mu_k)S_k(t), \\ \dot{V}_k(t) &= \xi_{v,k}S_k(t) - (1-\epsilon_{v,k})\lambda_k(t)V_k(t) - (\omega_{v,k} + \mu_k)V_k(t), \\ \dot{E}_k(t) &= \lambda_k(t)S_k(t) + (1-\epsilon_{v,k})\lambda_k(t)V_k(t) - (\sigma_k + \mu_k)E_k(t), \\ \dot{P}_k(t) &= \sigma_k E_k(t) - (\psi_k + \mu_k)P_k(t), \\ \dot{I}_k(t) &= r_k\psi_k P_k(t) - (\varphi_k + \gamma_{I,k} + \mu_k + \delta_{I,k})I_k(t), \\ \dot{A}_k(t) &= (1-r_k)\psi_k P_k(t) - (\gamma_{A,k} + \mu_k)A_k(t), \\ \dot{H}_k(t) &= \varphi_k I_k(t) - (\gamma_{H,k} + \mu_k + \delta_{H,k})H_k(t), \\ \dot{R}_k(t) &= \gamma_{I,k}I_k(t) + \gamma_{A,k}A_k(t) + \gamma_{H,k}H_k(t) - (\omega_{n,k} + \mu_k)R_k(t), \end{cases} \tag{2.3}$$

where, λ_k (the *force of infection*) is given by Equation (2.2). A flow diagram of the model (2.3) is depicted in Fig. 1 and the state variables and parameters of the model are described in Tables 1 and 2, respectively.

Some of the main assumptions made in the formulation of the model (2.3) are:

1. Individuals in the vaccinated compartment (V_k) are fully-vaccinated. That is, in line with the CDC definition of being fully-vaccinated, individuals in the V_k class are those that have received the single dose of the Janssen/Johnson & Johnson COVID-19 vaccine or the two doses of any of the approved mRNA COVID-19 vaccines at least 14 days earlier (Centers for Disease Control and Prevention (CDC), 2021).
2. Only unvaccinated susceptible individuals are vaccinated. Although the CDC recommends people with COVID-19 symptoms to wait to be vaccinated until the completion of the isolation period (Centers for Disease Control and Prevention, 2022), this still opens the possibility for exposed (i.e., infected but not infectious), pre-symptomatic, and asymptomatic individuals receiving the SARS-CoV-2 vaccine. Furthermore, although recovered individuals can choose to get vaccinated, our model does not allow for this possibility.

The model extends the heterogeneous $S_kV_kE_kI_kR_k$ model in (Elamin H Elbasha and Abba B Gumel, 2021) by adding compartments for pre-symptomatic (P_k), asymptomatic (A_k) and hospitalized (H_k) infectious individuals and also accounting for the waning of natural immunity (ω_{nk}). The study also contributes by providing detailed asymptotic stability of the model (including completed global asymptotic stability analysis of the disease-free and endemic equilibria of the homogeneous version of the original heterogeneous model).

2.1. Basic qualitative properties

In this section, the basic qualitative property of the m-group model (2.3) will be explored. In particular, the invariance properties of the solutions of the model will be rigorously analysed.

Consider the following biologically-feasible region for the model (2.3), with $k = \{1, 2, \ldots, m\}$:

$$\Omega = \left\{ (S_k, V_k, E_k, P_k, I_k, A_k, H_k, R_k) \in \mathbb{R}_+^{8m} : \sum_{k=1}^{m} (S_k + V_k + E_k + P_k + I_k + A_k + H_k + R_k) \leq N(0) \right\},$$

where $N(0)$ is the total initial size of the population. We claim the following result:

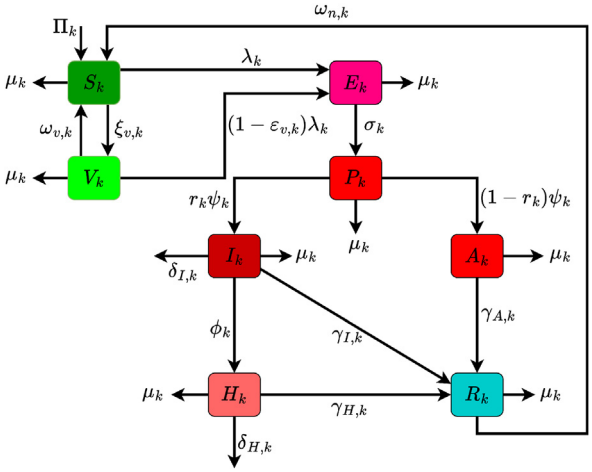

Fig. 1. The flow diagram describing the m-group heterogeneous model (2.3), with $k = \{1, 2, \ldots, m\}$ and the infection rate, λ_k, defined in (2.2).

Table 1
Description of the state variables of the m-group heterogeneous model (2.3), with $k = \{1, 2, \ldots, m\}$.

State variable	Description
S_k	Number of non-vaccinated susceptible individuals in subgroup k
V_k	Number of fully-vaccinated susceptible individuals in subgroup k
E_k	Number of exposed (newly-infected but not yet infectious) individuals in subgroup k
P_k	Number of pre-symptomatically-infectious individuals in subgroup k
I_k	Number of symptomatically-infectious individuals in subgroup k
A_k	Number of asymptomatically-infectious individuals in subgroup k
H_k	Number of hospitalized individuals in subgroup k
R_k	Number of recovered individuals in subgroup k

Table 2
Description of the parameters of the m-group heterogeneous model (2.3), with $k = \{1, 2, \ldots, m\}$.

Parameter	Description
Π_k	Recruitment rate into subgroup k
μ_k	Natural death rate for individuals in subgroup k
a_k	Average number of contacts *per* unit time made by individuals in subgroup k
$c_{k,l}$	Proportion of contacts individuals in subgroup k have with individuals in subgroup l
$\mathcal{P}_{P,k}(\mathcal{P}_{I,k})(\mathcal{P}_{A,k})(\mathcal{P}_{H,k})$	Transmission probability *per* contact for individuals in the $P_k(I_k)(A_k)(H_k)$ class
$\xi_{v,k}$	Rate at which susceptible individuals in subgroup k are fully-vaccinated
$\varepsilon_{v,k}$	Vaccine efficacy for vaccinated individuals in subgroup k
$\omega_{v,k}$	Waning rate of vaccine for vaccinated susceptible individuals in subgroup k
$\omega_{n,k}$	Waning rate of natural immunity for recovered individuals in subgroup k
σ_k	Progression rate from E_k to P_k class
r_k	Proportion of pre-symptomatic individuals in subgroup k who show clinical symptoms of the disease at the end of the pre-symptomatic period
$r_k\psi_k$	Progression rate from the P_k to the I_k class
$(1 - r_k)\psi_k$	Progression rate from the P_k to the A_k class
φ_k	Hospitalization rate for symptomatically-infectious individuals in subgroup k
$\gamma_{I,k}(\gamma_{A,k})(\gamma_{H,k})$	Recovery rate for individuals in the $I_k(A_k)(H_k)$ class
$\delta_{I,k}(\delta_{H,k})$	Disease-induced mortality rate for individuals in the $I_k(H_k)$ compartment

Theorem 2.1. *The region Ω is positively-invariant and attracts all solutions of the model* (2.3).
Proof. Adding all equations of the heterogeneous model (2.3) gives:

$$\dot{N} = \sum_{k=1}^{m} \left(\Pi_k - \mu_k N_k - \delta_{I,k} I_k - \delta_{H,k} H_k\right). \tag{2.4}$$

It is convenient to define $\Pi = \sum_{k=1}^{m} \Pi_k$. Then, Equation (2.4) can be rewritten as:

$$\dot{N} \leq \Pi - \sum_{k=1}^{m} (\mu_k N_k). \tag{2.5}$$

Let, $\mu_g = \min\{\mu_1, \mu_2, \ldots, \mu_m\}$, then it follows from (2.5) (and the definition of $N(t)$ in (2.1)) that:

$$\dot{N} \leq \Pi - \mu_g N(t). \tag{2.6}$$

Hence, if $N \geq \Pi/\mu_g$, then $\dot{N} \leq 0$. Furthermore, it follows, by applying a standard comparison theorem (Lakshmikantham et al., 1989) on (2.6), that:

$$N(t) \leq N(0)e^{-\mu_g t} + \frac{\Pi}{\mu_g}\left(1 - e^{-\mu_g t}\right). \tag{2.7}$$

In particular, $N(t) \leq \Pi/\mu_g$ if $N(0) \leq \frac{\Pi}{\mu_g}$. If $N(0) > \frac{\Pi}{\mu_g}$ (i.e., if the initial size of the population exceeds the carrying capacity, Π/μ_g, and the initial solutions are outside the region Ω), then $N(t) > \frac{\Pi}{\mu_g}$ for all $t > 0$ but with $\lim_{t\to\infty} N(t) = \frac{\Pi}{\mu_g}$ (and this initial solution trajectory eventually enters the region Ω (Gumel et al., 2006)). Thus, every solution of the model (2.3), with $\mu_g = \min\{\mu_1, \mu_2, \ldots, \mu_m\}$ and initial conditions in Ω, remains in Ω for all time $t > 0$, and all initial solutions outside Ω are eventually attracted into Ω. In other words, the region Ω is positively-invariant and attracts all initial solutions of the model (2.3). □

The epidemiological implication of Theorem 2.1 is that the model (2.3) is well-posed mathematically and epidemiology in the positively-invariant region Ω (Hethcote, 2000). Hence, it is sufficient to consider the dynamics of the flow generated by the heterogeneous model in Ω. Before analysing the heterogeneous model (2.3), it is instructive to study the dynamics of the model for the case where the population is assumed to be homogeneous (i.e., it is instructive to consider, first of all, the model (2.3) with $m = 1$). The objective is to determine whether the homogeneous model has certain qualitative features that may not be present in the full heterogeneous model or *vice versa*.

3. Model with homogeneous population

Before analyzing the qualitative features of the heterogeneous model (2.3), it is instructive to analyze the dynamics of the version of the model with a homogeneous population, obtained by setting $m = 1$ in the heterogeneous model (2.3). Setting $m = 1$ in the heterogeneous model gives the following homogeneous model (where Π is the recruitment rate into the population, and all other parameters are as defined in Table 2 with $m = 1$):

$$\begin{cases} \dot{S}(t) &= \Pi + \omega_v V(t) + \omega_n R(t) - \lambda S(t) - (\xi_v + \mu) S(t), \\ \dot{V}(t) &= \xi_v S(t) - (1-\epsilon_v)\lambda(t) V(t) - (\omega_v + \mu) V(t), \\ \dot{E}(t) &= \lambda(t) S(t) + (1-\epsilon_v)\lambda(t) V(t) - (\sigma + \mu) E(t), \\ \dot{P}(t) &= \sigma E(t) - (\psi + \mu) P(t), \\ \dot{I}(t) &= r\psi P(t) - (\varphi + \gamma_I + \mu + \delta_I) I(t), \\ \dot{A}(t) &= (1-r)\psi P(t) - (\gamma_A + \mu) A(t), \\ \dot{H}(t) &= \varphi I(t) - (\gamma_H + \mu + \delta_H) H(t), \\ \dot{R}(t) &= \gamma_I I(t) + \gamma_A A + \gamma_H H - (\omega_n + \mu) R(t), \end{cases} \tag{3.1}$$

where λ is the *force of infection* of the homogeneous model (3.1), given by:

$$\lambda = \left(\frac{\beta_P P + \beta_I I + \beta_A A + \beta_H H}{N} \right), \tag{3.2}$$

and β_P, β_I, β_A, and β_H are effective contact rates (i.e., the product of number of contacts during a given time period and the probability of transmission *per* contact) associated with disease transmission by individuals in the pre-symptomatic (P), symptomatic (I), asymptomatic (A), and the hospitalized (H) compartment, respectively. Let $D(t)$ represent the total number of individuals who have died from the disease by time t. Hence, it follows from the homogeneous model (3.1) that the rate of change of this population is given by:

$$\dot{D}(t) = \delta_I I + \delta_H H. \tag{3.3}$$

It is convenient to define the following feasible region for the homogeneous model (3.1):

$$\Omega_1 = \left\{ \left(S, V, E, P, I, A, H, R \right) \in \mathbb{R}_+^8 : N(t) \leq \frac{\Pi}{\mu} \right\}, \tag{3.4}$$

where $N(t)$ is the total population at time t. It can be shown (using the approach in Section 2.1) that the region Ω_1 is positively-invariant and attracts all solutions of the homogeneous model (3.1). Before analyzing the qualitative dynamics of the homogeneous model, with respect to the existence and asymptotic stability of its equilibria, we will first discuss the parameterization (and fitting) of the model, as below.

3.1. Fixed and estimated parameters of the homogeneous model

The homogeneous model (3.1) contains nineteen parameters. The values of thirteen of these parameters are well-known from the literature (these known parameters are defined as *fixed parameters*), while the values of the remaining six parameters (namely β_P, β_I, β_A, β_H, δ_I, and δ_H) are unknown, and will be estimated from observed COVID-19 data for the United States (these unknown parameters to be estimated from data are termed as *estimated parameters*). For fitting purposes, we will consider the following three time periods, corresponding to the major three waves of the COVID-19 pandemic in the United States, namely:

1. **Wave A:** time period from October 15, 2020 to April 5, 2021 (Alpha was the predominant variant in the United States during most of this period (Darroch, 2021; Paul et al., 2021)).
2. **Wave B:** time period from July 9, 2021 to November 7, 2021 (Delta was the dominant variant in the United States during this period (Cavazzoni, 2022; Christensen et al., 2022; Lauring et al., 2022)).
3. **Wave C:** time period from January 1, 2022 to May 7, 2022 (Omicron was the dominant variant during this period (Cavazzoni, 2022; Christensen et al., 2022; Lauring et al., 2022)).

The values of the fixed and estimated parameters are described below.

3.1.1. Fixed parameters of the homogeneous model

The derivation of the baseline values of the thirteen known parameters of the homogeneous model (3.1), given in Table 3, is described as follows: the value of the daily recruitment rate parameter (Π) is obtained from using the census data for the United States, and noting that the total population before the disease was introduced is Π/μ (where $1/\mu$ is the average lifespan). Thus, since the total population of the United States is approximately 331.4 million (Epstein & Lofquist, 2021) and the average lifespan is 77.8 years (Arias et al., 2020) (so that $1/\mu = 77.8$ years; hence, $\mu = 3.52 \times 10^{-5}$ *per* day), it follows that $\Pi = 331.4$ million $\times\ \mu = 11,670$ *per* day. The values of some of the fixed parameters, notably ξ_v, ε_v, σ, φ, and γ_H, vary from wave to wave. The time duration from initial infection to infectiousness of SARS-CoV-2 is given by $1/\sigma + 1/\psi$. The estimated duration of the pre-symptomatic stage associated with Alpha, Delta, and Omicron variants is 3.5 days, 2.91 days, and 1.92 days, respectively (so that $1/\sigma = 3.5$ days, 2.91 days, 1.92 days; hence, $\sigma = 1/3.5$, *per* day, 1/2.91 *per* day, 1.92 *per* day for Wave A, B, and C, respectively) (Wu et al., 2022; Xin et al., 2022). Similarly, the estimated duration for pre-symptomatic stage to the development of clinical symptomatic for Alpha, Delta, and Omicron variants is 2 days, 1.5 days, and 1.5 days, respectively (hence, $1/\psi = 2$ days, 1.5 days, 1.5 days, so that $\psi = 1/2$ *per* day, 1/1.5 *per* day, 1/1.5 *per* day for Wave A, B, and C, respectively) (Iboi et al., 2020b; Wu et al., 2022; Zhao et al., 2020a). Data from the CDC (Centers for Disease Control and Prevention, 2020) suggests that about 60% of new SARS-CoV-2 cases will develop clinical symptoms of the disease (and the remaining 40% will not show clinical symptoms and will remain asymptomatically-infectious). Hence, the parameter r is assigned the value $r = 0.6$ (Centers for Disease Control and Prevention, 2020; Iboi et al., 2020b; Ma et al., 2021). Ferguson et al. (Ferguson et al., 2020b) estimated the duration of recovery for symptomatically-infectious individuals ($1/\gamma_I$) to be 10 days (hence, $\gamma_I = 1/10$ *per* day). Infectious individuals that are asymptomatic recover within five days (Kissler et al., 2020) (hence, $\gamma_A = 1/5$ *per* day). Hospitalized individuals recover at a rate of γ_H *per* day. Iuliano et al. estimate the average hospital stay of an infected individual during Wave A, B, and C to be 8 days, 7.6 days, and 5.5 days, respectively (therefore, $\gamma_H = 1/8$ *per* day, 1/7.6 *per* day, 1/5.5 *per* day, for Wave A, B, and C, respectively) (Danielle Iuliano et al., 2022). The vaccine protective efficacy (ε_v) is assumed to vary for each wave. Specifically, for Waves A, B, and C, we assume that the protective efficacy of the vaccine is chosen to be the efficacy of the Pfizer vaccine against the Alpha ($\varepsilon_v = 0.90$), Delta ($\varepsilon_v = 0.86$), and Omicron ($\varepsilon_v = 0.70$) variants, respectively (Bruxvoort et al., 2021; Nasreen et al., 2022). We calculated the rate at which susceptible individuals become fully-vaccinated (ξ_v) during each wave using data from the CDC (NCIRD, 2022), and the fixed value of ξ_v for each of the three waves is tabulated in Table 3. Following Ngonghala et al. (Ngonghala et al., 2022), it is assumed that the vaccines wane (in fully-vaccinated individuals) after about 270 days (hence, $\omega_v = 1/270$ *per* day). Similarly, it is assumed that natural immunity wanes after 270 days (Ngonghala et al., 2022) (hence, $\omega_n = 1/270$ *per* day).

3.1.2. Estimated (fitted) parameters of the homogeneous model

The homogeneous model (3.1) was fitted with observed cumulative COVID-19 mortality data for the United States to obtain the best values of the six unknown parameters of the model, namely the effective contact rates (β_P, β_I, β_A, and β_H) and disease-induced death rates (δ_I and δ_H). The model fitting was done using a standard nonlinear least squares approach, which involved using the inbuilt MATLAB minimization function "lsqcurvefit" to minimize the sum of the squared differences between each observed cumulative mortality data point (obtained from Johns Hopkins University COVID-19 repository (CSSE at Johns Hopkins University, 2020)), and the corresponding cumulative mortality projection obtained from the simulation of the homogeneous model (3.1). The result of the fitting for Waves A, B, and C are depicted in Fig. 2a, b, and 2c, respectively (and the estimated values of these parameters, corresponding to each of the three waves, are tabulated in Table 4). The goodness of fit (for each of the figures) was assessed by plotting the predicted daily mortality and the predicted 7-day rolling averages against the observed daily mortality data and the observed 7-day rolling average data, respectively. The 7-day rolling average of day t_n is calculated by dividing the sum of the daily mortality on days t_{n-6}, …, t_n by 7.

Table 4 shows that the estimated (fitted) values for the parameters for the transmission rate of pre-symptomatic (β_P) and asymptomatic (β_A) individuals are larger than that for the transmission rate of symptomatic individuals (β_I), suggesting that pre-symptomatic and asymptomatic individuals accounted for majority of new cases of the disease during the three waves considered in this study. The relative contributions of pre-symptomatic, asymptomatic and symptomatic individuals towards generating new cases is further discussed in Section 3.2.1.1. Table 4 also shows that the estimated value of the parameter for the disease-induced mortality rate for hospitalized individuals (δ_H) exceeds that for the disease-induced mortality for symptomatically-infectious individuals (δ_I) during each of the three waves. Thus, our study shows that hospitalized individuals suffered a larger proportion of the COVID-19 mortality, in comparison to symptomatically-infectious individuals.

3.2. Asymptotic stability of disease-free equilibrium of the model (3.1)

In this section, the asymptotic stability property of the disease-free equilibrium (DFE) of the homogeneous model (3.1) is explored. The disease-free equilibrium of the homogeneous model (3.1) is given by:

$$\mathbb{E}_0 : (S^*, V^*, E^*, P^*, I^*, A^*, H^*, R^*) = \left(\frac{\Pi(\omega_v + \mu)}{\mu(\omega_v + \xi_v + \mu)}, \frac{\Pi\xi_v}{\mu(\omega_v + \xi_v + \mu)}, 0, 0, 0, 0, 0, 0\right). \tag{3.5}$$

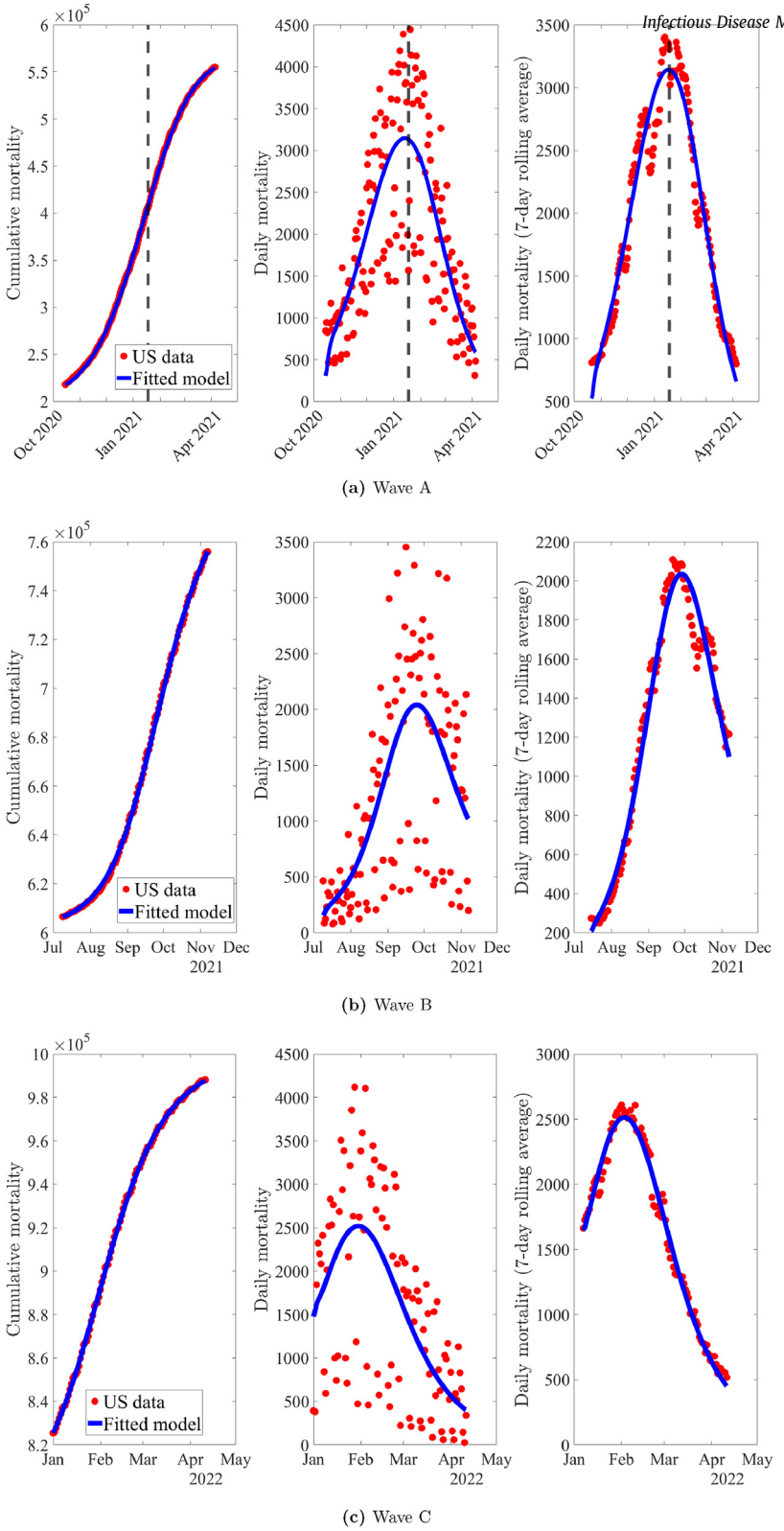

Fig. 2. The left figures are time series illustrations of the least squares fit of the homogeneous model (3.1), showing the model's output for the cumulative COVID-19 mortality compared to the observed cumulative mortality for the United States during the time periods associated with (a) Wave A, (b) Wave B, and (c) Wave (c). The middle figures are simulation result of the model (3.1), showing the daily COVID-19 mortality cases for the United States as a function of time, using the fixed (see Table 3) and estimated parameter (see Table 4) associated with (a) Wave A, (b) Wave B, and (c) Wave C. The right figures are a seven-day rolling average of daily mortality for (a) Wave A, (b) Wave B, and (c) Wave C. Red dots indicate data points, while the solid blue line represents output from the model. The dashed vertical line in Fig. 2 (a) marks the first day of susceptible individuals (S) entering the fully-vaccinated compartment (V). The initial conditions used to generate these figures are given in Table A1 of Appendix A.

Table 3
Baseline values of fixed parameters of the homogeneous model (3.1) for Waves A, B, and C. For Wave A, it should be noted that the rate at which susceptible (S) enter the fully-vaccinated compartment (V) from October 15, 2020 to January 3, 2021 is 0.

Parameter	Baseline value			Source
	Wave A	Wave B	Wave C	
Π	11, 670 day^{-1}	11, 670 day^{-1}	11, 670 day^{-1}	(Arias et al., 2020; Epstein & Lofquist, 2021)
μ	1/(77.8 × 365) day^{-1}	1/(77.8 × 365) day^{-1}	1/(77.8 × 365) day^{-1}	Arias et al. (2020)
r	0.6 (dimensionless)	0.6 (dimensionless)	0.6 (dimensionless)	(Centers for Disease Control and Prevention, 2020; Iboi et al., 2020b; Ma et al., 2021)
$1-r$	0.4 (dimensionless)	0.4 (dimensionless)	0.4 (dimensionless)	(Brozak et al., 2021; Centers for Disease Control and Prevention, 2020)
φ	1/5 day^{-1}	1/5 day^{-1}	1/5 day^{-1}	Ngonghala et al. (2022)
γ_I	1/10 day^{-1}	1/10 day^{-1}	1/10 day^{-1}	Ferguson et al. (2020b)
γ_A	1/5 day^{-1}	1/5 day^{-1}	1/5 day^{-1}	Kissler et al. (2020)
ω_v	1/(9 × 30) day^{-1}	1/(9 × 30) day^{-1}	1/(9 × 30) day^{-1}	Ngonghala et al. (2022)
ω_n	1/(9 × 30) day^{-1}	1/(9 × 30) day^{-1}	1/(9 × 30) day^{-1}	Ngonghala et al. (2022)
ξ_v	2.356 × 10^{-3} day^{-1}	8.029 × 10^{-4} day^{-1}	2.702 × 10^{-4} day^{-1}	NCIRD (2022)
ε_v	0.90 (dimensionless)	0.86 (dimensionless)	0.70 (dimensionless)	(Bruxvoort et al., 2021; Nasreen et al., 2022)
σ	1/3.5 day^{-1}	1/2.91 day^{-1}	1/1.92 day^{-1}	(Wu et al., 2022; Xin et al., 2022)
ψ	1/2 day^{-1}	1/1.5 day^{-1}	1/1.5 day^{-1}	(Iboi et al., 2020b; Wu et al., 2022; Xin et al., 2022; Zhao et al., 2020a)
γ_H	1/8 day^{-1}	1/7.6 day^{-1}	1/5.5 day^{-1}	Danielle Iuliano et al. (2022)

3.2.1. Local asymptotic stability of the DFE of the homogeneous model

The local asymptotic stability of the DFE ($\mathbb{E}_0$) of the homogeneous model will be explored using the *next generation operator method* (Diekmann et al., 1990; Pauline van den Driessche & Watmough, 2002). Using the notation in (Pauline van den Driessche & Watmough, 2002), it follows that the associated non-negative matrix of new infection terms (F) and the M-matrix of all linear transition terms (V) are given, respectively, by

$$F = \begin{bmatrix} 0 & \frac{\beta_P(S^*+(1-\epsilon_v)V^*)}{N^*} & \frac{\beta_I(S^*+(1-\epsilon_v)V^*)}{N^*} & \frac{\beta_A(S^*+(1-\epsilon_v)V^*)}{N^*} & \frac{\beta_H(S^*+(1-\epsilon_v)V^*)}{N^*} \\ 0 & 0 & 0 & 0 & 0 \\ 0 & 0 & 0 & 0 & 0 \\ 0 & 0 & 0 & 0 & 0 \\ 0 & 0 & 0 & 0 & 0 \end{bmatrix}, \tag{3.6}$$

and,

$$V = \begin{bmatrix} \sigma+\mu & 0 & 0 & 0 & 0 \\ -\sigma & \psi+\mu & 0 & 0 & 0 \\ 0 & -r\psi & \varphi+\gamma_I+\mu+\delta_I & 0 & 0 \\ 0 & -(1-r)\psi & 0 & \gamma_A+\mu & 0 \\ 0 & 0 & -\varphi & 0 & \gamma_H+\mu+\delta_H \end{bmatrix}. \tag{3.7}$$

It is also convenient to define the quantity (where ρ is the spectral radius) (Diekmann et al., 1990; Pauline van den Driessche & Watmough, 2002):

Table 4
Table of estimated (fitted) parameters of the homogeneous model (3.1) generated by fitting the model with the observed cumulative mortality data for the United States during Waves A, B, and C.

Parameter	Estimated (fitted) Value		
	Wave A	Wave B	Wave C
β_P	0.201 day^{-1}	0.448 day^{-1}	0.724 day^{-1}
β_I	0.110 day^{-1}	0.394 day^{-1}	0.448 day^{-1}
β_A	0.363 day^{-1}	0.604 day^{-1}	0.846 day^{-1}
β_H	2.468 × 10^{-8} day^{-1}	8.889 × 10^{-3} day^{-1}	1.950 × 10^{-3} day^{-1}
δ_I	1.998 × 10^{-4} day^{-1}	1.001 × 10^{-4} day^{-1}	1.014 × 10^{-5} day^{-1}
δ_H	5.472 × 10^{-4} day^{-1}	3.088 × 10^{-4} day^{-1}	1.015 × 10^{-3} day^{-1}

$$\mathcal{R}_v = \rho(FV^{-1}) = \mathcal{R}_{v,P} + \mathcal{R}_{v,I} + \mathcal{R}_{v,A} + \mathcal{R}_{v,H}, \tag{3.8}$$

where,

$$\begin{aligned}
\mathcal{R}_{v,P} &= \beta_P(1-\epsilon_v v^*)\frac{\sigma}{(\sigma+\mu)(\psi+\mu)},\\
\mathcal{R}_{v,I} &= \beta_I(1-\epsilon_v v^*)\frac{\sigma r\psi}{(\sigma+\mu)(\psi+\mu)(\varphi+\gamma_I+\mu+\delta_I)},\\
\mathcal{R}_{v,A} &= \beta_A(1-\epsilon_v v^*)\frac{\sigma(1-r)\psi}{(\sigma+\mu)(\psi+\mu)(\gamma_A+\mu)},\\
\mathcal{R}_{v,H} &= \beta_H(1-\epsilon_v v^*)\frac{\sigma r\psi\varphi}{(\sigma+\mu)(\psi+\mu)(\varphi+\gamma_I+\mu+\delta_I)(\gamma_H+\mu+\delta_H)},
\end{aligned} \tag{3.9}$$

with v^* defined as the proportion of individuals vaccinated at the disease-free equilibrium, given by

$$v^* = \frac{V^*}{N^*} = \frac{\xi_v}{\omega_v+\xi_v+\mu}, \tag{3.10}$$

from which it follows that,

$$1-\epsilon_v v^* = \frac{S^* + (1-\epsilon_v)V^*}{N^*}. \tag{3.11}$$

The quantity $\mathcal{R}_v$ is the *vaccination reproduction number* (or the *control reproduction number*) of the model (3.1). It measures the average number of new cases generated by a typical infected individual if introduced into a population almost completely consisting of susceptible and vaccinated individuals. The quantities $\mathcal{R}_{v,P}$, $\mathcal{R}_{v,I}$, $\mathcal{R}_{v,A}$, and $\mathcal{R}_{v,H}$ are the constituent vaccination reproduction numbers for the pre-symptomatic, symptomatic, asymptomatic, and hospitalized individuals, respectively.The result below follows from Theorem 2 of (Pauline van den Driessche & Watmough, 2002).

Theorem 3.1. *The disease-free equilibrium* ($\mathbb{E}_0$) *of the homogeneous model* (3.1)*, is locally-asymptotically stable (LAS) if* $\mathcal{R}_v < 1$*, and unstable if* $\mathcal{R}_v > 1$.

The epidemiological implication of Theorem 3.1 is that a small influx of COVID-19 cases will not generate a large outbreak in the community if $\mathcal{R}_v < 1$. The community-level transmission of the disease can be controlled if the initial number of infected individuals is small enough (i.e., if the initial conditions are in the basin of attraction of the disease-free equilibrium) and the vaccinated reproduction number ($\mathcal{R}_v$) can be brought to (and maintained at) a value less than one. It is worth mentioning that, using the definitions (3.10) and (3.11), the vaccination reproduction number ($\mathcal{R}_v$), given by (3.14), can be re-written as:

$$\mathcal{R}_v = (1-\epsilon_v v^*)\mathcal{R}_0, \tag{3.12}$$

where,

$$\mathcal{R}_0 = \beta_P\frac{\sigma}{k_3k_4} + \beta_I\frac{\sigma r\psi}{k_3k_4k_5} + \beta_A\frac{\sigma(1-r)\psi}{k_3k_4k_6} + \beta_H\frac{\sigma r\psi\varphi}{k_3k_4k_5k_7}, \tag{3.13}$$

with,

$$\begin{aligned}
k_1 &= \xi_v+\mu, \quad k_2 = \omega_v+\mu, \quad k_3 = \sigma+\mu, \quad k_4 = \psi+\mu,\\
k_5 &= \varphi+\gamma_I+\mu+\delta_I, \quad k_6 = \gamma_A+\mu, \quad k_7 = \gamma_H+\mu+\delta_H.
\end{aligned} \tag{3.14}$$

The quantity $\mathcal{R}_0$ is the *basic reproduction number* of the homogeneous model (3.1) (which measures the average number of new cases generated by a typical infected individual if introduced into a completely susceptible population). The values of the vaccination ($\mathcal{R}_v$) and basic ($\mathcal{R}_0$) reproduction numbers of the homogeneous model corresponding to the three waves are tabulated in Table 5 (this table shows a more severe epidemic during Waves B and C, in comparison to during Wave A, in line with the observed data depicted in Fig. 2). This is in agreement with the fact that the Delta and Omicron variants, circulating during Waves B and C, were more transmissible than the Alpha variant, which was the predominant variant during Wave A (Duong, 2021; Katella, 2022). The associated effective reproduction number (also known as *time-varying control reproduction number* (Gumel, Iboi, Ngonghala, & Elbasha, 2021)) of the homogeneous model (3.1) (denoted by $\mathcal{R}_e(t)$) is derived, for each of the three waves, in Appendix B, to show the changes, over time, of the reproduction number of the model during each of the three waves.

Table 5
Values of the control ($\mathcal{R}_v$) and basic ($\mathcal{R}_0$) reproduction numbers of the homogeneous model (3.1) for Waves A, B, and C. These values are obtained by substituting the fixed and estimated (fitted) parameters of the model, tabulated in Tables 3 and 4, respectively, into Equations (3.12) and (3.13), respectively.

Reproduction Numbers	Wave A	Wave B	Wave C
$\mathcal{R}_v$	0.88	2.28	3.50
$\mathcal{R}_0$	1.35	2.69	3.68

3.2.1.1. Epidemiological interpretation of the vaccination reproduction number ($\mathcal{R}_v$). The vaccination reproduction number of the homogeneous model (3.1), $\mathcal{R}_v$, is the sum of four constituent reproduction numbers for the number of new cases by pre-symptomatic individuals ($\mathcal{R}_{v,P}$), symptomatic individuals ($\mathcal{R}_{v,I}$), asymptomatic individuals ($\mathcal{R}_{v,A}$) and hospitalized individuals ($\mathcal{R}_{v,H}$). The constituent reproduction numbers are epidemiologically interpreted as follows.

Interpretation of $\mathcal{R}_{v,P}$: The term $\mathcal{R}_{v,P}$ is the product of the rate pre-symptomatically infectious individuals transmit infections near the disease-free equilibrium ($\beta_P(1-\epsilon_v v^*)$), the probability of surviving the exposed class and moving to the pre-symptomatic class $\left(\frac{\sigma}{\sigma+\mu}\right)$, and the average duration in the pre-symptomatically infectious class $\left(\frac{1}{\psi+\mu}\right)$.

Interpretation of $\mathcal{R}_{v,I}$: The term $\mathcal{R}_{v,I}$ is the product of the infection rate of symptomatically-infectious individuals near the disease-free equilibrium ($\beta_I(1-\epsilon_v v^*)$), the probability of surviving the exposed class and moving to the pre-symptomatic class $\left(\frac{\sigma}{\sigma+\mu}\right)$, the probability of surviving the pre-symptomatic class and moving to the symptomatic class $\left(\frac{r\psi}{\psi+\mu}\right)$, and the average duration in the symptomatically-infectious class $\left(\frac{1}{\varphi+\gamma_I+\mu+\delta_I}\right)$.

Interpretation of $\mathcal{R}_{v,A}$: The quantity $\mathcal{R}_{v,A}$ is the product of the infection rate of asymptomatically-infectious individuals near the disease-free equilibrium ($\beta_A(1-\epsilon_v v^*)$), the probability of surviving the exposed class and moving to the pre-symptomatic class $\left(\frac{\sigma}{\sigma+\mu}\right)$, the probability of surviving the pre-symptomatic class and moving to the asymptomatic class $\left(\frac{(1-r)\psi}{\psi+\mu}\right)$, and the average time spent in the asymptomatically-infectious class $\left(\frac{1}{\gamma_A+\mu}\right)$.

Interpretation of $\mathcal{R}_{v,H}$: The term $\mathcal{R}_{v,H}$ is the product of the transmission rate of hospitalized individuals near the disease-free equilibrium ($\beta_H(1-\epsilon_v v^*)$), the probability of surviving the exposed class and moving to the pre-symptomatic class $\left(\frac{\sigma}{\sigma+\mu}\right)$, the probability of surviving the pre-symptomatic class and moving to the symptomatic class $\left(\frac{r\psi}{\psi+\mu}\right)$, the probability of surviving the symptomatic class and moving to the hospitalized class $\left(\frac{\varphi}{\varphi+\gamma_I+\mu+\delta_I}\right)$, and the average duration spent in the hospitalized class $\left(\frac{1}{\gamma_H+\mu+\delta_H}\right)$.The sum of $\mathcal{R}_{v,P}$, $\mathcal{R}_{v,I}$, $\mathcal{R}_{v,A}$, and $\mathcal{R}_{v,H}$ gives $\mathcal{R}_v$.

The relative contributions of infectious individuals in the pre-symptomatic, symptomatic, asymptomatic and hospitalized compartments in the generation of new SARS-CoV-2 cases in the community are compared by computing the percent ratios of their associated constituent vaccination reproduction numbers, $(\mathcal{R}_{v,j}/\mathcal{R}_v) \times 100\%$ (with $j = \{P, I, A, H\}$) during each of the three waves. The percent contributions computed for the four infectious classes during each of the three waves are tabulated in Table 6, from which it follows that the main drivers of the pandemic (for all three waves) are the pre-symptomatic and asymptomatic individuals (accounting for a combined total of approximately 84% of all new cases during Wave A, 70% of all new cases during Wave B, and 76% of all new cases during Wave C). This result is in line with those reported in (Huff & Singh, 2020; Ngonghala, Iboi, & Gumel, 2020; Nikolai et al., 2020), which also showed that the main drivers of the COVID-19 pandemic (during the time periods considered in their study) were the pre-symptomatic and asymptomatic individuals. It is worth noting from Table 6 that the relative contribution of new cases generated by hospitalized infectious individuals is very low across the three waves (i.e., the vast majority of new SARS-CoV-2 cases were generated in the community, and not in the hospital setting).

Table 6
Percentage of new SARS-CoV-2 cases generated by infectious individuals in the pre-symptomatic (P), symptomatic (I), asymptomatic (A), and hospitalized (H) compartments during Waves A-C of the SARS-CoV-2 pandemic in the United States. The percentages presented in this table are calculated by considering the relative contribution of the constituent vaccination reproduction numbers for the pre-symptomatic, symptomatic, asymptomatic, and hospitalized individuals, given respectively by $\mathcal{R}_{v,P}$, $\mathcal{R}_{v,I}$, $\mathcal{R}_{v,A}$, and $\mathcal{R}_{v,H}$, and defined in (3.9), on $\mathcal{R}_v$, during Waves A-C.

Transmission Source	Percent Contribution for New Cases		
	Wave A	Wave B	Wave C
Pre-symptomatic ($\mathcal{R}_{v,P}$)	29.82%	24.94%	29.53%
Symptomatic ($\mathcal{R}_{v,I}$)	16.31%	29.23%	24.36%
Asymptomatic ($\mathcal{R}_{v,A}$)	53.86%	44.82%	46%
Hospitalized ($\mathcal{R}_{v,H}$)	0%	1%	0.12%

3.2.2. Global asymptotic stability of DFE of the homogeneous model: special case

The local asymptotic stability result established in Theorem 3.1 implies that the effective control of the disease when the vaccination reproduction number of the homogeneous model (3.1) is less than one depends on the initial sizes of the sub-populations of the model (i.e., the initial sizes of the sub-populations must lie within the basin of attraction of the disease-free equilibrium). For such effective control to be independent of the initial sizes of the sub-populations of the model, it is necessary that the disease-free equilibrium is proved to be globally-asymptotically stable when the vaccination reproduction number is less than one. This is explored for a special case below. Consider a special case of the homogeneous model with perfect protective efficacy of the vaccine (i.e., consider the homogeneous model (3.1) with $\varepsilon_v = 1$). It is convenient to define $\tilde{\mathcal{R}}_v = \mathcal{R}_v|_{\epsilon_v=1}$. We claim the following result:

Theorem 3.2. *The disease-free equilibrium of the special case of the homogeneous model* (3.1) *with perfect vaccine protective efficacy (i.e.,* $\varepsilon_v = 1$*) is globally-asymptotically stable in* Ω_1 *if* $\tilde{\mathcal{R}}_v \leq s^* < 1$, *where* $s^* = S^*/N^* = \frac{\omega_v+\mu}{\omega_v+\xi_v+\mu} < 1$.

The proof of Theorem 3.2, based on using Lyapunov function theory and LaSalle's Invariance Principle (Hale, 1969), is given in Appendix C. The epidemiological implication of Theorem 3.2 is that, for the special case of the homogeneous model with perfect vaccine-derived protection against acquisition of infection (i.e., $\varepsilon_v = 1$), the disease will be eliminated if $\tilde{\mathcal{R}}_v$ can be brought down to (and maintained at) a value less than $s^* < 1$. In other words, for the special case of the homogeneous model with $\varepsilon_v = 1$, the requirement $\tilde{\mathcal{R}}_v \leq s^* < 1$ is necessary and sufficient for the effective control or elimination of the SARS-CoV-2 pandemic. The results of Theorem 3.2 are numerically illustrated in Fig. 3, where all initial conditions converged to the disease-free equilibrium when the associated reproduction number ($\tilde{\mathcal{R}}_v$) is less than s^*.

The global asymptotic stability of the DFE of the homogeneous model can also be established for another special case as follows. Consider a special case of the homogeneous model (3.1) with negligible disease-induced mortality (i.e., consider the model (3.1) with $\delta_I = \delta_H = 0$). Setting $\delta_I = \delta_H = 0$ in the model (3.1), and adding all the equations, gives the following equation for the rate of change of the total population:

$$\dot{N} = \Pi - \mu N, \tag{3.15}$$

from which it follows that $N(t) \to \frac{\Pi}{\mu}$ as $t \to \infty$. Thus, $\frac{\Pi}{\mu}$ is an upper bound of $N(t)$ provided that $N(0) \leq \frac{\Pi}{\mu}$. Furthermore, if $N(0) > \frac{\Pi}{\mu}$, then $N(t)$ will decrease to this value asymptotically. Consequently, we can replace $N(t)$ with its limiting value, $\frac{\Pi}{\mu}$. Substituting $\frac{\Pi}{\mu}$ for $N(t)$ in the expression for the force of infection (3.2) shows that λ reduces to:

$$\lambda^\circ = \beta_P^\circ P + \beta_I^\circ I + \beta_A^\circ A + \beta_H^\circ H, \tag{3.16}$$

where,

$$\beta_j^\circ = \frac{\beta_j \mu}{\Pi}, \quad \text{with } j = \{P, I, A, H\}. \tag{3.17}$$

Then, it follows from Equations (3.1), (3.5) and (3.16) that:

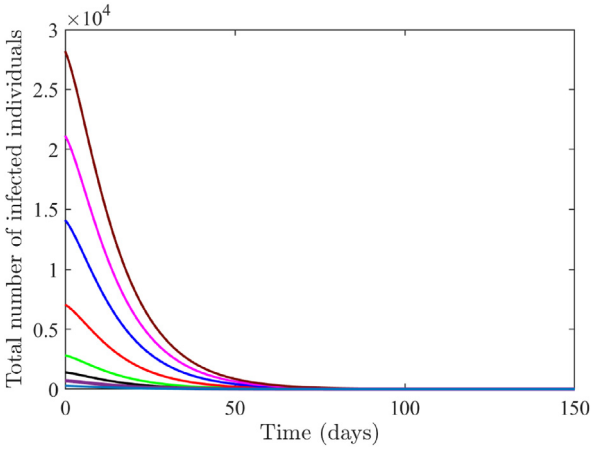

Fig. 3. Simulations of a special case of the homogeneous model (3.1) with $\varepsilon_v = 1$, showing convergence of initial solutions to the disease-free equilibrium when $\tilde{\mathcal{R}}_v < 1$. Parameter values used in these simulations are those for Wave C, given in Tables 3 and 4, with $\varepsilon_v = 1$, $\beta_P = \beta_I = \beta_A = 0.1$ (so that, $\tilde{\mathcal{R}}_v = 0.55 < s^* = 0.93 < 1$).

$$\begin{aligned}\dot{S} &= \Pi + \omega_v V - \lambda^\circ S - (\xi_v + \mu)S \\ &\leq \Pi + \omega_v V - (\xi_v + \mu)S \\ &\leq \Pi + \omega_v(\Pi/\mu - S - E - P - I - A - H - R) - (\xi_v + \mu)S \\ &\leq \frac{(\omega_v + \mu)\Pi}{\mu} - (\omega_v + \xi_v + \mu)S \\ &= (\omega_v + \xi_v + \mu)(S^* - S),\end{aligned}$$

from which it follows that if $S > S^*$, then $\dot{S} < 0$. Hence, $S \leq S^*$ provided that $S(0) \leq S^*$. Similarly, it follows from the second equation of (3.1) that $\dot{V} \leq -(\omega_v + \mu)V + \xi_v S = (\omega_v + \mu)(V^* - V)$. If $V > V^*$, then $\dot{V} < 0$. Thus, $V \leq V^*$ provided $V(0) \leq V^*$. It follows from these bounds that the region

$$\Omega^\circ = \{(S, V, E, P, I, A, H, R) \in \Omega_1 : S \leq S^*, V \leq V^*\},$$

is also positively invariant with respect to the flow generated by the homogeneous model (3.1), and attracts all solutions of the model in Ω_1.

It is convenient to define $\mathcal{R}_v^\circ = \mathcal{R}_v|_{\delta_I = \delta_H = 0}$, the reproduction number of the special case of the homogeneous model with $\delta_I = \delta_H = 0$. It follows from the definition of $\mathcal{R}_v$ in (3.12), with (3.13), that:

$$\mathcal{R}_v^\circ = (1 - \epsilon_v v^*)\left[\beta_P \frac{\sigma}{k_3 k_4} + \beta_I \frac{\sigma r \psi}{k_3 k_4 k_5^\circ} + \beta_A \frac{\sigma(1-r)\psi}{k_3 k_4 k_6} + \beta_H \frac{\sigma r \psi \varphi}{k_3 k_4 k_5^\circ k_7^\circ}\right], \tag{3.18}$$

where $k_5^\circ = \varphi + \gamma_I + \mu$ and $k_7^\circ = \gamma_H + \mu$ (and k_3 and k_4 are as defined in Equation (3.14)). We claim the following result.

Theorem 3.3. *Consider the homogeneous model* (3.1) *with negligible disease-induced mortality in the host population (i.e.,* $\delta_I = \delta_H = 0$*). The disease-free equilibrium of this special case of the homogeneous model* (3.1) *is globally-asymptotically stable in* Ω° *whenever* $\mathcal{R}_v^\circ < 1$.

The proof of Theorem 3.3, based on using a comparison theorem (Lakshmikantham et al., 1989), is given in Appendix D. The results of Theorem 3.3 are numerically illustrated in Fig. 4, where all initial conditions converged to the disease-free equilibrium when the associated reproduction number ($\mathcal{R}_v^\circ$) is less than one. Thus, based on the analyses above for the two special cases of the homogeneous model, we have identified two main mechanisms that could lead to the elimination of the pandemic (this is associated with bringing and maintaining the associated reproduction numbers of the homogeneous model to a value less than one). First, using highly efficacious vaccines, such that the vaccine protective efficacy (ε_v) approaches 100% could lead to SARS-CoV-2 elimination under the baseline parameter scenario (Theorem 3.2). Similarly, implementing effective therapeutic and other hospitalization measures that significantly reduce the disease-induced mortality for symptomatic and hospitalized individuals (e.g., the early detection and hospitalization of symptomatic individuals; use of highly effective drug therapies and ventilation systems etc.) can lead to the elimination of the pandemic (Theorem 3.3).

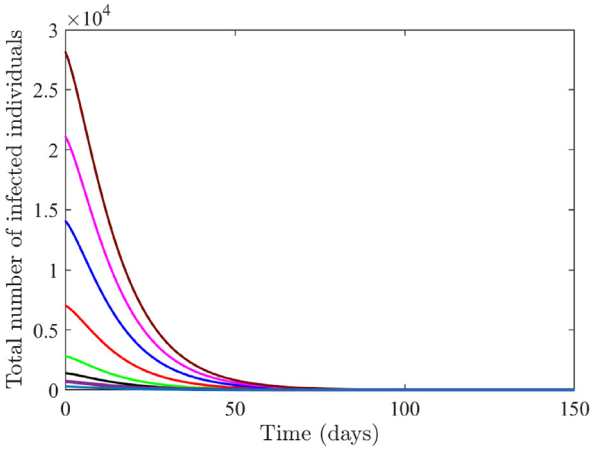

Fig. 4. Simulations of a special case of the homogeneous model (3.1) with $\delta_I = \delta_H = 0$, showing convergence of initial solutions to the disease-free equilibrium when $\mathcal{R}_v^\circ < 1$. Parameter values used are that of Wave C, given in Tables 3 and 4, with $\delta_I = \delta_H = 0$ and $\beta_P = \beta_I = \beta_A = 0.1$ (so that $\mathcal{R}_v^\circ = 0.53 < 1$).

3.3. Existence and asymptotic stability of endemic equilibria of the homogeneous model

In this section, conditions for the existence of endemic equilibria of the homogeneous model (i.e., equilibria where each of the state variable is nonzero) will be explored. Let (S^{**}, V^{**}, E^{**}, P^{**}, I^{**}, A^{**}, H^{**}, R^{**}) represent any arbitrary endemic equilibrium of the homogeneous model. It can be seen from (3.2) that the force of infection (λ) of the homogeneous model at an endemic equilibrium (denoted by λ^{**}) is given by:

$$\lambda^{**} = \left(\frac{\beta_P P^{**} + \beta_I I^{**} + \beta_A A^{**} + \beta_H H^{**}}{N^{**}}\right). \tag{3.19}$$

Setting the right-hand sides of the equations of the homogeneous model (3.1) to zero and solving gives the following expressions for the state variables of the model at an endemic steady-state (in terms of λ^{**}):

$$\begin{aligned} S^{**} &= \frac{\Pi[(1-\epsilon_v)\lambda^{**} + k_2]}{[(1-\epsilon_v)\lambda^{**} + k_2](\lambda + k_1 + \omega_n\tau\eta) - \omega_v\xi_v}, \quad V^{**} = \frac{\xi_v}{(1-\epsilon_v)\lambda^{**} + k_2}S^{**}, \\ E^{**} &= \eta S^{**}, \quad P^{**} = \frac{\sigma}{k_4}\eta S^{**}, \quad I^{**} = \frac{r\psi\sigma}{k_4k_5}\eta S^{**}, \quad A^{**} = \frac{(1-r)\psi\sigma}{k_4k_6}\eta S^{**}, \\ H^{**} &= \frac{\varphi r\psi\sigma}{k_4k_5k_7}\eta S^{**}, \quad R^{**} = \tau\eta S^{**}, \end{aligned} \tag{3.20}$$

where $\eta = \frac{\lambda^{**}[(1-\epsilon_v)\lambda^{**}+k_2+(1-\epsilon_v)\xi_v]}{k_3[(1-\epsilon_v)\lambda^{**}+k_2]}$ and $\tau = \frac{\gamma_I}{\omega_n+\mu}\frac{r\psi\sigma}{k_4k_5} + \frac{\gamma_A}{\omega_n+\mu}\frac{(1-r)\psi\sigma}{k_4k_6} + \frac{\gamma_H}{\omega_n+\mu}\frac{\varphi r\psi\sigma}{k_4k_5k_7}$. Substituting the expressions in (3.20) into (3.19) shows that the endemic equilibria of the homogeneous model satisfy the following quadratic equation (in terms of λ^{**}):

$$a_2(\lambda^{**})^2 + a_1\lambda^{**} + a_0 = 0, \tag{3.21}$$

where,

$$\begin{aligned} a_0 &= k_3(k_2 + \xi_v)(1 - \mathcal{R}_v), \\ a_1 &= [k_2 + (1-\epsilon_v)\xi_v]\rho - k_3(1-\epsilon_v)(\mathcal{R}_0 - 1), \\ a_2 &= (1-\epsilon_v)\rho, \end{aligned} \tag{3.22}$$

with $\rho = 1 + \frac{\sigma}{k_4} + \left(1 + \frac{\gamma_I}{\mu+\omega_n}\right)\frac{r\psi\sigma}{k_4k_5} + \left(1 + \frac{\gamma_A}{\mu+\omega_n}\right)\frac{(1-r)\psi\sigma}{k_4k_6} + \left(1 + \frac{\gamma_H}{\mu+\omega_n}\right)\frac{\varphi r\psi\sigma}{k_4k_5k_7} > 0$. The components of an endemic equilibrium of the homogeneous model can be obtained by solving for for λ^{**} in the quadratic equation (3.21) and substituting the result into the expressions in (3.22). Furthermore, it can be seen from (3.22) that the coefficient a_0 is positive (negative) whenever $\mathcal{R}_v < (>) 1$. Similarly, the coefficient a_2 is always positive (since $0 < \varepsilon_v < 1$). The result below follows from the quadratic (3.21) with (3.22).

Theorem 3.4. *The homogeneous model* (3.1) *has:*

(i) *a unique endemic equilibrium if* $a_0 < 0 \Leftrightarrow \mathcal{R}_v > 1$;
(ii) *a unique endemic equilibrium if* $a_1 < 0$ *and* $a_0 = 0$ *or* $a_1^2 - 4a_0a_2 = 0$;
(iii) *two endemic equilibria if* $a_2 > 0$, $a_1 < 0$, *and* $a_1^2 - 4a_0a_2 > 0$;
(iv) *no endemic equilibrium otherwise.*

While Case (i) of Theorem 3.4 implies the presence of a unique endemic equilibrium for the homogeneous model (3.1) whenever $\mathcal{R}_v > 1$, Case (iii) suggests the possibility of a *backward bifurcation*, a dynamic phenomenon characterized by the coexistence of the stable disease-free equilibrium (DFE) and a stable endemic equilibrium, when the associated vaccination reproduction number of the homogeneous model ($\mathcal{R}_v$) is less than one (see (Gumel, 2012) for further details about the causes and consequences of backward bifurcation in the transmission dynamics of infectious diseases).

It should be noted that in the case of a perfect vaccine ($\varepsilon_v = 1$), $a_2 = 0$, $a_1 > 0$ and the quadratic equation becomes linear in λ^{**} (with $\lambda^{**} = -a_0/a_1$). In this case, the homogeneous model (3.1) has a unique endemic equilibrium if and only if $a_0 > 0$ (i.e., $\mathcal{R}_v > 1$), ruling out backward bifurcation in this case (this is consistent with the result in Theorem 3.2, where it was shown that the disease-free equilibrium of the special case of the homogeneous model with $\varepsilon_v = 1$ is globally-asymptotically stable when the associated reproduction number is less than $s^* < 1$). It can be shown, following the approach in Section 3.3, that the special case of the homogeneous model (3.1) with $\delta_I = \delta_H = 0$ has a unique endemic equilibrium whenever $\mathcal{R}_v^\circ > 1$. That is, the result below holds.

Theorem 3.5. *The special case of the homogeneous model* (3.1) *with* $\delta_I = \delta_H = 0$ *has a unique positive endemic equilibrium whenever* $\mathcal{R}_v^\circ > 1$.Furthermore, let $\hat{\mathcal{R}}_v = \mathcal{R}_v|_{\delta_I=\delta_H=\omega_v=\omega_n=0,\ \epsilon=1}$. We claim the following result.

Theorem 3.6. *Consider the special case of the homogeneous model* (3.1) *with negligible disease-induced mortality (i.e.,* $\delta_I = \delta_H = 0$*), perfect vaccine* ($\varepsilon_v = 1$)*, and no waning* ($\omega_v = \omega_n = 0$)*. The associated unique endemic equilibrium of this special case of the homogeneous model is locally-asymptotically stable if* $\hat{\mathcal{R}}_v > 1$.

The proof of Theorem 3.6*, based on using a Krasnoselskii sub-linearity argument (see* (Hethcote & Thieme, 1985; Horst, 1985)*, and also* (Esteva et al., 2009; Esteva & Vargas, 2000)*), is given in Appendix E. The epidemiological implication of* Theorem 3.6 *is that the disease will persist in the population whenever* $\hat{\mathcal{R}}_v > 1$. *The local asymptotic stability result for the unique endemic equilibrium of the homogeneous model will be extended to global asymptotic stability as follows. It is, first of all, convenient to define the following region (the stable manifold of the disease-free equilibrium of the homogeneous model*):

$\Omega_0 = \{(S, V, E, P, I, A, H, R) \in \Omega_1 : E = P = I = A = H = R = 0\}$.*We claim the following result.*

***Theorem* 3.7.** *Consider the special case of the homogeneous model* (3.1) *with negligible disease-induced mortality (i.e.,* $\delta_I = \delta_H = 0$*), perfect vaccine* ($\varepsilon_v = 1$)*, and no waning* ($\omega_v = \omega_n = 0$)*. The unique endemic equilibrium of this special case of the homogeneous model is globally-asymptotically stable in* $\Omega_1 \setminus \Omega_0$ *whenever* $\hat{\mathcal{R}}_v > 1$.

The proof of Theorem 3.7*, based on using a nonlinear Lyapunov function of Goh-Volterra type, is given in Appendix F. The epidemiological implication of this result is that the disease will persist in the population whenever the associated reproduction threshold* ($\hat{\mathcal{R}}_v$) *exceeds unity. The results of Theorem* 3.7 *are numerically illustrated in* Fig. 5*, where all initial conditions converged to the unique endemic equilibrium when the associated reproduction number* ($\hat{\mathcal{R}}_v$) *exceeds one. Although the global asymptotic stability property of the endemic equilibrium of the homogeneous model was only established for a special case, extensive numerical simulations suggest that the endemic equilibrium of the full model is indeed globally-asymptotically stable whenever the reproduction number of the full model* ($\mathcal{R}_v$) *is greater than one. This suggests the following conjecture.*

***Conjecture* 1.** *The homogeneous model* (3.1) *has a unique and globally-asymptotically stable endemic equilibrium in* $\Omega_1 \setminus \Omega_0$ *whenever* $\mathcal{R}_v > 1$.

3.3.1. Computation of vaccine-derived herd immunity threshold for the homogeneous model

Herd immunity, also known as *mass immunity*, is a form of indirect protection from an infectious disease that occurs when a minimum percentage of the population is immune to the disease. The two main ways of achieving herd immunity are through vaccination and natural immunity developed through recovery from previous infection. Vaccination is the safest and fastest way to achieve herd immunity (Anderson & May 1985; Khalife & VanGennep, 2021; Roy, 1992). As noted in (Gumel, Iboi, Ngonghala, & Elbasha, 2021; Iboi et al., 2020b), "for vaccine-preventable diseases, such as COVID-19, not every susceptible member of the community can be vaccinated. For instance people with underlying health conditions, or females who are pregnant or people who opt out of vaccination for various reasons (traditional or other reasons) may not be vaccinated". Hence, it is critical to determine the minimum proportion of susceptible individuals in the community that need to be vaccinated in order to protect the ones that cannot be vaccinated (i.e., achieve herd immunity). To obtain the herd immunity threshold, we set the vaccination reproduction number ($\mathcal{R}_v$), given by Equation (3.12), to one and solve for the proportion of individuals fully-vaccinated at steady-state (v^*) (Gumel, Iboi, Ngonghala, & Elbasha, 2021; Iboi et al., 2020a). Doing so gives (for $\mathcal{R}_0 > 1$ and $0 < \varepsilon_v \leq 1$):

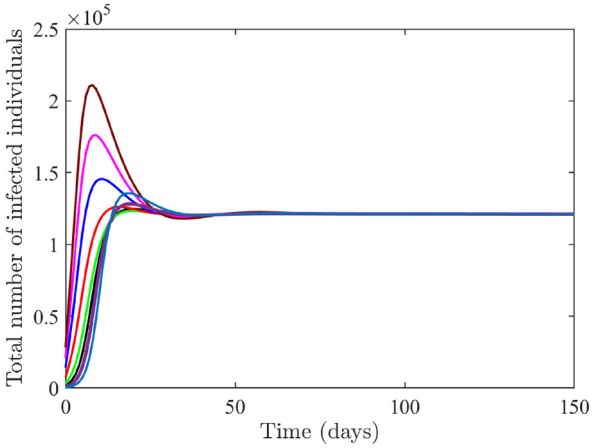

Fig. 5. *Simulations of a special case of the homogeneous model* (3.1) *with* $\delta_I = \delta_H = \omega_v = 0$ *and* $\varepsilon_v = 1$*, showing convergence of initial solutions to the unique endemic equilibrium when* $\hat{\mathcal{R}}_v > 1$. *Parameter values used are that of Wave B given in* Tables 3 and 4*, with* $\varepsilon_v = 1$, $\delta_I = \delta_H = \omega_v = \omega_n = 0$, *and* $\beta_P = \beta_I = \beta_A = 2$ (*so that* $\hat{\mathcal{R}}_v = 1.27 > 1$).

$$v^* = \frac{1}{\epsilon_v}\left(1 - \frac{1}{\mathcal{R}_0}\right) = v_c^*. \tag{3.23}$$

It follows from (3.12) and (3.23) that $\mathcal{R}_v < (>)1$ if $v^* > (<)v_c^*$. Further, $\mathcal{R}_v = 1$ whenever $v^* = v_c^*$. Hence, the result of Theorem 3.1 can be re-written in terms of the herd immunity threshold as follows:

Theorem 3.8. *The disease-free equilibrium* ($\mathbb{E}_0$) *of the homogeneous model* (3.1) *is locally-asymptotically stable if* $v^* > v_c^*$ ($\mathcal{R}_v < 1$), *and unstable if* $v^* < v_c^*$ ($\mathcal{R}_v > 1$).The global asymptotic stability results for the disease-free equilibrium (given in Theorems 3.2 and 3.3) can be similarly re-written in terms of the above herd immunity threshold.

Fig. 6 depicts a contour plot of the vaccination reproduction number ($\mathcal{R}_v$), as a function of coverage of fully-vaccinated susceptible individuals at steady-state (v^*) and vaccine efficacy (ε_v), during the three waves considered in this study.This figure shows that using the two-dose Pfizer vaccine (with an estimated protective efficacy of 90% (Bruxvoort et al., 2021; Nasreen et al., 2022)) during Wave A could lead to the effective control of the pandemic if at least 29% of the populace is fully-vaccinated (Fig. 6(a)). The vaccine coverage required to achieve such effective control during Wave B (Fig. 6(b)), using the same two-dose Pfizer vaccine (with an estimated efficacy of 85% during Wave B (Bruxvoort et al., 2021; Nasreen et al., 2022)), is 74%. However, these simulations show that using the same two-dose Pfizer vaccine during Wave C (with an estimated protective efficacy of 70% during this wave (Bruxvoort et al., 2021; Nasreen et al., 2022)) could not reduce the control reproduction number to a value below one (which is needed for achieving the vaccine-derived herd immunity, and consequently, eliminating the disease) even if every unvaccinated susceptible individual is fully vaccinated (Fig. 6(c)). This result can be attributed to the modest efficacy of the Pfizer vaccine (70% during Wave C (Bruxvoort et al., 2021; Nasreen et al., 2022)) and a higher basic reproduction number ($\mathcal{R}_0 = 3.68$), in comparison to the reproduction numbers for Wave A ($\mathcal{R}_0 = 1.35$) and Wave B ($\mathcal{R}_0 = 2.69$).

Fig. 6 also shows that if, on the other hand, a vaccine with moderate protective efficacy, such as the two-dose of AstraZeneca (with estimated protective efficacy of 67% (Lopez Bernal, Andrews, Gower, Gallagher, et al., 2021) during Wave B) is prioritized, the coverage needed to achieve herd immunity (and, consequently, disease elimination) during Wave B (Fig. 6(b)) is 94%. Likewise, the use of such a vaccine (with an estimated reduced efficacy of 49% during Wave C (Andrews et al., 2022)) will also fail to reduce the control reproduction number below one even if the coverage in its usage is 100% during Wave C (Fig. 6(c)).

3.4. Global sensitivity analysis for the homogeneous model

Global sensitivity analysis will be carried, using Latin Hypercube Sampling (LHS) and Partial Rank Correlation Coefficients (PRCCs) (Blower & Dowlatabadi, 1994; Marino et al., 2008; McLeod et al., 2006), on the homogeneous model (3.1) to determine the parameters that have the highest influence on the transmission dynamics of the disease (as measured by their impact on a chosen response function) during each of the three pandemic waves considered in this study. Specifically, the vaccination reproduction number ($\mathcal{R}_v$) is chosen as the response function. The application of this method entails using the baseline value of the 16 parameters in the expression for the vaccination reproduction number (given by (3.8)), corresponding to each of the three pandemic waves, listed in Tables 4 and 3 The parameters are assumed to obey the uniform distribution, and the range of each parameter in the response function is chosen to be 40% to the left and 40% to the right of its respective baseline value (Gao et al., 2023). The range of each parameter is sub-divided into 1, 000 equal sub-intervals. Since the parameter set is drawn from this set without replacement, this leads to 1, 000 × 18 parameter matrix (or hypercube) (Gao et al., 2023). A parameter with a negative (positive) PRCC value is said to be negatively (positively) correlated with the response function (typically, PRCC values in the range (0.5,1) in absolute value are considered to be correlated (Boloye Gomero, 2012), with values closer to −1 (+1) signifying a much higher negative (positive) correlation). The results

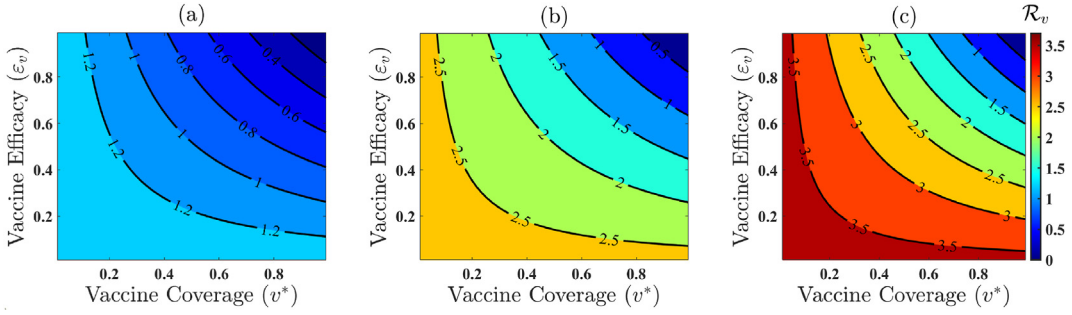

Fig. 6. Contour plot of the vaccine reproduction number ($\mathcal{R}_v$) of the homogeneous model (3.1), as a function of vaccine coverage at steady-state (v^*) and vaccine efficacy (ε_v), for the United States during (a) Wave A, (b) Wave B, and (c) Wave C. Parameter values used to generate the contour plots for each wave are given by their respective values in Tables 3 and 4

obtained for the PRCC values, depicted in Fig. 7 (see also Table 7), show that the correlated parameters (i.e., parameters with PRCC values higher than 0.5 in magnitude) during wave A of the pandemic are (Fig. 7 (a)):

(a) The proportion of pre-symptomatic individuals that become symptomatic at the end of the pre-symptomatic period (r; with PRCC value -0.85).
(b) The efficacy of the vaccine (ε_v; with PRCC value -0.82).
(c) The recovery rate of asymptomatically-infectious individuals (γ_A; with PRCC value -0.81).
(d) The transmission rate of asymptomatically infectious individuals (β_A; with PRCC value $+0.80$).
(e) The waning rate of the vaccine (ω_v; with PRCC value $+0.65$).
(f) The rate at which susceptible individuals become fully-vaccinated (ξ_v; with PRCC value -0.65).
(g) The rate at which pre-symptomatic individuals become symptomatic or asymptomatic (ψ; with PRCC value -0.64).
(h) The transmission rate of pre-symptomatic individuals (β_P; with PRCC value $+0.62$).

Thus, these results show that the implementation of control and mitigation strategies that focus on reducing the parameters β_A, β_P and ω_v and increasing r, γ_A, ψ, ε_v and ξ_v will be effective in reducing the burden of the pandemic during Wave A in the United States. The parameter β_A and β_P can be reduced by, for instance, the rapid detection of asymptomatic individuals, through measures such as mass random SARS-CoV-2 testing, isolation and contact tracing of symptomatic cases, and the use of high quality masks. Increasing ε_v entails designing and deploying a highly efficacious anti-SARS-CoV-2 vaccine. Similarly, ω_v can be reduced by using an effective vaccine that induces long-term vaccine-derived immunity. The parameter ξ_v can be increased by increasing the vaccine coverage in the community (this can be achieved by implementing effective public health campaign promoting the wide-scale use of the available vaccines). The recovery rate parameter for asymptomatic infectious individuals, γ_A, can be increased by using effective antiviral drugs, such as *remdesivir* (NIH) (*although* this may be challenging in practice due to the fact that this strategy requires large-scale random COVID-19 testing to detect asymptomatic infectious individuals and having a large number of such individuals to adhere to the prescribed antiviral treatment regimen. These

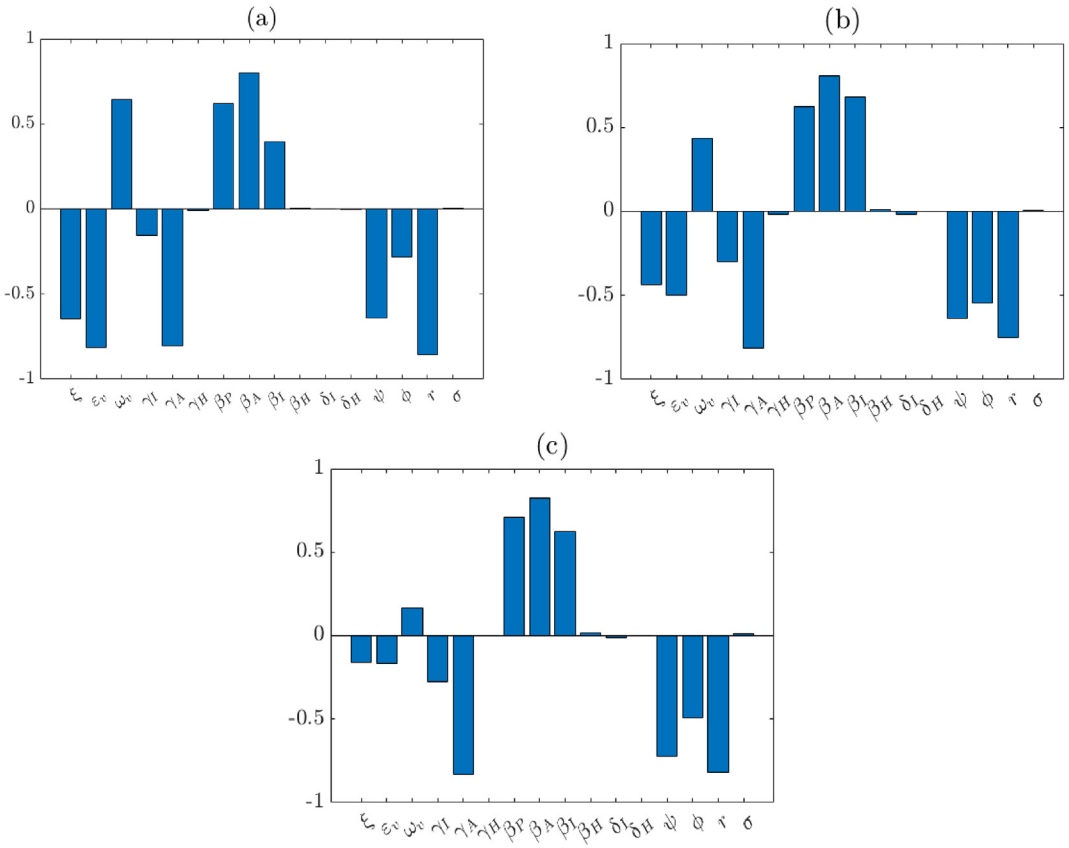

Fig. 7. Simulations of the homogeneous model (3.1), showing the partial rank correlation coefficients (PRCCs) values of the parameters in the chosen response function ($\mathcal{R}_v$) for (a): Wave A; (b): Wave B; and (c): Wave C. Parameter values used in the simulations are as given by the baseline values in Tables 3 and 4, and their ranges are taken to be 40% to the left and 40% to the right of the respective baseline value. All parameters are assumed to follow a uniform distribution.

Table 7
PRCC values of the parameters of the homogeneous model (3.1) using the vaccination reproduction number ($\mathcal{R}_v$) as the response function for the three waves considered in this study. The baseline values used are the parameter values listed in Tables 3 and 4, and their ranges are taken to be 40% to the left and 40% to the right of the respective baseline value. The PRCC value of 0.5 or higher in magnitude is highlighted in bold face.

Parameter	PRCC Value		
	Wave A	Wave B	Wave C
ξ_v	**−0.65**	−0.43	−0.16
ε_v	**−0.82**	−0.50	−0.16
ω_v	**+0.65**	+0.43	+0.16
γ_I	−0.16	−0.30	−0.27
γ_A	**−0.81**	**−0.81**	**−0.83**
γ_H	−0.007	−0.17	−0.002
β_P	**+0.62**	**+0.63**	**+0.71**
β_A	**+0.80**	**+0.81**	**+0.82**
β_I	+0.40	**+0.68**	**+0.62**
β_H	+0.007	+0.012	+0.018
δ_I	−0.001	−0.016	−0.011
δ_H	−0.005	−0.0001	−0.001
ψ	**−0.64**	**−0.63**	**−0.72**
φ	−0.28	**−0.54**	−0.49
r	**−0.85**	**−0.75**	**−0.82**
σ	+0.005	+0.003	+0.012

Table 8
Values of the fixed parameters of the two-group model (4.1) for Waves C.

Parameter ($k = \{1, 2\}$)	Value		Source
	Group 1 (age 0 to 64)	Group 2 (age 65 and above)	
Π_k	9, 622 day^{-1}	2, 048 day^{-1}	(The United States Census Bureau)
μ_k	1/(64 × 365) day^{-1}	1/(18.4 × 365) day^{-1}	[65, 116]
r_k	0.56 (dimensionless)	0.803 (dimensionless)	[68, 70, 71, 118]
$1 - r_k$	0.44 (dimensionless)	0.197 (dimensionless)	[21, 70, 118]
φ_k	1/6.69 day^{-1}	1/3.78 day^{-1}	Faes et al. (2020)
$\gamma_{I,i}$	1/10 day^{-1}	1/10 day^{-1}	Ferguson et al. (2020b)
$\gamma_{A,k}$	1/5 day^{-1}	1/5 day^{-1}	Kissler et al. (2020)
$\omega_{v,k}$	1/(9 × 30) day^{-1}	1/(9 × 30) day^{-1}	Ngonghala et al. (2022)
$\omega_{n,k}$	1/(9 × 30) day^{-1}	1/(9 × 30) day^{-1}	Ngonghala et al. (2022)
$\xi_{v,k}$	0.000418 day^{-1}	0.000102 day^{-1}	NCIRD (2022)
$\varepsilon_{v,k}$	0.70 (dimensionless)	0.70 (dimensionless)	[75, 76]
σ_k	1/1.92 day^{-1}	1/1.92 day^{-1}	[66, 67]
ψ_k	1/1.5 day^{-1}	1/1.5 day^{-1}	(Iboi et al., 2020b; Wu et al., 2022; Xin et al., 2022; Zhao et al., 2020a)
$\gamma_{H,k}$	1/3.9 day^{-1}	1/6.2 day^{-1}	Danielle Iuliano et al. (2022)

proved challenging during the COVID-19 pandemic in the United States (Peeling et al., 2021)). However, SARS-COV-2 vaccines are known to reduce the duration of infection in vaccinated individuals who acquired breakthrough infection (CDC, 2021; Emilia Paladino et al., 2021). Hence, it is plausible that increasing vaccination uptake may increase the recovery rate for asymptomatic infected individuals (i.e., vaccination can increase γ_A). Similarly, although increasing r decreases $\mathcal{R}_v$, it is not an ideal strategy since such an increase could also cause more disease-related hospitalizations and deaths. Although the results of our sensitivity analysis suggest that increasing ψ decreases $\mathcal{R}_v$, it is not a feasible strategy since it increases individuals with symptoms who may develop severe disease and potentially die of the disease.

Similarly, the correlated parameters during wave B of the pandemic are (Fig. 7(b)):

(i) The transmission rate of asymptomatically-infectious individuals (β_A; with PRCC value + 0.81).
(ii) The recovery rate of asymptomatically-infectious individuals (γ_A; with PRCC value −0.81).
(iii) The proportion of pre-symptomatic individuals that become symptomatic at the end of the pre-symptomatic period (r; with PRCC value −0.75).
(iv) The transmission rate of symptomatically-infectious individuals (β_I; with PRCC value + 0.68).
(v) The rate at which pre-symptomatic individuals become symptomatic or asymptomatic (ψ; with PRCC value + 0.63).
(vi) The transmission rate of pre-symptomatic individuals (β_P; with PRCC value −0.63).
(vii) The hospitalization rate of symptomatic individuals (φ; with PRCC value −0.54).

Hence, these results show that the implementation of control and mitigation strategies that focus on reducing the parameters β_A, β_I and β_P, and increasing γ_A, r, φ and ψ will be effective in reducing the burden of the pandemic during Wave C in the United States. It should be noted, first of all, that, while the correlated parameters β_A, γ_A, r, β_P and ψ for this wave are also correlated with the response function $\mathcal{R}_v$ in Wave A (so that the strategies associated with these parameters will also be

effective during Wave B), the correlated parameters β_I and φ are not correlated with the response function during Wave A. The parameter β_I can be reduced by implementing effective non-pharmaceutical interventions (with enough coverage), such as the quarantine of suspected cases, the isolation of confirmed/symptomatic cases (at home or in hospital), the use of high efficacy face mask in public and social distancing. The parameter φ can be increased by the rapid detection and hospitalization (and/or self-isolation) of symptomatic individuals. It is worth mentioning that the effectiveness of this strategy depends on whether or not the risk of disease transmission while in isolation (at home or in hospital) is greatly reduced or (better still) eliminated. In summary, these simulations show that the effective control of the pandemic during Wave B requires the implementation of strategies (targeting β_I and φ) that were not emphasized (or shown to be crucially-needed) during Wave A. In other words, these simulations show that the anti-SARS-CoV-2 intervention and mitigation strategies to be prioritized and implemented depends on the wave of the pandemic.

Finally, the correlated parameters during wave C of the pandemic are (Fig. 7(c)):

(a) The recovery rate of asymptomatically-infectious individuals (γ_A; with PRCC value -0.83).
(b) The proportion of pre-symptomatic individuals that become symptomatic at the end of the pre-symptomatic period (r; with PRCC value -0.82).
(c) The transmission rate of asymptomatically-infectious individuals (β_A; with PRCC value $+0.82$).
(d) The rate at which pre-symptomatic individuals become symptomatic or asymptomatic (ψ; with PRCC value -0.72).
(e) The transmission rate of pre-symptomatic individuals (β_P; with PRCC value $+0.71$).
(f) The transmission rate of symptomatically-infectious individuals (β_I; with PRCC value $+0.62$).

Here, too, five parameters (β_A, r, γ_A, β_P, and ψ) are also highly correlated (like in the cases of Waves A and B). Furthermore, like in the case of wave B, the parameter β_I is also highly correlated during wave C. Thus, these simulations show that strategies that focus on reducing the parameters β_P, β_A and β_I and increasing r and γ_A will be effective in reducing the burden of the pandemic during wave C in the United States. It should be noted that all six correlated parameters in Wave C also appear in Wave B (thus, all strategies that are effective to combat the pandemic during Wave C will also be effective during Wave B).

The discussion above (along with Fig. 7 and Table 7) shows that, while the vaccine coverage rate (ξ_v), efficacy (ε_v) and waning rate (ω_v) are correlated with the response function during Wave A, the relative influence of these parameters changes with the pandemic waves. For example, while ε_v has a PRCC value of -0.82 during Wave A, its PRCC value decreased to -0.43 and -0.16, respectively, during Wave B and Wave C. Although this result can be attributed to a decrease in vaccine coverage (ξ_v) and the decrease in vaccine-derived efficacy during subsequent waves, the result also underscores the fact that a control strategy that proved to be highly effective during one wave may not retain its high level of effectiveness during subsequent waves (suggesting that the optimal control strategies to be implemented will depend on the prevailing wave of the pandemic). Similarly, it has been observed that while the transmission rate of symptomatic individuals (β_I) during Waves B and C was correlated with the response function, this parameter was not correlated with the response function during Wave A. This suggests an increased adherence to non-pharmaceutical intervention by symptomatic individuals would have significantly helped reduce the spread of COVID-19 during Wave B and C. Finally, as stated above, the following three parameters are correlated with the response function during each of the three waves of the pandemic:

(a) The proportion of pre-symptomatic individuals that become symptomatic at the end of the pre-symptomatic period (r).
(b) The transmission rate of asymptomatically-infectious individuals (β_A).
(c) The recovery rate of asymptomatically-infectious individuals (γ_A).
(d) The rate at which pre-symptomatic individuals become symptomatic or asymptomatic (ψ).
(e) The transmission rate of pre-symptomatic individuals (β_P).

Hence, it follows that two parameters related to disease transmission dynamics by asymptomatically-infectious individuals (namely, β_A and γ_A) and two parameters related to disease transmission dynamics by pre-symptomatically-infectious individuals (namely, β_P and ψ) are highly correlated with the response function ($\mathcal{R}_v$) during each of the three waves of the pandemic. Consequently, this study shows that intervention strategies that target pre-symptomatic and asymptomatically-infectious individuals, such as contact tracing and mass random testing (implemented with the required coverage and level of effectiveness), will consistently be very effective in combating and mitigating the SARS-CoV-2 pandemic in the United States.

It is worth stating that, although the simulations carried out in this section shows that the proportion of individuals who become symptomatic at the end of the pre-symptomatic period (r) is highly (and negatively) correlated with the response function (i.e., an increase in r will result in a decrease in the response function) during each of the three waves, a strategy that focuses on increasing the value of r may not be realistic from public health standpoint (since such a strategy will result in an increase in SARS-CoV-2-related hospitalizations and, consequently, deaths) (Pant et al., 2024). Similarly, the parameters ψ and φ can negatively or positively affect the response function, $\mathcal{R}_v$ (depending on the choice of parameter values). Theoretical thresholds for the positive (negative) correlation of these parameters on the response function are derived in Appendix G. Finally, it is essential to emphasize the fact that SARS-CoV-2 vaccines can impact several parameters of the model (3.1). For example, these vaccines have been shown to reduce the duration of infection (CDC, 2021; Emilia Paladino et al., 2021) (i.e., increase γ_I, γ_A, and γ_H), thereby contributing to reductions in new transmission and overall burden (severity of disease, hospitalization and deaths).

4. Two-group heterogeneous model

In Section 3, the m-group heterogeneous model (2.3) was fitted and rigorously analysed for the (homogeneous) case with $m = 1$. In this section, the heterogeneous model (2.3) will be used to assess the impact of age heterogeneity and variable mixing patterns on the dynamics and burden of the SARS-CoV-2 pandemic. The SARS-CoV-2 pandemic is well known to disproportionately affect the elderly population (in terms of severity of disease, hospitalization and death) (CDCa; CDCb). In particular, although the population of people 65 years and older represents less than 20% of the total population of the United States (The United States Census Bureau), this population suffers the brunt of COVID-19 mortality (60.92%) and hospitalization (47.10%) in the United States (see Fig. 8(a) and (b)). Specifically, it can be seen from Fig. 8(a) that COVID-19-induced mortality *per* 100,000 people in this age group is 7.32 times higher than in the age group $0 - 64$. Similarly, Fig. 8(b) shows that hospitalization *per* 100,000 in the age group 65 and older is 4.18 times that of the age group $0 - 64$. It is also well known that most COVID-19 cases occur among younger individuals (Bosman & Mervosh, 2020; Lisa Lockerd Maragakis, 2020). For example, data from the California Department of Public Health showed that, by May 9, 2023, 89.1% of the total reported cases of COVID-19 in California were among people 64 years of age or under (CDPH. and COVID-19 age). This disproportionate effect of SARS-CoV-2 by age suggests the need to explicitly incorporate age structure (and the variable mixing patterns of the age groups considered) into mathematical models for the transmission dynamics and control of SARS-CoV-2 in a population. For this reason, we consider the heterogeneous model (2.3) for the case with two groups ($m = 2$) based on age. That is, we stratify the total population of the United States into those under 65 years of age (Group 1) and those 65 years and older (Group 2). Individuals in the two age groups also have variable mixing patterns with individuals in their age group, as well as with individuals in the other age group, and these variable mixing patterns need to also be incorporated into the model.

The main objective of this section is to determine whether or not adding these heterogeneities (age heterogeneity and the variable mixing patterns by age) significantly affects the level of the vaccine-derived herd immunity threshold needed to effectively control and mitigate the burden of the pandemic in the United States (i.e., we seek to compare the level of herd immunity threshold generated using the heterogeneous model of two groups (2.3) with the value obtained from the homogeneous model 3). Let $N_k(t)$, with $k = \{1, 2\}$, be the total number of individuals in Group k at time t. This population is split into the sub-populations of susceptible ($S_k(t)$), vaccinated ($V_k(t)$), exposed ($E_k(t)$), pre-symptomatic ($P_k(t)$), symptomatic ($I_k(t)$), asymptomatic ($A_k(t)$), hospitalized ($H_k(t)$) and recovered ($R_k(t)$) individuals, so that:

$$N_k(t) = S_k(t) + V_k(t) + E_k(t) + P_k(t) + I_k(t) + A_k(t) + H_k(t) + R_k(t);\ k = \{1, 2\}.$$

The two-group age-structured model for the transmission dynamics of SARS-CoV-2 in the United States (obtained by setting $m = 2$ in (2.3)) is given by the following system of nonlinear differential equations:

$$\begin{cases}
\dot{S}_1(t) &= \Pi_1 + \omega_{v,1}V_1(t) + \omega_{n,1}R_1(t) - \lambda_1(t)S_1(t) - (\xi_{v,1} + \mu_1)S_1(t),\\
\dot{S}_2(t) &= \Pi_2 + \omega_{v,2}V_2(t) + \omega_{n,2}R_2(t) - \lambda_2(t)S_2(t) - (\xi_{v,2} + \mu_2)S_2(t),\\
\dot{V}_1(t) &= \xi_{v,1}S_1(t) - (1 - \epsilon_{v,1})\lambda_1(t)V_1(t) - (\omega_{v,1} + \mu_1)V_1(t),\\
\dot{V}_2(t) &= \xi_{v,2}S_2(t) - (1 - \epsilon_{v,2})\lambda_2(t)V_2(t) - (\omega_{v,2} + \mu_2)V_2(t),\\
\dot{E}_1(t) &= \lambda_1(t)S_1(t) + (1 - \epsilon_{v,1})\lambda_1(t)V_1(t) - (\sigma_1 + \mu_1)E_1(t),\\
\dot{E}_2(t) &= \lambda_2(t)S_2(t) + (1 - \epsilon_{v,2})\lambda_2(t)V_2(t) - (\sigma_2 + \mu_2)E_2(t),\\
\dot{P}_1(t) &= \sigma_1E_1(t) - (\psi_1 + \mu_1)P_1(t),\\
\dot{P}_2(t) &= \sigma_2E_2(t) - (\psi_2 + \mu_2)P_2(t),\\
\dot{I}_1(t) &= r_1\psi_1P_1(t) - (\varphi_1 + \gamma_{I,1} + \mu_1 + \delta_1)I_1(t),\\
\dot{I}_2(t) &= r_2\psi_2P_2(t) - (\varphi_2 + \gamma_{I,2} + \mu_2 + \delta_2)I_2(t),\\
\dot{A}_1(t) &= (1 - r_1)\psi_1P_1(t) - (\gamma_{A,1} + \mu_1)A_1(t),\\
\dot{A}_2(t) &= (1 - r_2)\psi_2P_2(t) - (\gamma_{A,2} + \mu_2)A_2(t),\\
\dot{H}_1(t) &= \varphi_1I_1(t) - (\gamma_{H,1} + \mu_1 + \delta_{H,1})H_1(t),\\
\dot{H}_2(t) &= \varphi_2I_2(t) - (\gamma_{H,2} + \mu_2 + \delta_{H,2})H_2(t),\\
\dot{R}_1(t) &= \gamma_{I,1}I_1(t) + \gamma_{A,1}A_1(t) + \gamma_{H,1}H_1(t) - (\omega_{n,1} + \mu_1)R_1(t),\\
\dot{R}_2(t) &= \gamma_{I,2}I_2(t) + \gamma_{A,2}A_2(t) + \gamma_{H,2}H_2(t) - (\omega_{n,2} + \mu_2)R_2(t),
\end{cases} \tag{4.1}$$

where λ_k is the *force of infection* for group k, and is given by (the parameters in the model (4.1) and the expression 4.2 are as defined in Table 2 with $k = \{1, 2\}$):

$$\lambda_k = \sum_{l=1}^{2} a_k c_{kl}\left[\frac{\beta_{P,l}P_l(t) + \beta_{I,l}I_l(t) + \beta_{A,l}A_l(t) + \beta_{H,l}H_l(t)}{N_l(t)}\right];\quad k = \{1, 2\}. \tag{4.2}$$

It can be shown (using the approach in Section 3.2.2) that the region:

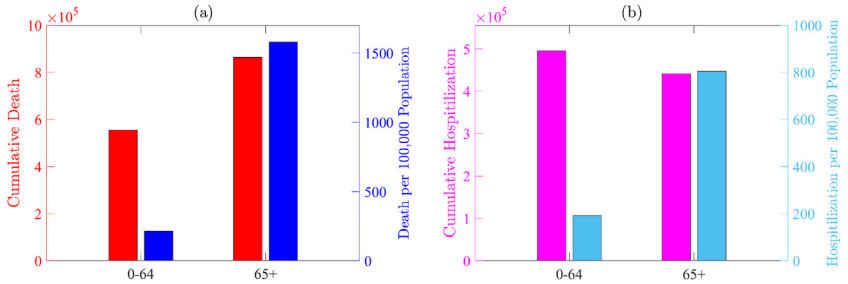

Fig. 8. Heterogeneity of COVID-19 burden by age groups, for individuals $0-64$ years of age and those that are 65 years of age and older, in the United States until August 26, 2023. (a) Cumulative COVID-19 mortality (cumulative deaths shown in red, while cumulative deaths *per* 100,000 shown in blue) and (b) cumulative COVID-19 hospitalization (cumulative hospitalization shown in magenta, while cumulative hospitalization *per* 100,000 is shown in cyan color). The mortality data (CDCa) used to generate this figure started in the first week of 2020, whereas the hospitalization data (CDCb) begins in the tenth week of 2020.

$$\Omega_2 = \left\{ \left(S_1, S_2, V_1, V_2, E_1, E_2, P_1, P_2, I_1, I_2, A_1, A_2, H_1, H_2, R_1, R_2 \right) \in \mathbb{R}_+^{16} : N_1(t) \leq \frac{\Pi_1}{\mu_2}, N_2(t) \leq \frac{\Pi_2}{\mu_2} \right\}, \tag{4.3}$$

is positively-invariant and attracting with respect to the two-group model (4.1). Thus, it is sufficient to study the dynamics of the model in Ω_2 (where it is well-posed mathematically and epidemiologically).

4.1. Contact matrix and parameterization for the two-group model

Before analyzing the qualitative dynamics of the two-group model, with respect to the existence and asymptotic stability of its equilibria, we will first discuss the derivation of the associated contact matrix as well as the values of the fixed and estimated parameters of the model, as follows.

4.1.1. Contact matrix

Using a large cross-sectional survey in eight European countries from 2005 to 2006 (as part of the EU-funded POLYMOD project (Improving public health policy in)), Mossong et al. (Mossong et al., 2008) showed that "contact patterns were highly assortative with age" (specifically, "schoolchildren and young adults, in particular, tended to mix with people of the same age"). Prem et al. (Prem et al., 2017) used the data from (Mossong et al., 2008), together with a Bayesian hierarchical model (using Markov chain Monte Carlo simulation), to estimate the age-and-location-specific contact patterns in 144 other countries across the globe, including the United States. Furthermore, the Prem et al. (Prem et al., 2017) study provided a 16×16 contact matrix that accounts for the general mixing patterns between sixteen age groups in the United States. Since our study considers two age-groups only (under 65 and 65 and older), we will use the data in the 16×16 contact matrix (given in Prem et al. (Prem et al., 2017)) and adapt it to the 2×2 contact matrix for the variable mixing patterns between our two age groups. Specifically, In order to accomplish this reduction, the total population of each of the 16 age groups will be used as a "weight", and weighted averages of the number of contacts made by individuals in this age group are computed and used to generate the entries of the reduced 2×2 contact matrix. This process is briefly described below.

Let $Q =$ denote the 16×16 contact matrix given in the Prem et al. (Prem et al., 2017) study, with the entries $q_{ij} (i, j = \{1, 2, \ldots, 16\})$ representing the number of contacts an individual in the age group i made with individuals in the age group j *per* day. The first 13 rows and columns of the matrix Q are related to age groups below 65 years of age (that is, individuals in the age range $0-64$), while the last three rows and columns are related to age groups 65 years and older. Let P_i be the total size of the population of individuals in the age group i. Let

$$N_1 = \sum_{k=1}^{13} P_k, \text{ and } \quad N_2 = \sum_{k=14}^{16} P_k,$$

represent, respectively, the total population of individuals under 65 years of age and the total population of individuals 65 years of age and older.

Hence, it follows that, the number of contacts *per* day made by an individual in group i with individuals under 65 years of age and those 65 years of age and older is given, respectively, by:

$$c_{i,u} = \sum_{l=1}^{13} q_{i,l} \text{ and } \quad c_{i,o} = \sum_{l=14}^{16} q_{i,l}.$$

Let the desired 2×2 matrix describing the number of contacts within and between the two age groups be given by E, where the entries e_{ij}, with $i \neq j$, represents the number of contacts *per* day an individual in age group i make with individuals in age group j, while $e_{ii}(i = \{1, 2\})$ represents the number of contacts *per* day an individual in age group i make with individuals in the same age group):

$$E = \begin{bmatrix} e_{11} & e_{12} \\ e_{21} & e_{22}. \end{bmatrix} \tag{4.4}$$

Using a weighted average, the number of contacts *per* day made by an individual under 65 years of age with other people under 65 years of age is given by:

$$e_{11} = \frac{\sum_{k=1}^{13} (c_{k,u} P_k)}{N_1}. \tag{4.5}$$

The number of contacts an individual 65 years of age and older makes with individuals under 65 years of age *per* day is given by:

$$e_{21} = \frac{\sum_{k=14}^{16} (c_{k,u} P_k)}{N_2}. \tag{4.6}$$

Since the total number of contacts made by all individuals under 65 years of age with those 65 years of age and older *per* day must equal the total number of contacts made by individuals 65 years of age and older with individuals under 65 years of age, the following conservation law of contacts must hold:

$$e_{12} N_1 = e_{21} N_2. \tag{4.7}$$

It follows from (4.7) that the number of contacts made by an individual under 65 with individuals 65 and older (e_{12}) is given by:

$$e_{12} = e_{21} \frac{N_2}{N_1}. \tag{4.8}$$

Finally, the number of contacts between individuals 65 years of age and older with other individuals in the same age group is given by:

$$e_{22} = \frac{\sum_{k=14}^{16} (c_{k,o} P_k)}{N_2}. \tag{4.9}$$

Thus, the four entries of the contact matrix E, given by 4.4, are given by the expressions in Equations (4.5), (4.6) and (4.8) and (4.9) (the matrix E is depicted in Fig. 9). It is evident from this matrix that individuals under 65 tend to mix with themselves more than with individuals 65 and older. Furthermore, individuals above 65 and older tend to mix more with individuals under 65 than themselves.

Finally, it is worth noting that the contact-related term $a_k c_{k,l}$ in the equation for the force of infection, λ, given by (4.2) (with a_k and $c_{k,l}$ as defined in Table 2) can be expressed in terms of the entries of the contact matrix E as:

$$a_k c_{kl} = e_{kl}, \quad k, l = \{1, 2\}. \tag{4.10}$$

Hence, Equation (4.10) allows for the computation of the force of infection, λ, using the entries of the age-stratified mixing matrix, E (4.4).

4.1.2. Estimated (fitted) and fixed parameters

In this section, the derivation of the values of the estimated (fitted) and fixed parameters of the two-group model (4.1) will be discussed.

(I) : Estimated (fitted) parameters of the two-group model

For convenience, we only fit the two-group model with the cumulative mortality data corresponding to wave C of the SARS-CoV-2 pandemic in the United States (and not data during previous waves A and B; we choose wave C for illustrative

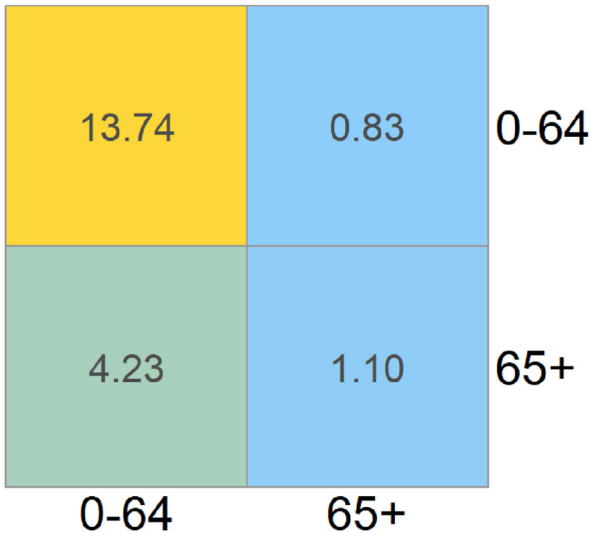

Fig. 9. Contact matrix accounting for the number of contacts made by individuals in Group 1 (age group 0–64 years of age) and Group 2 (age group 65 years of age and older) *per* day.

purposes). It should be recalled from Section 3.1 that we fitted six parameters for the homogeneous model (3.1), namely the disease-induced mortality rates (δ_I and δ_H) and the effective contact rates (β_P, β_I, β_A and β_H). For the two-group model (4.1), we will also fit the parameters related to the disease-induced mortality (i.e., $\delta_{I,1}$, $\delta_{I,2}$, $\delta_{H,1}$, and $\delta_{H,2}$) and those related to the effective contact rates. Since the effective contact rate parameters for the two-group model (4.1) are defined in terms of the product of the inter- and extra-group contact rates of individuals in the two age groups *per* day (a_1c_{11}, a_1c_{12}, a_2c_{21} and a_2c_{22}) and the probability of transmission *per* contact for the infectious compartments ($\mathcal{P}_{P,1}$, $\mathcal{P}_{P,2}$, $\mathcal{P}_{I,1}$, $\mathcal{P}_{I,2}$, $\mathcal{P}_{A,1}$, $\mathcal{P}_{A,2}$, $\mathcal{P}_{H,1}$ and $\mathcal{P}_{H,2}$), and the contact rates are known from the contact matrix E (Fig. 9), we only need to fit the aforementioned transmission probabilities. Furthermore, since it is reasonable to assume that no significant SARS-CoV-2 transmission (if at all) occurs in hospitals during wave C of the pandemic in the United States, the transmission probabilities $\mathcal{P}_{H,1}$ and $\mathcal{P}_{H,2}$ can be set to zero (it is worth recalling that the estimated value of the effective contact rate for SARS-CoV-2 transmission in hospital for the homogeneous model, given in Table 4, was very low. This justifies the assumption to set the transmission probabilities for SARS-CoV-2 in the hospital to zero for the two-group model). Furthermore, we make the simplifying assumption that the probability of transmission for pre-symptomatic and asymptomatic individuals, for both age groups, *per* contact is the same. That is, we assume $\tilde{\mathcal{P}} := \mathcal{P}_{P,1} = \mathcal{P}_{P,2} = \mathcal{P}_{A,1} = \mathcal{P}_{A,2}$ (hence, we only need to fit three transmission probabilities). Thus, in summary, we are fitting seven parameters of the two-group model (namely, $\delta_{I,1}$, $\delta_{I,2}$, $\delta_{H,1}$, $\delta_{H,2}$, $\tilde{\mathcal{P}}$, $\mathcal{P}_{I,1}$, and $\mathcal{P}_{I,2}$).

The two-group model (4.1) is used to fit the cumulative mortality of COVID-19 in the United States during wave C. The same data source (CSSE at Johns Hopkins University, 2020) and fitting procedure used for the homogeneous model (see Section 3.1.2 for details on the fitting of the homogeneous model to the data) are used here as well. Fig. 10(a) depicts the result obtained for fitting the two-group model with the cumulative mortality data for SARS-CoV-2 during wave C in the United States, and the estimated values of the seven fitted parameters are tabulated in Table 9. The goodness of fit of Fig. 10(a) is assessed by plotting the predicted daily mortality and the predicted 7-day rolling averages, against the observed daily SARS-CoV-2 mortality data and the observed 7-day rolling average data (shown in Fig. 10(b) and (c), respectively), showing a reasonably good fit, particularly the 7-day rolling average Fig. 10(c). In other words, Fig. 2 (b) and (c) and Fig. 10 (b) and (c) show, respectively, that the calibrated homogeneous and heterogeneous models predicted or captured the observed data (including the peaks) for the 7-day averages of the daily mortality better than that for the daily mortality (i.e., compare the blue curves and the data (red dots) in Figs. 2 and 10). The inability to accurately predict or capture the daily mortality data may be due to the prevailing delay in reporting of SARS-CoV-2 mortality over the weekend, during Wave C, in numerous jurisdictions across the United States (Bergman et al., 2020) (in fact, Bergman et al. (Bergman et al., 2020) noted that the process of adding previously unaccounted mortality data from weekends into the weekday mortality data can result in an increase in the reported mortality data during the weekdays). The values of the remaining parameters of the two-group model (known as the *fixed parameters*) will be obtained from the published literature and demographic (census) data, as described below.

(II) : Fixed parameters of the two-group model

It should also be mentioned that necessary adjustments in the values of the fixed parameters will be made to account for age-related heterogeneities (since the disease affects members of the two age groups differently). Data from the Census

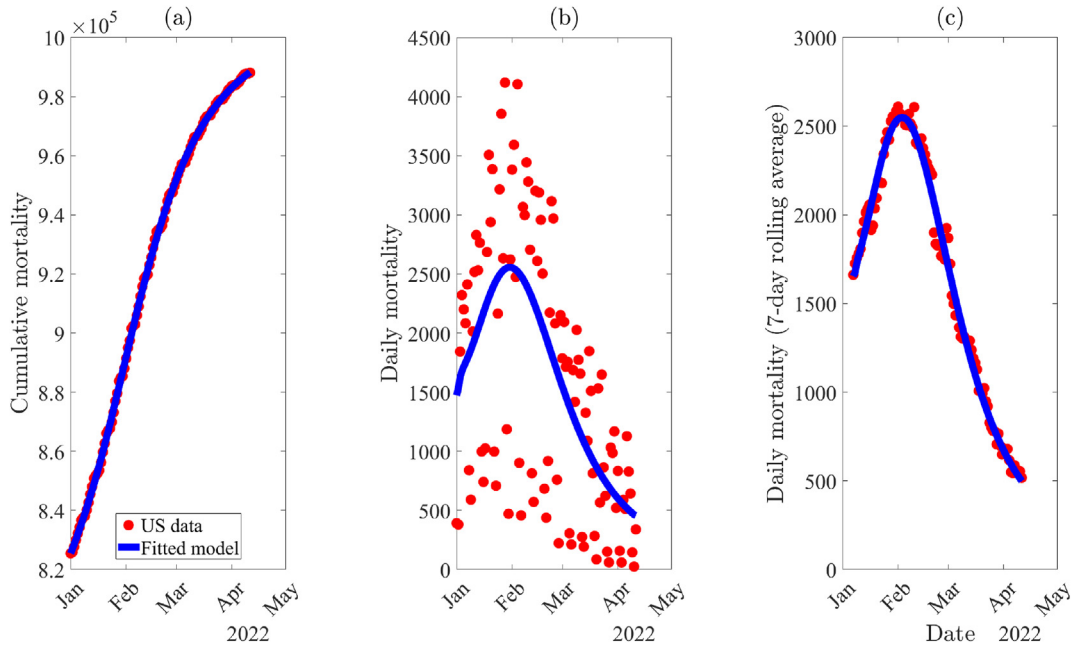

Fig. 10. (a) Time series illustrations of the least squares fit of the two-group model (4.1), showing the model's output for the cumulative COVID-19 mortality compared to the observed cumulative mortality for the United States during the time periods associated with Wave C. (b) The simulation result of the model (4.1), showing the daily COVID-19 mortality cases for the United States as a function of time, using the fixed (see Table 8) and estimated parameter (see Table 9) associated with Wave C. (c) The simulation result displaying seven-day rolling average of daily mortality for Wave C. Red dots indicate data points, while the solid blue line represents output from the model. The initial conditions used to generate this figure are given in Appendix A.

Bureau (The United States Census Bureau) for the year 2019 estimated the population of individuals in Group 1 (under 65) and Group 2 (65 and older) in the United States to be 257, 473, 015 (representing 82.45% of the total U.S. population) and 54, 792, 026 (which represents 17.55% of the U.S. population), respectively. It should be recalled that, for the homogeneous model (3.1), the recruitment rate in the population was $\Pi = 11,670$ *per* day. Hence, in order to be consistent with the homogeneous model, the recruitment rate of individuals into Group 1 (Π_1) and Group 2 (Π_2) is given by $\Pi_1 = 0.8245 \times \Pi = 9,622$ *per* day and $\Pi_2 = 0.1755 \times \Pi = 2,048$ *per* day. Current demographic data show that the average life expectancy of an individual in the United States is 78.8 years (Arias et al., 2020). Thus, it is reasonable to assume that, on average, individuals in Group 1 will live to be at least 64 years of age. Hence, the natural mortality rate of individuals in Group 1 (μ_1) is set to be $\mu_1 = 1/(64 \times 365)$ *per* day. On the other hand, data from the CDC shows that life expectancy at the age of 65 is 18.4 years (Kenneth et al., 2019). Consequently, the natural mortality rate for individuals in Group 2 (μ_2) is set at $\mu_2 = 1/(18.4 \times 365)$ *per* day.

The average duration from symptom onset to hospitalization (φ_1 and φ_2 for Group 1 and Group 2, respectively) can be estimated by computing the weighted average of the time delay reported between symptom onset to hospitalization for various age groups given in Table A2 of (Faes et al., 2020). For people under 65 years of age, the average duration is estimated to be 6.69 days (Faes et al., 2020). Consequently, the parameter φ_1 is set to $\varphi_1 = 1/6.69$ *per* day. Furthermore, the data in Table A2 of (Faes et al., 2020) show that the duration from the onset of symptoms to hospitalization for people 65 years of age or older is 3.78 days. Hence, the parameter φ_2 is set at $\varphi_2 = 1/3.78$ *per* day. Similarly, it follows from Table 2 of (Danielle Iuliano et al., 2022) that individuals under 65 stay in hospital for an average of 3.9 days. Thus, $\gamma_{H,1} = 1/3.9$ *per* day. Furthermore, these data show that people 65 and older stay in the hospital for approximately 6.2 days. Therefore, $\gamma_{H,2} = 1/6.2$ *per* day. Sah et al. (Sah et al., 2021) estimated that only 19.7% of infected individuals 60 years of age and older were asymptomatic. Consequently, we set the proportion of pre-symptomatic individuals in Group 2 who become asymptomatic at the end of the pre-symptomatic period (r_2) as $r_2 \approx 1 - 0.197 = 0.803$. Given that 60% of the population of infected individuals is symptomatic (recall that $r = 0.6$ in the homogeneous model (3.1)) and approximately 80% of the individuals in Group 2 are symptomatic (Sah et al., 2021), the proportion of pre-symptomatic individuals in Group 1 who become symptomatic at the end of the pre-symptomatic period (r_1) can be obtained from the relation:

$$r = r_1 \times \frac{\text{total population of Group 1}}{\text{total population of the United States}} + r_2 \times \frac{\text{total population of Group 2}}{\text{total population of the United States}},$$

so that:

Table 9
Table of estimated (fitted) parameters of the two-group heterogeneous model (4.1) generated by fitting the model with the observed cumulative mortality data for the United States during Waves C.

Parameter	Value
$\mathcal{P}_{P,1}$, $\mathcal{P}_{P,2}$, $\mathcal{P}_{A,1}$, $\mathcal{P}_{A,2}$	0.092 (dimensionless)
$\mathcal{P}_{I,1}$	0.062 (dimensionless)
$\mathcal{P}_{I,2}$	0.054 (dimensionless)
$\delta_{I,1}$	2.806×10^{-4} day^{-1}
$\delta_{I,2}$	2.836×10^{-4} day^{-1}
$\delta_{H,1}$	4.015×10^{-4} day^{-1}
$\delta_{H,2}$	5.281×10^{-4} day^{-1}

$$r_1 = \left(r - r_2 \times \frac{\text{total population of Group 2}}{\text{total population of the United States}}\right)\left(\frac{\text{total population of the United States}}{\text{total population of Group 1}}\right). \tag{4.11}$$

Substituting the values of the parameters and populations in Equation (4.11) gives $r_1 = 0.56$. The data (from the CDC (NCIRD, 2022)) used to estimate the complete vaccination rate (ξ_v) for the homogeneous model (3.1) are also used here to estimate the vaccination rates for the two-group model ($\xi_{v,1}$ and $\xi_{v,2}$). Using this data set and the approach in Section 3.1.1, it follows that $\xi_{v,1} = 0.000418$ *per* day and $\xi_{v,1} = 0.000102$ *per* day. The remaining fixed parameters of the two-group model (γ_I, γ_A, ω_v, ω_n, ε_v, σ, and ψ) are given the same values as in the homogeneous model (3.1) (see Section 3.1.1 for a detailed description of the fixed parameters of the homogeneous model and Table 8 for the values of the fixed parameters of the homogeneous model). The values of each of the fixed parameters for the two-group model (4.1) are given in Table 8.

4.2. Asymptotic stability of the DFE of the two-group model

The two-group model (4.1) has a unique disease-free equilibrium given by:

$$(S_1^*, S_2^*, V_1^*, V_2^*, E_1^*, E_2^*, P_1^*, P_2^*, A_1^*, A_2^*, I_1^*, I_2^*, H_1^*, H_2^*, R_1^*, R_2^*) = (S_1^*, S_2^*, V_1^*, V_2^*, 0, 0, 0, 0, 0, 0, 0, 0, 0, 0, 0, 0), \tag{4.12}$$

where,

$$S_k^* = \frac{\Pi_k(\omega_{v,k} + \mu_k)}{\mu_k(\omega_{v,k} + \mu_k + \xi_{v,k})} \quad \text{and} \quad V_k^* = \frac{\Pi_k \xi_{v,k}}{\mu_k(\omega_{v,k} + \mu_k + \xi_{v,k})}, \text{ with } k = \{1, 2\}.$$

The asymptotic stability of the DFE will be explored using the next generation operator method (Diekmann et al., 1990; Pauline van den Driessche & Watmough, 2002)(as in Section 3.2). Following Elbasha and Gumel (Elamin H Elbasha and Abba B Gumel, 2021), we make the simplifying assumption that the population in each of the two groups (N_k, with $k = \{1, 2\}$) has reached an equilibrium state. That is, we assume that:

$$N_k^* = N_k(0) = \frac{\Pi_k}{\mu_k}, \quad k = \{1, 2\}.$$

Furthermore, following Elbasha and Gumel (Elamin H Elbasha and Abba B Gumel, 2021), it is convenient to express the proportion of vaccinated individuals in group k (with respect to the total population), denoted by v_k^*. That is,

$$v_k^* = \frac{V_k^*}{N_1^* + N_2^*} = \frac{N_k^*}{N_1^* + N_2^*} \times \frac{V_k^*}{N_k^*} = n_k^* \times \frac{\xi_{v,k}}{\omega_{v,k} + \mu_k + \xi_{v,k}}, \ k = \{1, 2\} \tag{4.13}$$

where,

$$n_k^* = \frac{N_k^*}{N_1^* + N_2^*} \tag{4.14}$$

is the fraction of individuals in group k.

The derivation of the vaccination reproduction number of the two-group model (denoted by $\mathcal{R}_v^\dagger$), using the next generation operator method, is presented in Appendix H. It follows from Equation H.1 that the vaccination reproduction number for the two-group model (4.1) is given by

$$\mathcal{R}_v^\dagger = \frac{1}{2}\left(\Delta_1 + \sqrt{\Delta_1^2 - 4\Delta_2}\right), \tag{4.15}$$

where,

$$\begin{aligned} \Delta_1 &= (1-\nu_1^*\epsilon_{v,1})\mathcal{R}_{11}^\dagger + (1-\nu_2^*\epsilon_{v,2})\mathcal{R}_{22}^\dagger, \\ \Delta_2 &= (1-\nu_1^*\epsilon_{v,1})(1-\nu_2^*\epsilon_{v,2})(\mathcal{R}_{12}^\dagger\mathcal{R}_{21}^\dagger - \mathcal{R}_{11}^\dagger\mathcal{R}_{22}^\dagger), \end{aligned} \tag{4.16}$$

with $\mathcal{R}_{11}^\dagger$, $\mathcal{R}_{12}^\dagger$, $\mathcal{R}_{21}^\dagger$, and $\mathcal{R}_{22}^\dagger$ defined by

$$\mathcal{R}_{kl}^\dagger = \mathcal{R}_{kl,P}^\dagger + \mathcal{R}_{kl,I}^\dagger + \mathcal{R}_{kl,A}^\dagger + \mathcal{R}_{kl,H}^\dagger, \quad k,l = \{1,2\}, \tag{4.17}$$

where,

$$\begin{aligned} \mathcal{R}_{kl,P}^\dagger &= a_k c_{kl}\beta_{k,P}\frac{\sigma_l}{(\sigma_l+\mu_l)(\psi_l+\mu_l)}, \\ \mathcal{R}_{kl,I}^\dagger &= a_k c_{kl}\beta_{k,I}\frac{\sigma_l r_l\psi_l}{(\sigma_l+\mu_l)(\psi_l+\mu_l)(\varphi_l+\gamma_{l,I}+\delta_{l,I}+\mu_l)}, \\ \mathcal{R}_{kl,A}^\dagger &= a_k c_{kl}\beta_{k,A}\frac{\sigma_l(1-r_l)\psi_l}{(\sigma_l+\mu_l)(\psi_l+\mu_l)(\gamma_A+\mu)}, \\ \mathcal{R}_{kl,H}^\dagger &= a_k c_{kl}\beta_{k,H}\frac{\sigma_l r\psi_l\varphi_l}{(\sigma_l+\mu_l)(\psi_l+\mu_l)(\varphi_l+\gamma_{l,I}+\delta_{l,I}+\mu_l)(\gamma_{l,H}+\delta_{l,H}+\mu_l)}. \end{aligned} \tag{4.18}$$

The quantity $\mathcal{R}_{kl}^\dagger$, defined in (4.17), is the *constituent reproduction number* associated with disease transmission by individuals in group k to those in group l, while the quantities $\mathcal{R}_{kl,P}^\dagger$, $\mathcal{R}_{kl,I}^\dagger$, $\mathcal{R}_{kl,A}^\dagger$, and $\mathcal{R}_{kl,H}^\dagger$, given in (4.18), represent the constituent reproduction numbers associated with disease transmission between groups k and l by infectious individuals in the P, I, A and H compartments.

The result below follows from Theorem 2 of (Pauline van den Driessche & Watmough, 2002).

Theorem 4.1. *The disease-free equilibrium, given by* (4.12)*, of the two-group model* (4.1) *is locally-asymptotically stable (LAS) in* Ω_2 *whenever* $\mathcal{R}_v^\dagger < 1$*, and unstable if* $\mathcal{R}_v^\dagger > 1$.

Using Equation (4.15), the vaccination reproduction number for the two-group model (4.1) during Wave C is calculated to be 3.72.

It should be mentioned that the *basic reproduction number* ($\mathcal{R}_0$) associated with the two-group model (4.1) can be obtained by setting the vaccination-related parameters in Equation (4.15) to zero (i.e., $\nu_1^* = \nu_2^* = 0$) (Elamin H Elbasha and Abba B Gumel, 2021):

$$\mathcal{R}_0^\dagger = \frac{1}{2}\left[\mathcal{R}_{11}^\dagger + \mathcal{R}_{22}^\dagger + \sqrt{\left(\mathcal{R}_{11}^\dagger + \mathcal{R}_{22}^\dagger\right)^2 - 4\mathcal{R}_{12}^\dagger\mathcal{R}_{21}^\dagger}\right]. \tag{4.19}$$

The local asymptotic stability result (Theorem 4.1) can be extended to global asymptotic stability for a special case of the two-group model, as follows. Consider a special case of the two-group model (4.1) with negligible disease-induced mortality (i.e., set $\delta_{I,1} = \delta_{I,2} = \delta_{H,1} = \delta_{H,2} = 0$). Using the approach in Section 3.2.2, it can be shown that the feasible region is positively-invariant with respect to the flow generated by the two-group model (4.1), and attracts all solutions of the model that reside in the region Ω_2. It is convenient to define $\mathcal{R}_v^\Delta = \mathcal{R}_v^\dagger|_{\delta_{I,k}=\delta_{H,k}=0}$ (with $k = \{1,2\}$), the reproduction number of the special case of the two-group model (4.1) with $\delta_{I,k} = \delta_{H,k} = 0$ (with $k = \{1,2\}$). We claim the following result.

$$\Omega_2^\Delta = \left\{\left(S_1,S_2,V_1,V_2,E_1,E_2,P_1,P_2,I_1,I_2,A_1,A_2,H_1,H_2,R_1,R_2\right) \in \mathbb{R}_+^{16} : S_1 < S_1^*, S_2 < S_2^*, V_1 < V_1^*, V_2 < V_2^*\right\},$$

Theorem 4.2. *The disease-free equilibrium of the special case of the two-group model* (4.1) *with negligible disease-induced mortality (i.e.,* $\delta_{I,k} = \delta_{H,k} = 0$*, with* $k = \{1,2\}$*), given by* (4.12)*, is globally-asymptotically stable in* Ω_2^Δ *whenever* $\mathcal{R}_v^\Delta < 1$.

The proof of Theorem 3.3, based on using a comparison theorem (Lakshmikantham et al., 1989), is given in Appendix I. Like in the case of Theorem 3.3 for the special case of the homogeneous model without disease-induced mortality, the epidemiological implication of Theorem 4.2 is that, for the special case of the two-group model without disease-induced mortality, bringing (and maintaining) the reproduction threshold ($\mathcal{R}_v^\Delta$) to a value less than one is necessary and sufficient for the elimination of the pandemic in the population. Therefore, this result shows that the implementation of a vaccination program

that can bring (and maintain) the reproduction threshold, $\mathcal{R}_v^{\Delta}$, to a value below one will lead to the elimination of the pandemic in the United States.

Owing to the assortative mixing pattern shown by the data used to generate Fig. 9, it can be seen, using the expressions for the constituent reproduction numbers (4.17), that the transmission of COVID-19 occurs more due to mixing within each group than mixing between groups. That is, the following inequality holds (as a natural consequence of the assortative mixing in favor of within-group mixing):

$$\mathcal{R}_{11}^{\dagger}\mathcal{R}_{22}^{\dagger} > \mathcal{R}_{12}^{\dagger}\mathcal{R}_{21}^{\dagger}.$$

It should also be noted from Equations (4.17) and (4.18) that the mixing terms (a_k and c_{kl}) determine the sign of the expression of $\mathcal{R}_{11}^{\dagger}\mathcal{R}_{22}^{\dagger} - \mathcal{R}_{12}^{\dagger}\mathcal{R}_{21}^{\dagger}$. Specifically, as shown by Elbasha and Gumel (Elamin H Elbasha and Abba B Gumel, 2021),

$$\text{sign}(\mathcal{R}_{11}^{\dagger}\mathcal{R}_{22}^{\dagger} - \mathcal{R}_{12}^{\dagger}\mathcal{R}_{21}^{\dagger}) = \text{sign}(a_1c_{11}a_2c_{22} - a_1c_{12}a_2c_{21}), \tag{4.20}$$

from which, using (4.10), it follows that

$$\text{sign}(\mathcal{R}_{11}^{\dagger}\mathcal{R}_{22}^{\dagger} - \mathcal{R}_{12}^{\dagger}\mathcal{R}_{21}^{\dagger}) = \text{sign}(e_{11}e_{12} - e_{12}e_{21}). \tag{4.21}$$

Thus, the entries of the mixing matrix (Fig. 9) determine the biased assortative nature of the mixing patterns (in favor of within-group mixing) in the population.

4.3. Vaccine-derived herd immunity threshold for the two-group model

In this section, the result of Theorem 4.2 will be used to compute an expression for the vaccine-derived herd immunity threshold (HIT) needed to eliminate the pandemic using the two-group model. The objective is to determine whether the level of vaccine-derived HIT obtained using the two-group model differs from the HIT value obtained for the homogeneous model (given in Section 3.3.1). The approach here follows closely the approach introduced by Elbasha and Gumel (Elamin H Elbasha and Abba B Gumel, 2021). Specifically, in order to compute the HIT for the two-group model, it is convenient to re-write the proportion of vaccinated individuals at steady-state as (Elamin H Elbasha and Abba B Gumel, 2021):

$$\frac{V_1^* + V_2^*}{N_1^* + N_2^*} = \left(\frac{N_1^*}{N_1^* + N_2^*}\right)\frac{V_1^*}{N_1^*} + \left(\frac{N_2^*}{N_1^* + N_2^*}\right)\frac{V_2^*}{N_2^*} = n_1^*\nu_1^* + n_2^*\nu_2^*, \tag{4.22}$$

where n_k^* and ν_k^* are defined by Equations (4.14) and (4.13), respectively. Hence, following Elbasha and Gumel (Elamin H Elbasha and Abba B Gumel, 2021), the computation of the vaccine-derived HIT for the two-group model (4.1) entails solving the following optimization problem (Elamin H Elbasha and Abba B Gumel, 2021):

$$\text{minimize}(n_1^*\nu_1^* + n_2^*\nu_2^*) \quad \text{subject to,} \quad 0 \le \nu_1^*, \nu_2^* \le 1, \mathcal{R}_v^{\dagger} \le 1. \tag{4.23}$$

Since individuals in each of the two age groups continued to receive SARS-CoV-2 vaccines in the United States during wave C of the pandemic (i.e., $0 \le \nu_1^*, \nu_2^* \le 1$), and considering the fact that contact matrix 9 produces biased assortative mixing (i.e., $\mathcal{R}_{11}^{\dagger}\mathcal{R}_{22}^{\dagger} > \mathcal{R}_{12}^{\dagger}\mathcal{R}_{21}^{\dagger}$), the HIT for Wave C is given by (the derivation of this expression is given in (Elamin H Elbasha and Abba B Gumel, 2021), and not repeated here):

$$n_1^*\nu_1^* + n_2^*\nu_2^* = \frac{\epsilon_1 n_2^*(\mathcal{R}_{11}^{\dagger} + \mathcal{R}_{12}^{\dagger}\mathcal{R}_{21}^{\dagger} - \mathcal{R}_{22}^{\dagger}\mathcal{R}_{11}^{\dagger}) + \epsilon_2 n_1^*(\mathcal{R}_{22}^{\dagger} + \mathcal{R}_{12}^{\dagger}\mathcal{R}_{21}^{\dagger} - \mathcal{R}_{22}^{\dagger}\mathcal{R}_{11}^{\dagger}) - 2\sqrt{\epsilon_1 n_2^*\epsilon_2 n_1^*\mathcal{R}_{12}^{\dagger}\mathcal{R}_{21}^{\dagger}}}{\epsilon_1\epsilon_2(\mathcal{R}_{12}^{\dagger}\mathcal{R}_{21}^{\dagger} - \mathcal{R}_{11}^{\dagger}\mathcal{R}_{22}^{\dagger})}. \tag{4.24}$$

Substituting the values of constituent reproduction numbers ($\mathcal{R}_{11}^{\dagger}$, $\mathcal{R}_{12}^{\dagger}$, $\mathcal{R}_{21}^{\dagger}$ and $\mathcal{R}_{22}^{\dagger}$), vaccine efficacy ($\varepsilon_1$ and ε_2) and the fraction of the total population that belongs to a group (n_1^* and n_2^*) into the right-hand side of Equation (4.24) shows that the value of HIT for the two-group model is $n_1^*\nu_1^* + n_2^*\nu_2^* = 0.61$. That is, the computation in this section shows that, using the two-group model (4.1), vaccine-derived herd immunity can be achieved in the United States if at least 61% of the population is fully vaccinated. It should be recalled that, for the homogeneous model (3.1), it was shown that vaccine-derived herd immunity could not be achieved during Wave C even if all unvaccinated susceptible individuals were fully vaccinated during that wave. Thus, this study shows that adding age-related heterogeneity into a homogeneous model for SARS-CoV-2 pandemic that includes a vaccination significantly reduces the vaccination coverage needed to eliminate the disease. This result is consistent with (Elamin H Elbasha and Abba B Gumel, 2021) where it was theoretically shown that the value of the herd immunity threshold obtained using the (two-group) heterogeneous model was smaller than that obtained using the (one-group) homogeneous model.

5. Discussion and conclusions

The novel pneumonia-like illness that emerged late in December 2019 (COVID-19, caused by SARS-CoV-2) became the most devastating public health and socio-economic challenge humans have faced since the 1918 influenza pandemic (Morens & Fauci, 2007; Ngonghala, Iboi, Eikenberry, et al., 2020; Samuel Faust et al., 2020). The SARS-CoV-2 pandemic, which caused over 700 million confirmed cases and nearly 7 million deaths globally (World Health Organization), affected different segments of society differently. For example, healthcare professionals, grocery store workers, public transport workers, law enforcement and other emergency public service providers, retail workers, the elderly, residential care residents and workers, were more vulnerable to acquire SARS-CoV-2 infection than other members of the public (Chen et al., 2021, 2022; Ing et al., 2020; Iyengar et al., 2020; Matz et al., 2022; Mutambudzi et al., 2021). Furthermore, individuals with underlying health conditions (such as diabetes and hypertension), in comparison to individuals without such co-morbidities, are more vulnerable against SARS-CoV-2 (Callender et al., 2020; Djaharuddin et al., 2021; Omame et al., 2021; Sanyaolu et al., 2020; Wang et al., 2020). Although the elderly population (i.e., people 65 years of age and older) had higher vaccine acceptance (Jeffrey et al., 2021), they suffered the brunt of the SARS-CoV-2 burden (for instance, despite representing less than 20% of the total population, the elderly accounted for 47.10% of hospitalizations and 60.92% of deaths in the United States (CDCa; CDCb)). This study is based on using mathematical modeling approaches, together with data analytics and computation, to unravel the combined population-level impacts of the disproportionate effect of the SARS-CoV-2 pandemic on the elderly (i.e., age heterogeneity and associated mixing patterns), which represents the highest risk group (Applegate & Ouslander, 2020), and vaccination on the transmission dynamics and control of the SARS-CoV-2 pandemic in the United States.

The objective of this study was achieved via the design of a generalized multigroup mathematical model, which takes the form of a deterministic system of nonlinear differential equations for the temporal dynamics of the disease within a population with m heterogeneous subgroups (the m heterogeneous sub-populations could represent various heterogeneities, such as heterogeneities with respect to age, risk of acquiring infection, mixing patterns, socioeconomic status etc.). The m-group model was shown to be well-posed mathematically and epidemiologically, by rigorously establishing the non-negativity, boundedness and invariance of its solutions. A special case of the model with homogeneous mixing (i.e., the model with $m = 1$) was considered first of all. The disease-free equilibrium of this (*homogeneous*) model was shown to be locally-asymptotically stable whenever a certain epidemiological threshold, known as the *vaccination reproduction number*, is less than one. The implication of this result is that the vaccination program implemented in the United States could lead to the elimination of the pandemic if the reproduction number could be brought to (and maintained at) a value less than one, provided the initial number of infected individuals is small enough. This result was extended to the global asymptotic stability of the disease-free equilibrium for two special cases (one where the vaccines used offer perfect protection against the acquisition of SARS-CoV-2 infection, and another where the disease-induced mortality is negligible). The epidemiological implication of this global asymptotic stability of the disease-free equilibrium is that bringing the vaccination reproduction number less than the proportion of wholly-susceptible individuals at the disease-free steady-state (which is less than one) is necessary and sufficient for the elimination of the pandemic, regardless of the initial sizes of the sub-populations of the model. This result is in line with the results presented in models for SARS-CoV-2 pandemic that incorporate an imperfect vaccine, such as those in (Gumel, 2012; Gumel, Iboi, Ngonghala, & Elbasha, 2021). For the case where the vaccination reproduction number exceeds the value one, the homogeneous model has a unique endemic equilibrium which was shown, using a Krasnasolskii sub-linearity approach, to be locally-asymptotically stable when it exists. This equilibrium was shown to be globally-asymptotically stable, using a nonlinear Lyapunov function of Goh-Volterra type. The implication of these results is that, for the case where the vaccination reproduction number exceeds one, the vaccination program implemented (despite its ability to decrease disease burden) will fail to lead to the elimination of the pandemic. In such a case, the vaccination program needs to be supplemented with other control and mitigation programs, such as mask usage and social-distancing.

The homogeneous model was fitted using the observed cumulative mortality data for the United States during three waves of the pandemic. The three waves (denoted Wave A, B and C) correspond to the time periods when the pandemic was mostly dominated by the Alpha, Delta and Omicron variants, respectively. The calibrated model was used to estimate the unknown parameters of the homogeneous model and to compute the level of vaccine-derived herd immunity threshold needed to eliminate the pandemic. Our simulations showed that, for the one-group homogeneous model, vaccine-derived herd immunity cannot be achieved during Wave C even if all the unvaccinated susceptible individuals in the population are fully vaccinated during Wave C. We conducted a detailed global sensitivity analysis to determine the parameters of the model that have the highest impact on the vaccination reproduction number (hence, the burden of the pandemic). A number of parameters (such as parameters related to asymptomatically-infectious individuals) were identified as the most influential in driving the disease dynamics during the three waves considered in this study. We used these parameters to suggest the most effective control and mitigation interventions to be implemented during each of the three waves of the pandemic. Our study shows that some interventions that may be very effective during one of the three waves may not always be as effective during the other wave or waves. However, we showed that interventions related to targeting asymptomatic infectious individuals is always very effective across the three waves. Therefore, another novel finding in this study is that strategies that focus on rapidly detecting and isolating asymptomatic infectious individuals (such as wide-scale random testing, rapid detection, and contact tracing of contacts of identified asymptomatic individuals) will be very effective in controlling and mitigating the spread of respiratory pathogens, such as SARS-CoV-2, where asymptomatic transmission is a major feature of its transmission dynamics.

To account for the disproportionate effect of SARS-CoV-2 on the elderly, we considered another special case of the generalized m-group model where the total population of the United States is stratified into two sub-groups of individuals under 65 years of age (Group 1) and those that are 65 and older (Group 2). The resulting two-group model (i.e., the heterogeneous model with $m = 2$) was rigorously analysed and fitted with the cumulative mortality data for Wave C (as in the case of the aforementioned homogeneous model). The main objective is to determine whether age heterogeneity (together with the associated variability in mixing patterns by age) affects the size of the vaccination coverage needed to achieve vaccine-derived herd immunity in the United States (in comparison to the case where the model assumes a homogeneous population). Our results showed that, for the two-group model, vaccine-derived herd immunity can be achieved in the United States during wave C of the pandemic (for example) if at least 61% of the population is fully vaccinated. Thus, this study shows that adding age heterogeneity to a vaccination model for SARS-CoV-2 that assumes a homogeneous population dramatically decreases the size of the herd immunity threshold needed to eliminate the pandemic (it should be recalled that, for the case where the homogeneous model was used, such vaccine-derived herd immunity was not attainable during Wave C even if all unvaccinated susceptible members of the community are fully vaccinated). Thus, adding the realism of the well-known heterogeneities associated with the SARS-CoV-2 pandemic makes the likelihood of its elimination using a vaccine more realistically achievable (because it requires vaccination coverage that can perhaps be readily and realistically achieved). This finding strongly supports the study by Britton et al. (Britton et al., 2020) (which shows, via numerical simulations, that the herd immunity threshold obtained through a heterogeneous model is "substantially less" than one obtained through a homogeneous model) and the theoretical study by Elbasha and Gumel (Elamin H Elbasha and Abba B Gumel, 2021) (which used a geometric approach to rigorously show that the herd immunity threshold of a vaccination model for an infectious disease that uses heterogeneous populations is lower than that of an equivalent model with a homogeneous population).

This study has some limitations. For instance, one of the main assumptions made in the formulation of the $k-$ group heterogeneous model is that only unvaccinated susceptible individuals are vaccinated (i.e., recovered and asymptomatic infected individuals are not vaccinated). Furthermore, the SARS-CoV-2 vaccines considered in this study are assumed to only offer preventive efficacy against the acquisition infection and offer no therapeutic benefits with regards to slowing disease progression, severity, hospitalization and mortality (the SARS-CoV-2 vaccines have been shown to reduce the duration of infection (CDC, 2021; Emilia Paladino et al., 2021), the likelihood of hospitalization (Lopez Bernal, Andrews, Gower, Robertson, et al., 2021; Moline et al., 2021; Rahmani et al., 2022) and disease-induced mortality (Lopez Bernal, Andrews, Gower, Robertson, et al., 2021; Rahmani et al., 2022)).

In summary, in addition to highlighting the importance of adding heterogeneities to mathematical models for the transmission dynamics and control of diseases such as SARS-CoV-2 and showing that control and mitigation strategies that are very effective during one wave may not always be very effective during other waves, this study shows that the prospect for the elimination of SARS-CoV-2 using a vaccination program is highly promising, provided the coverage level is high enough to achieve herd immunity (adding heterogeneity reduces the coverage level of the herd immunity threshold needed to achieve herd immunity; hence, makes the elimination of the pandemic more likely).

Acknowledgments

ABG acknowledges the support, in part, of the National Science Foundation (Grant Number: DMS-2052363; transferred to DMS-2330801). The authors are grateful to the anonymous reviewers for their very constructive comments.

CRediT authorship contribution statement

Binod Pant: Writing – review & editing, Writing – original draft, Visualization, Validation, Software, Methodology, Investigation, Formal analysis, Data curation, Conceptualization. **Abba B. Gumel:** Writing – review & editing, Visualization, Validation, Supervision, Project administration, Methodology, Investigation, Funding acquisition, Formal analysis, Conceptualization.

Declaration of competing interest

None.

Appendix. A Initial Conditions for the Models

A.1Homogeneous Model

The initial conditions for the state variables of the homogeneous model (3.1), corresponding to Waves A, B and C, are given in Table A1.

A.2 Two-group Model (During Wave C)

For the two-group model (4.1), the initial conditions for the state variables for individuals in Group 1 (i.e., individuals 64 years and younger) during Wave C is denoted by X_{01}, where:

$$X_{01} = (S_{01}, V_{01}, P_{01}, I_{01}, A_{01}, H_{01}, R_{01}), \tag{A.1}$$

with,

$$\begin{aligned} S_{01} &= 54,168,536, V_{01} = 76,784,154, E_{01} = 73,596, P_{01} = 366,386, \\ I_{01} &= 4,126,977, A_{01} = 3,558,881, H_{01} = 42,140 \text{ and } R_{01} = 118,643,401. \end{aligned} \tag{A.2}$$

Similarly, the initial conditions for the state variables for individuals in Group 2 (i.e., individuals 65 and older), denoted by X_{02}, are computed from the relation:

$$X_{02} = X_0 - X_{01}, \quad \text{where} \quad X_i = \{S_i, V_i, E_i, P_i, I_i, A_i, H_i, R_i\}, \ \text{with } i = \{0, 01\}, \tag{A.3}$$

where X_0 is the vector of the initial conditions for the state variables of the homogeneous model (given in Table A1) and X_{01} is the set of the initial conditions for the state variables of the individuals in Group 1 (as given in (A.1)).

Table A.1
The initial conditions of the state variables of the homogeneous model (3.1) used to generate Fig. 2 (obtained by fitting the homogeneous model with the observed cumulative mortality data for the United States during Waves A, B, and C). The initial value of the susceptible population (S_0) was obtained by subtracting the initial values of remaining state variables of the homogeneous model (V_0, E_0, P_0, I_0, A_0, H_0 and R_0) and the observed cumulative mortality (recorded at the beginning of each of the three waves) from the total population of the United States (331.69 million (The United States Census Bureau)). The initial conditions for the hospitalized individuals and the cumulative mortality (at the beginning of each of the three waves) are obtained from data (CSSE at Johns Hopkins University, 2020; NCIRD, 2022).

Initial Condition	Value		
	Wave A	Wave B	Wave C
S_0	327,433,290	155,108,886	73,443,709
V_0	0	54,250,695	100,070,766
E_0	800, 109	300, 105	97, 860
P_0	800, 032	400, 302	388, 859
I_0	1, 091, 821	1, 293, 500	4, 169, 424
A_0	311, 949	748, 501	3, 586, 032
H_0	32, 604	14, 085	84, 281
R_0	1, 009, 051	118, 974, 149	149, 030, 355

A.3 Profiles of Susceptible and Recovered Individuals for Model (3.1)

Fig. 11 depicts the time-series profile of the susceptible and recovered individuals generated using the homogeneous model (3.1) during Waves A, B and C of the SARS-CoV-2 in the United States. The figure was generated by simulating the homogeneous model (3.1) with the baseline values of the parameters in Tables 3 and 4 and the initial conditions given in Table A1.

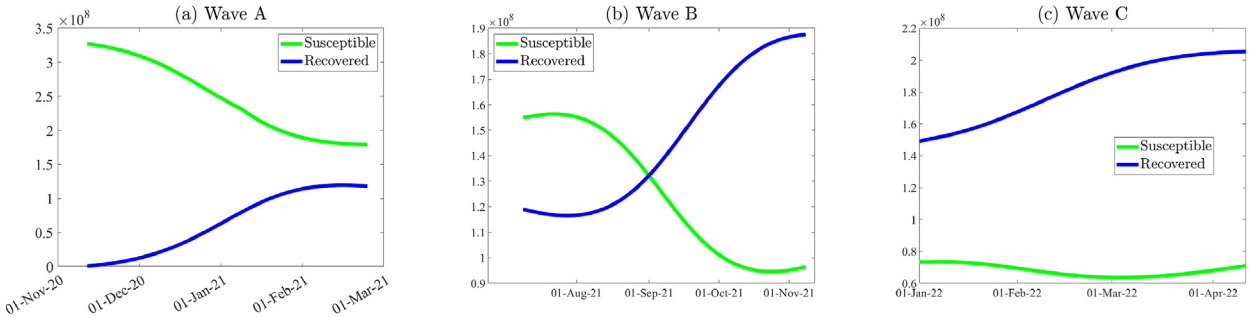

Fig. 11. Time-series of populations of susceptible (green curve) and recovered (blue curve) individuals during Waves A, B, and C, as functions of time, generated by simulating the homogeneous model (3.1) using the baseline values of the parameters in Tables 3 and 4 and the initial conditions given in Table A1. (a) Wave A, (b) Wave B and (c) Wave C.

B Effective Reproduction Number For the Homogeneous Model During Each Wave

The effective reproduction number (also known as *time-varying reproduction number* (Gumel, Iboi, Ngonghala, & Elbasha, 2021)), denoted by $\mathcal{R}_e(t)$, is the average number of new infections generated by a typical infected individual at any given time t. In the absence of vaccination, the effective reproduction number for the homogeneous model (3.1), denoted by $\mathcal{R}_{e0}(t)$, is given by (Ngonghala, Iboi, Eikenberry, et al., 2020; Nishiura & Chowell, 2009):

$$\mathcal{R}_{e0}(t) = (\mathcal{R}_0)\left(\frac{S(t)}{N(t)}\right), \tag{B.1}$$

where $\mathcal{R}_0$ is defined by (3.14). Similarly, in the presence of vaccination, it follows, from (Kim et al., 2022; Zhao, Musa, et al., 2020) and Equations (3.11) and (3.12), that the effective reproduction number, denoted by $\mathcal{R}_{ev}(t)$, for the homogeneous model (3.1) is given by (where the basic reproduction number, $\mathcal{R}_0$, is given by (3.14)):

$$\mathcal{R}_{ev}(t) = (\mathcal{R}_0)\left(\frac{S(t) + (1-\epsilon_v)V(t)}{N(t)}\right). \tag{B.2}$$

The time profile of the effective reproduction number and the prevalence of the disease during Waves A, B, and C is depicted in Fig. 12. Sustained SARS-CoV-2 transmission occurs when the effective reproduction number ($\mathcal{R}_{e0}(t)$ or $\mathcal{R}_{ev}(t)$) exceeds one, and declines when the effective reproduction number is less than one. Additionally, disease prevalence peaks, for each of the three waves, when the effective reproduction equals one.

For Wave A, which runs from October 15, 2020, to April 5, 2021, it should be noted that there are no individuals in the fully-vaccinated compartment until January 3, 2021. Hence, the effective reproduction number ($\mathcal{R}_e(t)$) for Fig. 12(a) is given by the following piece-wise function (depicted by the blue curve in Fig. 12(a)):

$$\mathcal{R}_e(t) = \begin{cases} \mathcal{R}_{e0}(t) & \text{for } t \in [\text{October } 15,\ 2020 \text{ to January } 3,\ 2021], \\ \mathcal{R}_{ev}(t) & \text{for } t \in [\text{January } 4,\ 2021 \text{ to April } 5,\ 2021]. \end{cases} \tag{B.3}$$

Fig. 12(b) and (c) are generated using the effective reproduction number $\mathcal{R}_{ev}(t)$.

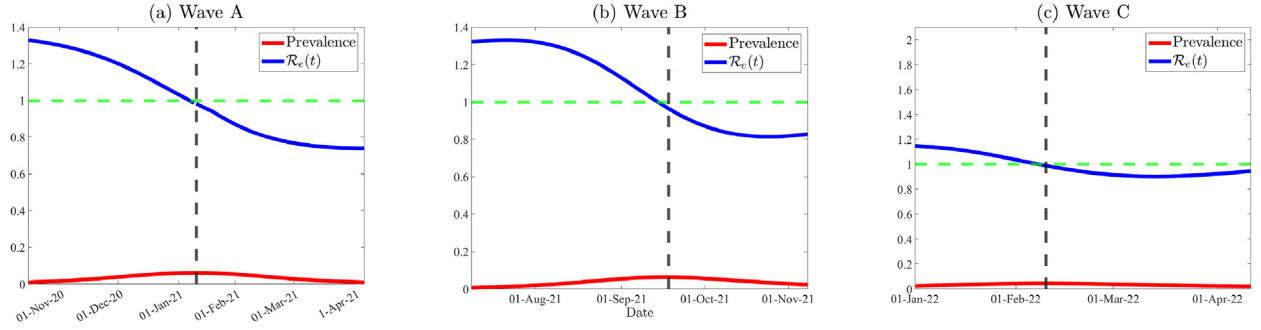

Fig. 12. Profiles of the effective reproduction numbers ($\mathcal{R}_{e0}(t)$ or $\mathcal{R}_{ev}(t)$) of the homogeneous model (blue curve) and disease prevalence (red curve). Panels (a), (b) and (c) depict the profiles for Waves A, B, and C, respectively. The effective reproduction number associated with Wave A is represented as a piece-wise function, given by Equation (B.3), to account for the fact that vaccination against SARS-CoV-2 did not start until middle to late December 2020; hence there were no fully vaccinated individuals at the beginning of Wave A. The effective reproduction for Wave A was computed using $\mathcal{R}_{e0}(t)$ during the period from October 15, 2020 to January 3, 2021, and using $\mathcal{R}_{ev}(t)$ for the period from January 4, 2021 until the end of Wave A. In other words, Fig. 12(a) was obtained by using Equation (B.1) for the period from October 15, 2020 to January 3, 2021 (shown by the left lower-right segment to the left of the vertical dashed lines), and Equation (B.2) for the remaining period from January 4, 2021 to the end of the first wave, as well as for Waves B and C (shown in Figures (b) and (c). The dashed vertical black line represents the day peak prevalence is attained. Dashed horizontal green line depicts when the effective reproduction number ($\mathcal{R}_{e0}(t)$ or $\mathcal{R}_{ev}(t)$ equals one).

C Proof of Theorem 3.2

Proof. Consider the homogeneous model (3.1) with a perfect vaccine (i.e., $\varepsilon_v = 1$). Let $\tilde{\mathcal{R}}_v \leq s^* < 1$ (where $s^* = S^*/N^* = \frac{\omega_v+\mu}{\omega_v+\xi_v+\mu}$). Further, consider the following linear Lyapunov function:

$$\mathcal{L} = \alpha_0 E + \alpha_1 P + \alpha_2 I + \alpha_3 A + \alpha_4 H,$$

where,

$$\alpha_0 = \frac{1}{\sigma+\mu},\ \alpha_1 = \frac{\alpha_0\beta_P + r\psi\alpha_2 + (1-r)\psi\alpha_3}{(\psi+\mu)},\ \alpha_2 = \frac{\alpha_0\beta_I + \varphi\alpha_4}{\varphi+\gamma_I+\delta_I+\mu},$$
$$\alpha_3 = \alpha_0\frac{\beta_A}{\gamma_A+\mu} \text{ and } \alpha_4 = \alpha_0\frac{\beta_H}{\gamma_H+\delta_H+\mu}.$$

The Lyapunov derivative is given by (where a dot represents differentiation with respect to time t):

$$\dot{\mathcal{L}} = \alpha_0\dot{E} + \alpha_1\dot{P} + \alpha_2\dot{I} + \alpha_3\dot{A} + \alpha_4\dot{H},$$

which can be simplified to

$$\begin{aligned}\dot{\mathcal{L}} &= \left[\alpha_0\beta_P\frac{S}{N} - \alpha_1(\psi+\mu) + \alpha_2 r\psi + \alpha_3(1-r)\psi\right]P + \left[\alpha_0\beta_A\frac{S}{N} - \alpha_3(\gamma_A+\mu)\right]A\\ &+\left[\alpha_0\beta_I\frac{S}{N} - \alpha_2(\varphi+\gamma_I+\delta_I+\mu) + \alpha_4\varphi\right]I + \left[\alpha_0\beta_H\frac{S}{N} - \alpha_4(\gamma_H+\delta_H+\mu)\right]H\\ &+[-\alpha_0(\sigma+\mu) + \alpha_1\sigma]E,\end{aligned}$$

so that (noting $S(t) \le N(t)$ for all t in Ω_1),

$$\begin{aligned}\dot{\mathcal{L}} &\le \left[\frac{\sigma}{\sigma+\mu}\left\{\frac{\beta_P}{\psi+\mu} + \frac{r\psi\beta_I}{(\psi+\mu)(\varphi+\gamma_I+\delta_I+\mu)} + \frac{r\psi\varphi\beta_H}{(\gamma_H+\delta_H+\mu)(\varphi+\gamma_I+\delta_I+\mu)} + \frac{(1-r)\psi\beta_A}{(\psi+\mu)(\gamma_A+\mu)}\right\} - 1\right]E,\\ \dot{\mathcal{L}} &\le (\mathcal{R}_0 - 1)E,\\ \dot{\mathcal{L}} &\le \left[\left(\frac{1-v^*}{1-v^*}\right)\mathcal{R}_0 - 1\right]E,\\ \dot{\mathcal{L}} &= \left(\frac{\tilde{\mathcal{R}}_v}{1-v^*} - 1\right)E.\end{aligned}$$

Thus, $\dot{\mathcal{L}} \le \left(\frac{\tilde{\mathcal{R}}_v}{s^*} - 1\right)E$, where $s^* = 1 - v^*$ (with v^* defined in Equation (3.11)). That is, the Lyapunov derivative $\dot{\mathcal{L}} \le 0$ if $\tilde{\mathcal{R}}_v \le s^* < 1$, and $\dot{\mathcal{L}} = 0$ if and only if $E(t) = 0$. Thus, $\mathcal{L}$ is a Lyapunov function in Ω_1 and it follows from LaSalle's Invariance Principle (Hale, 1969) that every solution to the model (3.1) (with $\varepsilon_v = 1$ and initial conditions in Ω_1) converges to DFE as $t \to \infty$. That is, $(S(t), V(t), E(t), P(t), I(t), A(t), H(t), R(t)) \to (S^*, V^*, 0, 0, 0, 0, 0, 0)$ as $t \to \infty$ for $\tilde{\mathcal{R}}_v \le s^*$. Hence, the DFE is globally-asymptotically stable in Ω_1 if $\tilde{\mathcal{R}}_v \le s^*$ for the special case of the model (3.1) with $\varepsilon_v = 1$. This completes the proof. □

D Proof of Theorem 3.3

Proof. Consider a special case of the homogeneous model (3.1) with negligible disease-induced mortality (i.e., consider the model (3.1) with $\delta_I = \delta_H = 0$). Furthermore, let $\mathcal{R}_v^\circ < 1$. The proof is based on using a comparison theorem (Lakshmikantham et al., 1989).

It is convenient to define:

$$W = \frac{S + (1-\epsilon_v)V}{\Pi/\mu} \quad \text{and} \quad W^* = \frac{S^* + (1-\epsilon_v)V^*}{N^*}. \tag{D.1}$$

The equations for the infected compartments of this special case of the model (3.1) can be re-written in terms of the next generation matrices F and $V^\circ = V|_{\delta_I=\delta_H=0}$ (with F and V matrices given in Section 3.2.1) as:

$$\frac{d}{dt}\begin{bmatrix}E(t)\\P(t)\\I(t)\\A(t)\\H(t)\end{bmatrix} = (F - V^\circ)\begin{bmatrix}E(t)\\P(t)\\I(t)\\A(t)\\H(t)\end{bmatrix} - M^\circ\begin{bmatrix}E(t)\\P(t)\\I(t)\\A(t)\\H(t)\end{bmatrix}, \tag{D.2}$$

where,

$$F - V^{\circ} = \begin{bmatrix} -(\sigma+\mu) & \beta_P W^* & \beta_I W^* & \beta_A W^* & \beta_H W^* \\ \sigma & -(\psi+\mu) & 0 & 0 & 0 \\ 0 & r\psi & -(\varphi+\gamma_I+\mu) & 0 & 0 \\ 0 & (1-r)\psi & 0 & -(\gamma_A+\mu) & 0 \\ 0 & 0 & \varphi & 0 & -(\gamma_H+\mu) \end{bmatrix}, \tag{D.3}$$

and,

$$M^{\circ} = \begin{bmatrix} 0 & \beta_P(W^*-W) & \beta_I(W^*-W) & \beta_A(W^*-W) & \beta_H(W^*-W) \\ 0 & 0 & 0 & 0 & 0 \\ 0 & 0 & 0 & 0 & 0 \\ 0 & 0 & 0 & 0 & 0 \\ 0 & 0 & 0 & 0 & 0 \end{bmatrix}. \tag{D.4}$$

Since $S^* \geq S$ and $V^* \geq V$ in Ω° (so that $W^* > W$) and $N^* = \Pi/\mu$, it follows that the matrix M°, defined in (D.4), is non-negative. Thus, Equation (D.2) can be re-written as the following inequality:

$$\frac{d}{dt}\begin{bmatrix} E(t) \\ P(t) \\ I(t) \\ A(t) \\ H(t) \end{bmatrix} \leq (F - V^{\circ})\begin{bmatrix} E(t) \\ P(t) \\ I(t) \\ A(t) \\ H(t) \end{bmatrix}. \tag{D.5}$$

If $\mathcal{R}_v^{\circ} < 1$, then $\rho(FV^{\circ -1}) < 1$ (see Section 3.2.1), which is equivalent to all eigenvalues of $F - V^{\circ}$ matrix being negative (Pauline van den Driessche & Watmough, 2002). Hence, the linearized differential inequality (D.5) is stable whenever $\mathcal{R}_v^{\circ} < 1$, so $(E(t), P(t), I(t), A(t), H(t)) \to (0, 0, 0, 0, 0)$ as $t \to \infty$ for this linear ODE system. It follows, using a standard comparison theorem (Lakshmikantham et al., 1989), that: $(E(t), P(t), I(t), A(t), H(t)) \to (0, 0, 0, 0, 0)$. Substituting $E(t) = P(t) = I(t) = A(t) = H(t) = 0$, into the equations for $\dot{S}$, $\dot{V}$, and $\dot{R}$ of the homogeneous model (3.1) gives:

$$S(t) \to S^*, V(t) \to V^* \text{ and } R(t) \to 0, \text{ as } t \to \infty.$$

Hence, the disease-free equilibrium of the special case of the model (3.1) with negligible disease-induced mortality (i.e., model (3.1) with $\delta_I = \delta_H = 0$) is globally-asymptomatically stable in Ω°, whenever $\mathcal{R}_v^{\circ} < 1$. □

E Proof of Theorem 3.6

Proof. Consider the special case of the homogeneous model (3.1) with negligible disease-induced mortality (i.e., $\delta_I = \delta_H = 0$), perfect vaccine ($\varepsilon_v = 1$), and no waning of immunity ($\omega_v = \omega_n = 0$). The proof of Theorem 3.6 is based on using a Krasnoselskii sub-linearity trick (see (Hethcote & Thieme, 1985; Horst, 1985), and also (Esteva et al., 2009; Esteva & Vargas, 2000)). The substitution $S = N^* - V - E - P - I - A - H - R$ (along with (3.14)) is used to rewrite this special case of model (3.1) as:

$$\begin{aligned} \dot{V}(t) &= \xi_v(N^* - V - E - P - I - A - H - R) - k_2 V, \\ \dot{E}(t) &= \lambda^{\circ}(N^* - V - E - P - I - A - H - R) - k_3 E, \\ \dot{P}(t) &= \sigma E - k_4 P, \\ \dot{I}(t) &= r\psi P - k_5^{\circ} I, \\ \dot{A}(t) &= (1-r)\psi P - k_6 A, \\ \dot{H}(t) &= \varphi I - k_7^{\circ} H, \\ \dot{R}(t) &= \gamma_I I + \gamma_A A + \gamma_H H - \mu R, \end{aligned} \tag{E.1}$$

where $k_5^{\circ} = \varphi + \gamma_I + \mu$, $k_7^{\circ} = \gamma_H + \mu$, and λ°, the force of infection obtained by substituting $N = N^*$ in (3.2), is given by

$$\lambda^{\circ} = \frac{\beta_P P + \beta_I I + \beta_A A + \beta_H H}{N^*}. \tag{E.2}$$

Linearizing the system (E.1) around the endemic equilibrium, $\mathbb{E}_1^{\circ}$, gives

$$\begin{aligned}
\dot{V}(t) &= -\xi_v(V+E+P+I+A+H+R) - k_2 V,\\
\dot{E}(t) &= -a_0 V - (a_0+k_3)E + (a_1-a_0)P + (a_2-a_0)I + (a_3-a_0)A + (a_4-a_0)H - a_0 R,\\
\dot{P}(t) &= \sigma E - k_4 P,\\
\dot{I}(t) &= r\psi P - k_5^{\diamond} I,\\
\dot{A}(t) &= (1-r)\psi P - k_6 A,\\
\dot{H}(t) &= \varphi I - k_7^{\diamond} H,\\
\dot{R}(t) &= \gamma_I I + \gamma_A A + \gamma_H H - \mu R,
\end{aligned} \tag{E.3}$$

where, $a_0 = \frac{\beta_P P^{**} + \beta_I I^{**} + \beta_A A^{**} + \beta_H H^{**}}{N^*}$, $a_1 = \beta_P \frac{S^{**}}{N^*}$, $a_2 = \beta_I \frac{S^{**}}{N^*}$, $a_3 = \beta_A \frac{S^{**}}{N^*}$, and $a_4 = \beta_H \frac{S^{**}}{N^*}$.

It follows that the Jacobian of the system (E.3), evaluated at $\mathbb{E}_1^{\diamond}$, is given by

$$J(\mathbb{E}_1^{\diamond}) = \begin{pmatrix}
-\xi_v - k_2 & -\xi_v & -\xi_v & -\xi_v & -\xi_v & -\xi_v & -\xi_v\\
-a_0 & -a_0 - k_3 & a_1 - a_0 & a_2 - a_0 & a_3 - a_0 & a_4 - a_0 & -a_0\\
0 & \sigma & -k_4 & 0 & 0 & 0 & 0\\
0 & 0 & r\psi & -k_5^{\diamond} & 0 & 0 & 0\\
0 & 0 & (1-r)\psi & 0 & -k_6 & 0 & 0\\
0 & 0 & 0 & \varphi & 0 & -k_7^{\diamond} & 0\\
0 & 0 & 0 & \gamma_I & \gamma_A & \gamma_H & -\mu
\end{pmatrix}.$$

Assume that the linearized system (E.3) has a solution of the form

$$\mathbf{Z}(t) = \mathbf{Z}_0 e^{\omega t}, \tag{E.4}$$

with $\mathbf{Z}_0 = (Z_1, Z_2, Z_3, Z_4, Z_5, Z_6, Z_7)$, $\omega, Z_i \in \mathbb{C}$ ($i = \{1, 2, \ldots, 7\}$). Substituting the solution of the form (E.4) into the linearized system (E.3) gives

$$\begin{aligned}
\omega Z_1 &= -\xi_v(Z_1+Z_2+Z_3+Z_4+Z_5+Z_6+Z_7) - k_2 Z_1,\\
\omega Z_2 &= -a_0 Z_1 - (a_0+k_3)Z_2 + (a_1-a_0)Z_3 + (a_2-a_0)Z_4 + (a_3-a_0)Z_5 + (a_4-a_0)Z_6 - a_0 Z_7,\\
\omega Z_3 &= \sigma Z_2 - k_4 Z_3,\\
\omega Z_4 &= r\psi Z_3 - k_5^{\diamond} Z_4,\\
\omega Z_5 &= (1-r)\psi Z_3 - k_6 Z_5,\\
\omega Z_6 &= \varphi Z_4 - k_7^{\diamond} Z_6,\\
\omega Z_7 &= \gamma_I Z_4 + \gamma_A Z_5 + \gamma_H Z_6 - \mu Z_7.
\end{aligned} \tag{E.5}$$

The third to the seventh equation in system (E.5) can be rewritten by moving negative terms to their respective left-hand side as

$$\begin{aligned}
\left(1+\frac{\omega}{k_4}\right)Z_3 &= \frac{\sigma}{k_4} Z_2,\\
\left(1+\frac{\omega}{k_5^{\diamond}}\right)Z_4 &= \frac{r\psi}{k_5^{\diamond}} Z_3,\\
\left(1+\frac{\omega}{k_6}\right)Z_5 &= \frac{(1-r)\psi}{k_6} Z_3,\\
\left(1+\frac{\omega}{k_7^{\diamond}}\right)Z_6 &= \frac{\varphi}{k_7^{\diamond}} Z_4,\\
\left(1+\frac{\omega}{\mu}\right)Z_7 &= \frac{\gamma_I}{\mu} Z_4 + \frac{\gamma_A}{\mu} Z_5 + \frac{\gamma_H}{\mu} Z_6.
\end{aligned} \tag{E.6}$$

To get a similar expression from first and second equations in system (E.5), we first rewrite all equations in system (E.6) in terms of Z_2 as

$$\begin{aligned}
Z_3 &= \frac{\sigma}{\omega + k_4} Z_2 = A_1 Z_2,\\
Z_4 &= \frac{r\psi\sigma}{(\omega + k_4)(\omega + k_5^\diamond)} Z_2 = A_2 Z_2,\\
Z_5 &= \frac{\sigma(1-r)\psi}{(\omega + k_4)(\omega + k_6)} = A_3 Z_2,\\
Z_6 &= \frac{\varphi r\psi\sigma}{(\omega + k_4)(\omega + k_6)(\omega + k_7^\diamond)} Z_2 = A_4 Z_2,\\
Z_7 &= \frac{1}{\mu}(\gamma_I A_4 + \gamma_A A_5 + \gamma_H A_6) Z_2 = A_5 Z_2.
\end{aligned} \tag{E.7}$$

Then, using the first two equations of (E.5) and expressions in (E.7), we obtain

$$\begin{aligned}
\left(1 + \frac{\omega + \xi_v}{k_2}\right) Z_1 + \left[1 + \frac{\omega + a_0}{k_3} + \frac{\xi_v}{k_2} + \left(\frac{\xi_v}{k_2} + \frac{a_0}{k_3}\right) \right. & \left. (A_3 + A_4 + A_5 + A_6 + A_7)\right] Z_2 \\
&= \frac{a_1}{k_3} Z_3 + \frac{a_2}{k_3} Z_4 + \frac{a_3}{k_3} Z_5 + \frac{a_4}{k_3} Z_6.
\end{aligned} \tag{E.8}$$

System (E.6) along with (E.8) can be rewritten as

$$\begin{aligned}
[1 + F_1(\omega)] Z_1 + [1 + F_2(\omega)] Z_2 &= \frac{a_1}{k_3} Z_3 + \frac{a_2}{k_3} Z_4 + \frac{a_3}{k_3} Z_5 + \frac{a_4}{k_3} Z_6,\\
[(1 + F_3(\omega)] Z_3 &= \frac{\sigma}{k_4} Z_2 = (MZ)_3,\\
[1 + F_4(\omega)] Z_4 &= \frac{r\psi}{k_5^\diamond} Z_3 = (MZ)_5,\\
[1 + F_5(\omega)] Z_5 &= \frac{(1-r)\psi}{k_6} Z_3 = (MZ)_5,\\
[1 + F_6(\omega)] Z_6 &= \frac{\varphi}{k_7^\diamond} Z_4 = (MZ)_6,\\
[1 + F_7(\omega)] Z_7 &= \frac{\gamma_I}{\mu} Z_4 + \frac{\gamma_A}{\mu} Z_5 + \frac{\gamma_H}{\mu} Z_6 = (MZ)_7,
\end{aligned} \tag{E.9}$$

where,

$$\begin{aligned}
F_1(\omega) &= \frac{\omega + \xi_v}{k_2} + \frac{a_0}{k_3},\\
F_2(\omega) &= \frac{\omega + a_0}{k_3} + \frac{\xi_v}{k_2} + \left(\frac{\xi_v}{k_2} + \frac{a_0}{k_3}\right)\left(A_1 + A_2 + A_3 + A_4 + A_5\right),\\
F_3(\omega) &= \frac{\omega}{k_4}, \quad F_4(\omega) = \frac{\omega}{k_5^\diamond}, \quad F_5(\omega) = \frac{\omega}{k_6}, \quad F_6(\omega) = \frac{\omega}{k_7^\diamond}, \text{ and } F_7(\omega) = \frac{\omega}{\mu},
\end{aligned} \tag{E.10}$$

with,

$$M = \begin{pmatrix} 0 & 0 & 0 & 0 & 0 & 0 & 0 \\ 0 & 0 & \frac{a_1}{k_3} & \frac{a_2}{k_3} & \frac{a_3}{k_3} & \frac{a_4}{k_4} & 0 \\ 0 & \frac{\sigma}{k_4} & 0 & 0 & 0 & 0 & 0 \\ 0 & 0 & \frac{r\psi}{k_5^\diamond} & 0 & 0 & 0 & 0 \\ 0 & 0 & \frac{(1-r)\psi}{k_6} & 0 & 0 & 0 & 0 \\ 0 & 0 & 0 & \frac{\varphi}{k_7^\diamond} & 0 & 0 & 0 \\ 0 & 0 & 0 & \frac{\gamma_I}{\mu} & \frac{\gamma_A}{\mu} & \frac{\gamma_H}{\mu} & 0 \end{pmatrix}.$$

In the above expressions, the notation $(M\mathbf{Z})_i$ (with $i = 1, \ldots, 7$) denotes the ith coordinate of the vector MZ. Furthermore, note that the matrix M has non-negative entries and the endemic equilibrium $\mathbb{E}_1^\diamond$ satisfies $\mathbb{E}_1^\diamond = M\mathbb{E}_1^\diamond$. Hence, if $\mathbf{Z}$ is a solution of (E.9), then it is possible to find a minimal positive real number b such that (Esteva et al., 2009; Esteva & Vargas, 2000)

$$\|\mathbf{Z}\| \leq b\mathbb{E}_1^\diamond, \tag{E.11}$$

where, $\|\mathbf{Z}\| = (\|Z_1\|, \|Z_2\|, \|Z_3\|, \|Z_4\|, \|Z_5\|, \|Z_6\|, \|Z_7\|)$ with lexicographic order, and $\|.\|$ is a norm in $\mathbb{C}$. Now it is sufficient to show that $\mathrm{Re}(\omega) < 0$. Assume the contrary (i.e., $\mathrm{Re}(\omega) \geq 0$) and consider the following two cases.

Case 1: $\omega = 0$.

In this case, (E.5) is the homogeneous linear system in the variables Z_i (with $i = 1, \ldots, 7$). The determinant of this system is given by

$$\Delta = -A + \left(S^{**}\frac{\hat{\mathcal{R}}_v}{N^*} - 1\right)\mu(\xi_v + k_2)k_3k_4k_5^\diamond k_6k_7^\diamond, \tag{E.12}$$

where,

$$\begin{aligned} A = \; & \mu\sigma k_2k_5^\diamond k_6k_7^\diamond + \mu k_2k_4k_5^\diamond k_6k_7^\diamond + r\mu\sigma\varphi\psi k_2k_6 + r\mu\sigma\psi k_2k_6k_7^\diamond + (1-r)\mu\sigma\psi k_2k_5^\diamond k_7^\diamond \\ & + r\sigma\psi\gamma_I k_2k_6k_7^\diamond + (1-r)\sigma\psi\gamma_A k_2k_5^\diamond k_7^\diamond + r\sigma\varphi\psi\gamma_H k_2k_5^\diamond > 0. \end{aligned}$$

To determine the sign of Δ it is enough to determine that of $S^{**}\frac{\hat{\mathcal{R}}_v}{N^*}$. To do this, we first solve the system (E.1) at the endemic steady-state $(\mathbb{E}_1^\diamond)$ as

$$\frac{S^{**}}{N^*} = \frac{k_3E^{**}}{\beta_P P + \beta_I I^{**} + \beta_A A^{**} + \beta_H H^{**}}, \tag{E.13}$$

$$P^{**} = \frac{\sigma}{k_4}E^{**}, \quad I^{**} = \frac{r\psi\sigma}{k_5^\diamond}E^{**}, \quad A^{**} = \frac{(1-r)\psi\sigma}{k_4k_6}E^{**}, \quad H^{**} = \frac{r\psi\sigma\varphi}{k_4k_5k_7^\diamond}E^{**}. \tag{E.14}$$

Then, we observe that

$$\beta_P P^{**} + \beta_I I^{**} + \beta_A A^{**} + \beta_H H^{**} = \left[\beta_P\frac{\sigma}{k_4} + \beta_I\frac{r\psi\sigma}{k_4k_5^\diamond} + \beta_A\frac{(1-r)\psi\sigma}{k_4k_6} + \beta_H\frac{r\psi\sigma\varphi}{k_4k_5^\diamond k_7^\diamond}\right]E^{**} = k_3\mathcal{R}_v^\diamond E^{**}, \tag{E.15}$$

and substitute the expression from equation (E.15) into (E.13) to get

$$\frac{S^{**}}{N^*} = \frac{1}{\hat{\mathcal{R}}_v}. \tag{E.16}$$

This implies that $S^{**}\frac{\hat{\mathcal{R}}_v}{N^*} - 1 = 0$, which means (E.12) can be simplified as

$$\Delta = -A < 0. \tag{E.17}$$

Since the determinant Δ is negative, it follows that the system (E.5) has a unique solution, given by $\mathbf{Z} = 0$ (which corresponds to the DFE $(\mathbb{E}_0)$).

Case 2: $\omega \neq 0$.

In this case, since by assumption $\mathrm{Re}(\omega) > 0$, so $|1 + F_i(\omega)| > 1$ for all $i = 1, \ldots, 7$. Define $F(\omega) = \min|1 + F_i(\omega)|$ for $i = 1, \ldots, 7$. Then, $F(\omega) > 1$, and $\frac{b}{F(\omega)} < b$. Since b is a minimal positive real number such that $\|\mathbf{Z}\| \leq b\mathbb{E}_1^\diamond$, then (Safi & Gumel, 2010)

$$\|\mathbf{Z}\| > \frac{b}{F(\omega)}\mathbb{E}_1^\diamond. \tag{E.18}$$

On the other hand, by taking the norm of both sides of the second equation in (E.9) and noting that M is a non-negative matrix, we have (Safi & Gumel, 2010)

$$F(\omega)\|Z_2\| \leq |1 + F_2(\omega)\|Z_2\| = \|(MZ)_2\| \leq M\|Z_2\| \leq bM(\mathbb{E}_1^\diamond)_2 = b(\mathbb{E}_1^\diamond)_2 = bI^{**}. \tag{E.19}$$

It follows from (E.19) that $\|Z_2\| \leq \frac{b}{F(\omega)}I^{**}$, which contradicts (E.18). Hence, $\mathrm{Re}(\omega) < 0$. Thus, all eigenvalues of the characteristic equation associated with the linearized system (E.3) will have a negative real part, so that the unique endemic equilibrium, $\mathbb{E}_1^\diamond$, is LAS whenever $\hat{\mathcal{R}_v} > 1$. This completes the proof. □

F Proof of Theorem 3.7

Proof. Consider a special case of the homogeneous model (3.1) with negligible disease-induced mortality (i.e., $\delta_I = \delta_H = 0$), perfect vaccine ($\varepsilon_v = 1$) and no waning of immunity ($\omega_v = \omega_n = 0$). For this special case of the model, the fully-vaccinated (V) and recovered (R) terms are not featured in the remaining equations of model (3.1), so it is enough to consider the following non-linear Lyapunov function (non-linear functions of this type have been used in ecology and epidemiology literature, such as in (Freedman & So, 1985; Gumel, 2009; Guo & Yi Li, 2006)):

$$\begin{aligned}\mathcal{F} = \quad & S - S^{**} - S^{**}\ln\left(\frac{S}{S^{**}}\right) + E - E^{**} - E^{**}\ln\left(\frac{E}{E^{**}}\right) + a_1\left[P - P^{**} - P^{**}\ln\left(\frac{S}{S^{**}}\right)\right] \\ & + a_2\left[I - I^{**} - I^{**}\ln\left(\frac{I}{I^{**}}\right)\right] + a_3\left[A - A^{**} - A^{**}\ln\left(\frac{A}{A^{**}}\right)\right] + a_4\left[H - H^{**} - H^{**}\ln\left(\frac{H}{H^{**}}\right)\right],\end{aligned} \tag{F.1}$$

where,

$$a_1 = \frac{k_3}{\sigma}, \quad a_2 = \frac{\beta_I k_7 + \beta_H \varphi}{k_5 k_7}S^{**}, \quad a_3 = \frac{\beta_A}{k_6}S^{**}, \quad a_4 = \frac{\beta_H}{k_7}S^{**}. \tag{F.2}$$

Taking the time derivative of (F.1) gives

$$\begin{aligned}\dot{\mathcal{F}} \quad & = \dot{S} - \frac{S^{**}}{S}\dot{S} + \dot{E} - \frac{E^*}{E}\dot{E} + a_1\left(\dot{P} - \frac{P^{**}}{P}\dot{P}\right) + a_2\left(\dot{I} - \frac{I^{**}}{I}\dot{I}\right) + a_3\left(\dot{A} - \frac{A^{**}}{A}\dot{A}\right) + a_4\left(\dot{H} - \frac{H^{**}}{H}\dot{H}\right) \\ & = \Pi - k_1 S - \frac{S^{**}}{S}[\Pi - (\beta_P P + \beta_I I + \beta_A A + \beta_H H)S - k_1 S] - k_3 E - \frac{E^{**}}{E}[(\beta_P P + \beta_I I + \beta_A A + \beta_H H)S - k_3 E] \\ & \quad + a_1\left[\sigma E - k_4 P - \frac{P^{**}}{P}(\sigma E - k_4 P)\right] + a_2\left[r\psi P - k_5 I - \frac{I^{**}}{I}(r\psi P - k_5 I)\right] \\ & \quad + a_3\left[\left((1-r)\psi P - k_6 A - \frac{A^{**}}{A}((1-r)\psi P - k_6 A\right] + a_4\left[\varphi I - k_7 H - \frac{H^{**}}{H}(\varphi I - k_7 H)\right].\end{aligned} \tag{F.3}$$

It can be shown from this special case of the model (3.1) that, at endemic steady-state,

$$\begin{aligned}\Pi \quad & = (\beta_P P^{**} + \beta_I I^{**} + \beta_A A^{**} + \beta_H H^{**})S^{**} - k_1 S^{**}, \\ a_2\sigma \quad & = \frac{k_3 k_4 P^{**}}{\sigma E^{**}}, \quad a_3 r\psi = \frac{\beta_I S^* S^*}{P^*} + \beta_H \frac{S^* H^*}{P^*}, \\ a_4(1-r)\psi \quad & = \frac{\beta_A S^{**} A^{**}}{P^{**}}, \quad a_5\varphi = \frac{\beta_H S^{**} H^{**}}{I^{**}}.\end{aligned} \tag{F.4}$$

Plugging in the first equation from (F.4) into (F.3) and simplifying, gives

$$\begin{aligned}\dot{\mathcal{F}} = \quad & k_1 S^{**}\left[2-\frac{S^{**}}{S}-\frac{S}{S^{**}}\right]+(\beta_P P^{**}+\beta_I I^{**}+\beta_A A^{**}+\beta_H H^{**})S^{**}+k_3 E^{**}+a_1 k_4 P^{**}+a_2 k_5 I^{**}\\ & +a_3 k_6 A^{**}+a_4 k_7 H^{**}-(\beta_P P^{**}+\beta_I I^{**}+\beta_A A^{**}+\beta_H H^{**})\frac{S^{**2}}{S}-(\beta_P P+\beta_I I+\beta_A A+\beta_H H)\frac{SE^{**}}{E}\\ & -a_1\sigma\frac{EP^{**}}{P}-a_3 r\psi\frac{PI^{**}}{I}-a_4(1-r)\psi\frac{PA^{**}}{A}-a_5\varphi\frac{IH^{**}}{H}.\end{aligned} \tag{F.5}$$

Then, making use of the remaining equations in (F.4), the equation (F.5) can be re-written as

$$\begin{aligned}\dot{\mathcal{F}} = \quad & k_1 S^{**}\left[2-\frac{S^{**}}{S}-\frac{S}{S^{**}}\right]+4(\beta_P P^{**}+\beta_I I^{**}+\beta_A A^{**}+\beta_H H^{**})S^{**}\\ & -(\beta_P P^{**}+\beta_I I^{**}+\beta_A A^{**}+\beta_H H^{**})\frac{S^{**2}}{S}-(\beta_P P+\beta_I I+\beta_A A+\beta_H H)\frac{SE^{**}}{E}\\ & -(\beta_P P^{**}+\beta_I^{**}+\beta_A A^{**}+\beta_H H^{**})\frac{S^{**}EP^{**}}{E^{**}P}-\beta_I\frac{S^{**}I^{**2}P}{IP^{**}}-\beta_H\frac{S^{**}PI^{**}H^{**}}{P^{**}I}\\ & -\beta_A\frac{S^{**}A^{**2}P}{AP^{**}}-\beta_H\frac{S^{**}IH^{**2}}{I^{**}H},\end{aligned} \tag{F.6}$$

$$\begin{aligned}\dot{\mathcal{F}} = \quad & k_1 S^{**}\left[2-\frac{S^{**}}{S}-\frac{S}{S^{**}}\right]+\beta_P S^{**}P^{**}\left[3-\frac{S^{**}}{S}-\frac{SPE^{**}}{S^{**}P^{**}E}-\frac{EP^{**}}{E^{**}P}\right]\\ & +\beta_I S^{**}I^{**}\left[4-\frac{S^{**}}{S}-\frac{SIE^{**}}{S^{**}I^{**}E}-\frac{EP^{**}}{E^{**}P}-\frac{I^{**}P}{IP^{**}}\right]+\beta_A S^{**}A^{**}\left[4-\frac{S^{**}}{S}-\frac{SAE^{**}}{S^{**}A^{**}E}-\frac{EP^{**}}{E^{**}P}-\frac{A^{**}P}{AP^{**}}\right]\\ & +\beta_H S^{**}H^{**}\left[5-\frac{S^{**}}{S}-\frac{SHE^{**}}{S^{**}H^{**}E}-\frac{EP^{**}}{E^{**}P}-\frac{PI^{**}}{P^{**}I}-\frac{IH^{**}}{I^{**}H}\right].\end{aligned}$$

Since the arithmetic mean exceed the geometric mean, it implies that

$$\begin{aligned}& k_1 S^{**}\left[2-\frac{S^{**}}{S}-\frac{S}{S^{**}}\right]\le 0,\\ & \beta_P S^{**}P^{**}\left[3-\frac{S^{**}}{S}-\frac{SPE^{**}}{S^{**}P^{**}E}-\frac{EP^{**}}{E^{**}P}\right]\le 0,\\ & \beta_I S^{**}I^{**}\left[4-\frac{S^{**}}{S}-\frac{SIE^{**}}{S^{**}I^{**}E}-\frac{EP^{**}}{E^{**}P}-\frac{I^{**}P}{IP^{**}}\right]\le 0,\\ & \beta_A S^{**}A^{**}\left[4-\frac{S^{**}}{S}-\frac{SAE^{**}}{S^{**}A^{**}E}-\frac{EP^{**}}{E^{**}P}-\frac{A^{**}P}{AP^{**}}\right]\le 0,\\ & \beta_H S^{**}H^{**}\left[5-\frac{S^{**}}{S}-\frac{SHE^{**}}{S^{**}H^{**}E}-\frac{EP^{**}}{E^{**}P}-\frac{PI^{**}}{P^{**}I}-\frac{IH^{**}}{I^{**}H}\right]\le 0\end{aligned} \tag{F.7}$$

Thus $\dot{\mathcal{F}}\le 0$ for $\mathcal{R}_v>1$. Hence, $\mathcal{F}$ is a Lyapunov function for the aforementioned special case of the model (3.1) on Ω_1/Ω_0. Therefore, it follows, by LaSalle's Invariance Principle (Hale, 1969), that

$$\begin{aligned}&\lim_{x\to\infty}S(x) = S^{**},\quad \lim_{x\to\infty}E(x)=E^{**},\quad \lim_{x\to\infty}P(x)=P^{**},\\ &\lim_{x\to\infty}I(x) = I^{**},\quad \lim_{x\to\infty}A(x)=A^{**},\quad \lim_{x\to\infty}H(x)=H^{**}.\end{aligned}$$

Thus, $\lim\inf_{t\to\infty} S = \lim\sup_{t\to\infty} S = S^{**}$. Since, $\lim\sup_{t\to\infty} S = S^{**}$, it follows that, for sufficiently small $\zeta>0$, there exists a $T_1>0$ such that $\lim\sup_{t\to\infty} S \le S^{**}+\zeta$ for all $t>T_1$. It follows from (3.14) and the $\dot{V}$ equation of the special case of the model (3.1) that, for $t>T_1$,

$$\dot{V}\le \xi_v(S^{**}+\zeta)-k_2 V.$$

So, by comparison theorem (Lakshmikantham et al., 1989),

$$V^{\infty} = \lim_{t\to\infty}\sup V \leq \frac{\xi_v(S^{**}+\zeta)}{k_2} \to \frac{\xi_v S^{**}}{k_2} \quad \text{as } \zeta \to 0. \tag{F.8}$$

Similarly, by using $\lim_{t\to\infty}\inf S = S^{**}$, we can show that

$$V_{\infty} = \lim_{t\to\infty}\inf V \geq \frac{\xi_v(S^{**}+\zeta)}{k_2} \to \frac{\xi_v S^{**}}{k_2} \quad \text{as } \zeta \to 0. \tag{F.9}$$

Then, it follows from (F.8) and (F.9) that

$$V_{\infty} \geq \frac{\xi_v S^{**}}{k_2} \geq V^{\infty}. \tag{F.10}$$

Hence, $\lim_{t\to\infty} V = \frac{\xi_v S^{**}}{k_2} = V^{**}$. Similarly, it can be shown that $\lim_{t\to\infty} R = R^{**}$. Thus, for $\hat{\mathcal{R}}_v > 1$, every solution of the system (3.1), with initial conditions in Ω_1/Ω_0, approaches the unique endemic equilibrium for $t \to \infty$. □

G Threshold Analysis of Reproduction Number for Model (3.1)

Consider the homogeneous model (3.1). The effect or sensitivity of parameters of the model on the vaccination reproduction number (i.e., the response function), $\mathcal{R}_v$ (given by (3.8)), can also be measured from the sign of the partial derivative of the response function with respect to each of the chosen model parameters (where a positive (negative) sign of the partial derivative with respect to a parameter shows that an increase in that parameter will increase (decrease) the response function, which correspondingly lead to an increase (decrease) in disease burden). It can be shown, for instance, that the partial derivative of $\mathcal{R}_v$ with respect to the parameters β_P, β_I, β_A, β_H, and ω_v is always positive. Hence, an increase in the values of any of these parameters will correspondingly lead to an increase in the value of the reproduction number (hence, increase the burden of the pandemic). Similarly, the sign of the partial derivative of $\mathcal{R}_v$ with respect to the parameters ε_v, ξ_v, γ_I, γ_A, γ_H, δ_I, and δ_H is always negative. Hence, an increase in the values of these parameters will lead to a corresponding decrease in the response function (and, consequently, a decrease in disease burden). However, the sign of the partial derivative of $\mathcal{R}_v$ with respect to the parameters r, φ and ψ, can be positive or negative. In other words, depending on the values of the parameters of the model (3.1), these three parameters can have a positive or negative impact on the response function, $\mathcal{R}_v$. We explore the impact of these three parameters in detail below.

The partial derivative of the control reproduction number, $\mathcal{R}_v$, with respect to the parameter for the proportion of pre-symptomatic individuals who become symptomatic at the end of pre-symptomatic period (r) of the homogeneous model is given by (where k_i ($i = 3, \ldots 7$) are as defined in Equation (3.14)):

$$\frac{\partial \mathcal{R}_v}{\partial r} = (1-\epsilon_v v^*)\frac{\sigma\psi}{k_3 k_4}\left(\frac{k_6\beta_I}{k_5} + \frac{k_6\varphi\beta_H}{k_5 k_7} - \beta_A\right), \tag{G.1}$$

from which it follows that,

$$\frac{\partial \mathcal{R}_v}{\partial r} > 0 (<0) \text{ if and only if } \beta_A < \beta_A^c (>\beta_A^c),$$

where,

$$\beta_A^c = \frac{k_6}{k_5}\beta_I + \frac{k_6\varphi}{k_5 k_7}\beta_H.$$

The result below follows from the derivations above.

Lemma G.1. *Increasing the value of the proportion of pre-symptomatic individuals who become symptomatic at the end of the pre-symptomatic period (r) will decrease (increase) the vaccination reproduction number ($\mathcal{R}_v$) if $\beta_A > (<)\beta_A^c$.*

Lemma G.1 implies that if the transmission rate of symptomatic (β_I) and hospitalized (β_H) individuals reaches a certain threshold (given by β_A^c), then any further increase in the proportion of pre-symptomatic individuals who become symptomatic at the end of the pre-symptomatic period (r) will lead to an increase in the reproduction number $\mathcal{R}_v$ (and, consequently, an increase in the burden of the disease). Similar threshold dynamics for the proportion of asymptomatic individuals was numerically observed in (Pant et al., 2024).

The partial derivative of $\mathcal{R}_v$ with respect to the parameter for the rate at which symptomatic individuals are hospitalized (φ) is given by:

$$\frac{\partial \mathcal{R}_v}{\partial \varphi} = (1-\epsilon_v v^*)\frac{\sigma r \psi}{k_3 k_4 k_5^2}\left(\frac{\gamma_I+\delta_I+\mu}{\gamma_H+\delta_H+\mu}\beta_H - \beta_I\right), \tag{G.2}$$

from which it follows that,

$$\frac{\partial \mathcal{R}_v}{\partial \psi} > 0 (<0) \text{ if and only if } \beta_H > \beta_H^c (<\beta_H^c),$$

where,

$$\beta_H^c = \frac{\gamma_H+\mu+\delta_H}{\gamma_I+\mu+\delta_I}\beta_I,$$

suggesting the following result.

Lemma G.2. *An increase in the hospitalization rate of symptomatic individuals* (φ) *will decrease (increase)* $\mathcal{R}_v$ *if* $\beta_H < (>)\beta_H^c$.

Lemma G.2 implies that if the transmission rate of hospitalized individuals (β_H) is "large enough", then an increase in the hospitalization rate (φ) will increase $\mathcal{R}_v$ (and, consequently, increase disease burden). In other words, if the rate at which hospitalized individuals transmits the infection (β_H) reaches and exceeds a certain threshold (given by β_H^c; which may arise due to poor implementation of safety protocols such as hand washing, sanitation and masking at a hospital), any further increase in the hospitalization rate of symptomatic individuals (φ) will $\mathcal{R}_v$ (i.e., under this scenario hospitalization of symptomatically-infectious individuals make things worse).

Finally, partial derivative of $\mathcal{R}_v$ with respect to the parameter for the rate at which pre-symptomatic individuals become symptomatic or asymptomatic (ψ) is given by:

$$\frac{\partial \mathcal{R}_v}{\partial \psi} = (1-\epsilon_v v^*)\frac{\sigma}{k_3 k_4^2}\left[\frac{r\mu}{k_5}\left(\beta_I + \frac{\varphi}{k_7}\beta_H\right) + \frac{\mu(1-r)}{k_6}\beta_A - \beta_P\right], \tag{G.3}$$

from which it follows that,

$$\frac{\partial \mathcal{R}_v}{\partial \psi} > 0 (<0) \text{ if and only if } \beta_P < \beta_P^c (>\beta_P^c),$$

where,

$$\beta_P^c = \frac{r\mu}{k_5}\left(\beta_I + \frac{\varphi}{k_7}\beta_H\right) + \frac{\mu(1-r)}{k_6}\beta_A,$$

suggesting the following result.

Lemma G.3. *Increase in the rate at which pre-symptomatic individuals become symptomatic or asymptomatic* (ψ) *will decrease (increase) vaccination reproduction number* ($\mathcal{R}_v$) *if* $\beta_P > (<)\beta_P^c$.

Lemma G.3 implies that the impact of the rate at which pre-symptomatic individuals become symptomatic or asymptomatic (ψ) on $\mathcal{R}_v$ largely depends on the transmission rate of pre-symptomatic individuals, in comparison to asymptomatic, symptomatic and hospitalized infectious individuals. If the transmission rate of a pre-symptomatic individual reaches the threshold (β_P^c), then an increase in ψ decreases $\mathcal{R}_v$ (hence, decrease disease burden). In summary, this study identifies three parameters of the model that exhibits key threshold dynamics with respect to increasing or decreasing disease burden. Intervention strategies should target these parameters to enhance the likelihood of effective control or elimination of the pandemic.

H Computation of Reproduction Number of the Two-group Model (4.1)

Using the *next generation operator method* (Diekmann et al., 1990; Pauline van den Driessche & Watmough, 2002), the non-negative matrix of new infection terms (F_2) and M-Matrix (V_2) of linear transition term in the infected compartments corresponding to two-group heterogeneous model (4.1) are given, respectively, by:

$$F_2 = \begin{bmatrix} 0 & 0 & f_{1,3} & f_{1,4} & f_{1,5} & f_{1,6} & f_{1,7} & f_{1,8} & f_{1,9} & f_{1,10} \\ 0 & 0 & f_{2,3} & f_{2,4} & f_{2,5} & f_{2,6} & f_{2,7} & f_{2,8} & f_{2,9} & f_{2,10} \\ 0 & 0 & 0 & 0 & 0 & 0 & 0 & 0 & 0 & 0 \\ 0 & 0 & 0 & 0 & 0 & 0 & 0 & 0 & 0 & 0 \\ 0 & 0 & 0 & 0 & 0 & 0 & 0 & 0 & 0 & 0 \\ 0 & 0 & 0 & 0 & 0 & 0 & 0 & 0 & 0 & 0 \\ 0 & 0 & 0 & 0 & 0 & 0 & 0 & 0 & 0 & 0 \\ 0 & 0 & 0 & 0 & 0 & 0 & 0 & 0 & 0 & 0 \\ 0 & 0 & 0 & 0 & 0 & 0 & 0 & 0 & 0 & 0 \\ 0 & 0 & 0 & 0 & 0 & 0 & 0 & 0 & 0 & 0 \end{bmatrix},$$

and

$$V_2 = \begin{bmatrix} \sigma_1+\mu_1 & 0 & 0 & 0 & 0 & 0 & 0 & 0 & 0 & 0 \\ 0 & \sigma_2+\mu_2 & 0 & 0 & 0 & 0 & 0 & 0 & 0 & 0 \\ -\sigma_1 & 0 & \psi_1+\mu_1 & 0 & 0 & 0 & 0 & 0 & 0 & 0 \\ 0 & -\sigma_2 & 0 & \psi_2+\mu_2 & 0 & 0 & 0 & 0 & 0 & 0 \\ 0 & 0 & -r_1\psi_1 & 0 & \varphi_1+\gamma_{I,1}+\delta_1+\mu_1 & 0 & 0 & 0 & 0 & 0 \\ 0 & 0 & 0 & -r_2\psi_2 & 0 & \varphi_2+\gamma_{I,2}+\delta_2+\mu_2 & 0 & 0 & 0 & 0 \\ 0 & 0 & -(1-r_1)\psi_1 & 0 & 0 & 0 & \gamma_{A,1}+\mu_1 & 0 & 0 & 0 \\ 0 & 0 & 0 & -(1-r_2)\psi_2 & 0 & 0 & 0 & \gamma_{A,2}+\mu_2 & 0 & 0 \\ 0 & 0 & 0 & 0 & -\varphi_1 & 0 & 0 & 0 & \gamma_{H,1}+\delta_{H,1}+\mu_1 & 0 \\ 0 & 0 & 0 & 0 & 0 & -\varphi_2 & 0 & 0 & 0 & \gamma_{H,2}+\delta_{H,2}+\mu_2 \end{bmatrix},$$

where,

$$\begin{aligned}
f_{1,3} &= a_1c_{11}\mathcal{P}_{P,1}\frac{S_1^*+(1-\epsilon_v)V_1^*}{N_1^*}, & f_{1,4} &= a_1c_{12}\mathcal{P}_{P,2}\frac{S_1^*+(1-\epsilon_v)V_1^*}{N_2^*},\\
f_{1,5} &= a_1c_{11}\mathcal{P}_{I,1}\frac{S_1^*+(1-\epsilon_v)V_1^*}{N_1^*}, & f_{1,6} &= a_1c_{12}\mathcal{P}_{I,2}\frac{S_1^*+(1-\epsilon_v)V_1^*}{N_2^*},\\
f_{1,7} &= a_1c_{11}\mathcal{P}_{A,1}\frac{S_1^*+(1-\epsilon_v)V_1^*}{N_1^*}, & f_{1,8} &= a_1c_{12}\mathcal{P}_{A,2}\frac{S_1^*+(1-\epsilon_v)V_1^*}{N_2^*},\\
f_{1,9} &= a_1c_{11}\mathcal{P}_{H,1}\frac{S_1^*+(1-\epsilon_v)V_1^*}{N_1^*}, & f_{1,10} &= a_1c_{12}\mathcal{P}_{H,2}\frac{S_1^*+(1-\epsilon_v)V_1^*}{N_2^*},\\
f_{2,3} &= a_2c_{21}\mathcal{P}_{P,1}\frac{S_2^*+(1-\epsilon_v)V_2^*}{N_1^*}, & f_{2,4} &= a_2c_{22}\mathcal{P}_{P,2}\frac{S_2^*+(1-\epsilon_v)V_2^*}{N_2^*},\\
f_{2,5} &= a_2c_{21}\mathcal{P}_{I,1}\frac{S_2^*+(1-\epsilon_v)V_2^*}{N_1^*}, & f_{2,6} &= a_2c_{22}\mathcal{P}_{I,2}\frac{S_2^*+(1-\epsilon_v)V_2^*}{N_2^*},\\
f_{2,7} &= a_2c_{21}\mathcal{P}_{A,1}\frac{S_2^*+(1-\epsilon_v)V_2^*}{N_1^*}, & f_{2,8} &= a_2c_{22}\mathcal{P}_{A,2}\frac{S_2^*+(1-\epsilon_v)V_2^*}{N_2^*},\\
f_{2,9} &= a_2c_{21}\mathcal{P}_{H,1}\frac{S_2^*+(1-\epsilon_v)V_2^*}{N_1^*}, & f_{2,10} &= a_2c_{22}\mathcal{P}_{H,2}\frac{S_2^*+(1-\epsilon_v)V_2^*}{N_2^*}.
\end{aligned}$$

Hence, it follows from (Elamin H Elbasha and Abba B Gumel, 2021) that the vaccination reproduction number for the two-group model (4.1) is given by (Diekmann et al., 1990; Pauline van den Driessche & Watmough, 2002):

$$\mathcal{R}_v^{\dagger} = \rho(F_2V_2^{-1}) \tag{H.1}$$

I Proof of Theorem 4.2

Proof. Consider a special case of the two-group model (4.1) with negligible disease-induced mortality (i.e., $\delta_{I,k} = \delta_{H,k} = 0$). Let k, $l = \{1, 2\}$ and $\mathcal{R}_v^{\Delta} < 1$. Adding all the equations with indices k in (2.3) gives

$$\dot{N}_k = \Pi_k - \mu_k N_k - \delta_{I,k} I_k - \delta_{H,k} H_k.$$

In the absence of disease-included mortality (i.e., we set $\delta_{k,I} = \delta_{k,H} = 0$ into the model), it can be seen that $N_k \to \frac{\Pi_k}{\mu_k}$ as $t \to \infty$, and $\frac{\Pi_k}{\mu_k}$ is an upper bound of $N_k(t)$ provided that $N_k(0) \leq \frac{\Pi_k}{\mu_k}$. If $N_k(0) > \frac{\Pi_k}{\mu_k}$, then N_k will decrease to that level. Hence, in Ω_2, $N_k \leq \frac{\Pi_k}{\mu_k}$. Then, it follows from first equation in (2.3) and (2.2) that

$$\begin{aligned}\dot{S_k} &= \Pi_k + \omega_{v,k}V_k - \lambda_k S_k - (\xi_{v,k} + \mu_k)S_k \\ &\leq \Pi_k + \omega_{v,k}V_k - (\xi_{v,k} + \mu_k)S_k \\ &\leq \Pi_k + \omega_{v,k}(\Pi_k/\mu_k - S_k - E_k - P_k - I_k - A_k - H_k - R_k) - (\xi_{v,k} + \mu_k)S_k \\ &\leq \frac{(\omega_{v,k} + \mu_k)\Pi_k}{\mu_k} - (\omega_{v,k} + \xi_{v,k} + \mu_k)S_k = (\omega_{v,k} + \xi_{v,k} + \mu_k)(S_k^* - S_k).\end{aligned}$$

So, if $S_k > S_k^*$, then $\dot{S}_k < 0$; hence $S_k \leq S_k^*$ given $S_k(0) \leq S_k^*$ is true. Following a similar argument, one can show that $\dot{V}_k \leq -(\omega_{v,k} + \mu_k)V_k + \xi_{v,k}S_k = (\omega_{v,k} + \mu_k)(V_k^* - V_k)$. If $V_k > V_k^*$ then $\dot{V}_k < 0$; hence $V_k \leq V_k^*$ given $V_k(0) \leq V_k^*$ is true.

It follows from these bounds that the region

$$\tilde{\Omega}_2^{\Delta} = \{(S_1, S_2, V_1, V_2, E_1, E_2, P_1, P_2, I_1, I_2, A_1, A_2, H_1, H_2, R_1, R_2) \in \Omega_2 : S_k \leq S_k^*, V_k \leq V_k^*\},$$

is also positively invariant and attracts all solutions in Ω_2. It is convenient to define the following

$$\begin{aligned}&\bar{a}_k = \sigma_k + \mu_k, \quad \bar{b}_k = \psi_k + \mu_k, \quad \bar{c}_k = \psi_k + \gamma_{I,k} + \mu_k + \delta_{I,k}, \\ &\bar{d}_k = \gamma_{A,k} + \mu_k, \quad \bar{e}_k = \gamma_{H,k} + \mu_k + \delta_{H,k}, \\ &W_{kl} = \frac{S_k + (1 - \epsilon_{v,k})V_k}{\Pi_l/\mu_l}, \quad W_{kl}^* = \frac{S_k^* + (1 - \epsilon_{v,k})V_k^*}{N_l^*},\end{aligned} \tag{I.1}$$

Since $S_k^* \geq S_k$, $V_k^* \geq V_k$, observe that

$$W_{kl}^* \geq W_{kl}. \tag{I.2}$$

The equations of the infected component of this special case of the model (4.1) can be re-written in terms of the next generation matrices F_2 and $V_2^{\Delta} = V_2|_{\delta_{I,k} = \delta_{H,k} = 0}$, given in Appendix H as:

$$\frac{d}{dt}\begin{pmatrix} E_1(t) \\ E_2(t) \\ P_1(t) \\ P_2(t) \\ I_1(t) \\ I_2(t) \\ A_1(t) \\ A_2(t) \\ H_1(t) \\ H_2(t) \end{pmatrix} = (F_2 - V_2^{\Delta})\begin{pmatrix} E_1(t) \\ E_2(t) \\ P_1(t) \\ P_2(t) \\ I_1(t) \\ I_2(t) \\ A_1(t) \\ A_2(t) \\ H_1(t) \\ H_2(t) \end{pmatrix} - J_2\begin{pmatrix} E_1(t) \\ E_2(t) \\ P_1(t) \\ P_2(t) \\ I_1(t) \\ I_2(t) \\ A_1(t) \\ A_2(t) \\ H(t) \\ H_2(t) \end{pmatrix}, \tag{I.3}$$

where,

$$F_2 - V_2^{\Delta} = \begin{bmatrix} -\bar{a}_1 & 0 & f_{1,3} & f_{1,4} & f_{1,5} & f_{1,6} & f_{1,7} & f_{1,8} & f_{1,9} & f_{1,10} \\ 0 & -\bar{a}_2 & f_{2,3} & f_{2,4} & f_{2,5} & f_{2,6} & f_{2,7} & f_{2,8} & f_{2,9} & f_{2,10} \\ \sigma_1 & 0 & -\bar{b}_1 & 0 & 0 & 0 & 0 & 0 & 0 & 0 \\ 0 & \sigma_2 & 0 & -\bar{b}_2 & 0 & 0 & 0 & 0 & 0 & 0 \\ 0 & 0 & r_1\psi_1 & 0 & -\bar{c}_1 & 0 & 0 & 0 & 0 & 0 \\ 0 & 0 & 0 & r_2\psi_2 & 0 & -\bar{c}_2 & 0 & 0 & 0 & 0 \\ 0 & 0 & (1-r_1)\psi_1 & 0 & 0 & 0 & -\bar{d}_1 & 0 & 0 & 0 \\ 0 & 0 & 0 & (1-r_2)\psi_2 & 0 & 0 & 0 & -\bar{d}_2 & 0 & 0 \\ 0 & 0 & 0 & 0 & \varphi_1 & 0 & 0 & 0 & -\bar{e}_1 & 0 \\ 0 & 0 & 0 & 0 & 0 & \varphi_2 & 0 & 0 & 0 & -\bar{e}_2 \end{bmatrix}, \tag{I.4}$$

and,

$$J_2 = \begin{pmatrix} 0 & 0 & J_{1,3} & J_{1,4} & J_{1,5} & J_{1,6} & J_{1,7} & J_{1,8} & J_{1,9} & J_{1,10} \\ 0 & 0 & J_{2,3} & J_{2,4} & J_{2,5} & J_{2,6} & J_{2,7} & J_{2,8} & J_{2,9} & J_{2,10} \\ 0 & 0 & 0 & 0 & 0 & 0 & 0 & 0 & 0 & 0 \\ 0 & 0 & 0 & 0 & 0 & 0 & 0 & 0 & 0 & 0 \\ 0 & 0 & 0 & 0 & 0 & 0 & 0 & 0 & 0 & 0 \\ 0 & 0 & 0 & 0 & 0 & 0 & 0 & 0 & 0 & 0 \\ 0 & 0 & 0 & 0 & 0 & 0 & 0 & 0 & 0 & 0 \\ 0 & 0 & 0 & 0 & 0 & 0 & 0 & 0 & 0 & 0 \\ 0 & 0 & 0 & 0 & 0 & 0 & 0 & 0 & 0 & 0 \\ 0 & 0 & 0 & 0 & 0 & 0 & 0 & 0 & 0 & 0 \end{pmatrix}, \tag{I.5}$$

with

$$\begin{aligned} J_{1,3} &= a_1 c_{11}\mathcal{P}_{P,1}(W_{11}^* - W_{11}), & J_{1,4} &= a_1 c_{12}\mathcal{P}_{P,2}(W_{12}^* - W_{12}), \\ J_{1,5} &= a_1 c_{11}\mathcal{P}_{I,1}(W_{11}^* - W_{11}), & J_{1,6} &= a_1 c_{12}\mathcal{P}_{I,2}(W_{12}^* - W_{12}), \\ J_{1,7} &= a_1 c_{11}\mathcal{P}_{A,1}(W_{11}^* - W_{11}), & J_{1,8} &= a_1 c_{12}\mathcal{P}_{A,2}(W_{12}^* - W_{12}), \\ J_{1,9} &= a_1 c_{11}\mathcal{P}_{H,1}(W_{11}^* - W_{11}), & J_{1,10} &= a_1 c_{12}\mathcal{P}_{H,2}(W_{12}^* - W_{12}), \\ J_{2,3} &= a_2 c_{21}\mathcal{P}_{P,1}(W_{21}^* - W_{21}), & J_{2,4} &= a_2 c_{22}\mathcal{P}_{P,2}(W_{22}^* - W_{22}), \\ J_{2,5} &= a_2 c_{21}\mathcal{P}_{I,1}(W_{21}^* - W_{21}), & J_{2,6} &= a_2 c_{22}\mathcal{P}_{I,2}(W_{22}^* - W_{22}), \\ J_{2,7} &= a_2 c_{21}\mathcal{P}_{A,1}(W_{21}^* - W_{21}), & J_{2,8} &= a_2 c_{22}\mathcal{P}_{A,2}(W_{22}^* - W_{22}), \\ J_{2,9} &= a_2 c_{21}\mathcal{P}_{H,1}(W_{21}^* - W_{21}), & J_{2,10} &= a_2 c_{22}\mathcal{P}_{H,2}(W_{22}^* - W_{22}). \end{aligned} \tag{I.6}$$

Since (I.2) holds, J_2 is a non-negative matrix. Thus, Equation (I.3) can be re-written as the following inequality:

$$\frac{d}{dt}\begin{pmatrix} E_1(t) \\ E_2(t) \\ P_1(t) \\ P_2(t) \\ I_1(t) \\ I_2(t) \\ A_1(t) \\ A_2(t) \\ H_1(t) \\ H_2(t) \end{pmatrix} \leq (F - V)\begin{pmatrix} E_1(t) \\ E_2(t) \\ P_1(t) \\ P_2(t) \\ I_1(t) \\ I_2(t) \\ A_1(t) \\ A_2(t) \\ H_1(t) \\ H_2(t) \end{pmatrix}. \tag{I.7}$$

If $\mathcal{R}_v^{\Delta} < 1$, then $\rho(F_2 {V_2^{\Delta}}^{-1}) < 1$, which is equivalent to all eigenvalues of $F - V^{\diamond}$ matrix being negative (Pauline van den Driessche & Watmough, 2002). Hence, the linearized differential inequality (D.5) is stable whenever $\mathcal{R}_v^{\diamond} < 1$, so

$(E_1(t), E_2(t), P_1(t), P_2(t), I_1(t), I_2(t), A_1(t), A_2(t), H_1(t), H_2(t)) \to (0,0,0,0,0,0,0,0,0,0)$ as $t \to \infty$ for this linear ODE system. It follows, using a standard comparison theorem (Lakshmikantham et al., 1989), that:

$(E_1(t),\ E_2(t),\ P_1(t),\ P_2(t),\ I_1(t),\ I_2(t),\ A_1(t),\ A_2(t),\ H_1(t),\ H_2(t)) \to (0,\ 0,\ 0,\ 0,\ 0,\ 0,\ 0,\ 0,\ 0,\ 0)$. Substituting $E_k(t) = P_k(t) = I_k(t) = A_k(t) = H_k(t) = 0$, into the equations for $\dot{S}$, $\dot{V}$, and $\dot{R}$ of the homogeneous model (3.1) gives:

$$S_k(t)\to S_k^*, V_k(t)\to V_k^* \text{ and } R_k(t)\to 0, \text{ as } t\to\infty.$$

Hence, the disease-free equilibrium of the special case of the two-group model (4.1) with negligible disease-induced mortality (i.e, (4.1) with $\delta_I = \delta_H = 0$) is globally-asymptomatically stable in Ω_2^Δ, whenever $\mathcal{R}_v^\Delta < 1$. □

References

Almagor, J., & Picascia, S. (2020). Exploring the effectiveness of a COVID-19 contact tracing app using an agent-based model. *Scientific Reports, 10*(1), 1–11.

Anderson, R. M., & May, R. M. (1985). Vaccination and herd immunity to infectious diseases. *Nature, 318*(6044), 323–329.

Andrews, N., Stowe, J., Kirsebom, F., Toffa, S., Rickeard, T., Gallagher, E., Gower, C., Kall, M., Groves, N., O'Connell, A.-M., et al. (2022). COVID-19 vaccine effectiveness against the Omicron (B. 1.1. 529) variant. *New England Journal of Medicine, 386*(16), 1532–1546.

Applegate, W. B., & Ouslander, J. G. (2020). COVID-19 presents high risk to older persons. *Journal of the American Geriatrics Society, 68*(4), 681.

Arias, E., Tejada-Vera, B., & Ahmad, F. (2020). Provisional life expectancy estimates for January through June. https://www.cdc.gov/coronavirus/2019-ncov/hcp/planning-scenarios.html. (Accessed 20 May 2021). February 2020.

Bergman, A., Sella, Y., Agre, P., & Casadevall, A. (2020). Oscillations in US COVID-19 incidence and mortality data reflect diagnostic and reporting factors. *mSystems, 5*(4).

Blower, S. M., & Dowlatabadi, H. (1994). Sensitivity and uncertainty analysis of complex models of disease transmission: An HIV model, as an example. *International Statistical Review/Revue Internationale de Statistique*, 229–243.

Bo, Y., Guo, C., Lin, C., Zeng, Y., Bi Li, H., Zhang, Y., Hossain, M. S., Chan, J. W. M., Yeung, D. W., Kwok, K. O., et al. (2021). Effectiveness of non-pharmaceutical interventions on COVID-19 transmission in 190 countries from 23 January to 13 April 2020. *International Journal of Infectious Diseases, 102*, 247–253.

Boloye Gomero. (2012). *Latin hypercube sampling and partial rank correlation coefficient analysis applied to an optimal control problem*. TRACE.

Bosman, J., & Mervosh, S. (2020). As virus surges, younger people account for 'disturbing' number of cases. https://www.nytimes.com/2020/06/25/us/coronavirus-cases-young-people.html. (Accessed 18 September 2023).

Britton, T., Ball, F., & Trapman, P. (2020). A mathematical model reveals the influence of population heterogeneity on herd immunity to SARS-CoV-2. *Science, 369*(6505), 846–849.

Brozak, S. J., Pant, B., Safdar, S., & Gumel, A. B. (2021). *Dynamics of COVID-19 pandemic in India and Pakistan: A metapopulation modelling approach*. Infectious Disease Modelling.

Bruxvoort, K. J., Sy, L. S., Qian, L., Ackerson, B. K., Luo, Y., Lee, G. S., Tian, Y., Florea, A., Aragones, M., Tubert, J. E., et al. (2021). Effectiveness of mRNA-1273 against delta, mu, and other emerging variants of SARS-CoV-2: Test negative case-control study. *BMJ, 375*.

Callender, L. A., Curran, M., Bates, S. M., Mairesse, M., Weigandt, J., & Betts, C. J. (2020). The impact of pre-existing comorbidities and therapeutic interventions on COVID-19. *Frontiers in Immunology, 11*, 1991.

Calvetti, D., Hoover, A. P., Rose, J., & Somersalo, E. (2020). Metapopulation network models for understanding, predicting, and managing the coronavirus disease COVID-19. *Frontiers in Physics, 8*, 261.

Cavazzoni, P. (2022). Coronavirus (COVID-19) update: FDA limits use of certain monoclonal antibodies to treat COVID-19 due to the Omicron variant. *US Food and Drug Administration*.

CDC. Deaths by select demographic and geographic characteristics. https://www.cdc.gov/nchs/nvss/vsrr/covid_weekly/index.htm. Accessed September 04, 2023..

CDC. Laboratory-confirmed COVID-19-associated hospitalizations. https://gis.cdc.gov/grasp/covidnet/covid19_5.html. Accessed September 04, 2023..

CDC. (2021). *CDC COVID-19 study shows mRNA vaccines reduce risk of infection by 91 percent for fully vaccinated people*.

CDPH. COVID-19 age, race and ethnicity data. https://www.cdph.ca.gov/Programs/CID/DCDC/Pages/COVID-19/Age-Race-Ethnicity.aspx. Accessed September 04, 2023..

Centers for Disease Control and Prevention (CDC). (2021). *Requirement for proof of COVID-19 vaccination for air passengers*.

Centers for Disease Control and Prevention. (2020). COVID-19 pandemic planning scenarios. https://www.cdc.gov/coronavirus/2019-ncov/hcp/planning-scenarios.html. (Accessed 20 May 2021).

Centers for Disease Control and Prevention. (2022). Frequently asked questions about COVID-19 vaccination. https://www.cdc.gov/coronavirus/2019-ncov/vaccines/faq.html. (Accessed 13 June 2022).

Chen, Y.-H., Glymour, M., Riley, A., Balmes, J., Duchowny, K., Harrison, R., Matthay, E., & Bibbins-Domingo, K. (2021). Excess mortality associated with the COVID-19 pandemic among Californians 18–65 years of age, by occupational sector and occupation: March through November 2020. *PLoS One, 16*(6), Article e0252454.

Chen, Y.-H., Riley, A. R., Duchowny, K. A., Aschmann, H. E., Chen, R., Kiang, M. V., Mooney, A. C., Stokes, A. C., Glymour, M. M., & Bibbins-Domingo, K. (2022). COVID-19 mortality and excess mortality among working-age residents in California, USA, by occupational sector: A longitudinal cohort analysis of mortality surveillance data. *The Lancet Public Health, 7*(9), e744–e753.

Christensen, P. A., Olsen, R. J., Long, S. W., Snehal, R., Davis, J. J., Saavedra, M. O., Reppond, K., Shyer, M. N., Cambric, J., Gadd, R., et al. (2022). Signals of significantly increased vaccine breakthrough, decreased hospitalization rates, and less severe disease in patients with coronavirus disease 2019 caused by the Omicron variant of severe acute respiratory syndrome coronavirus 2 in Houston, Texas. *American Journal Of Pathology, 192*(4), 642–652.

COVID-19 map. https://coronavirus.jhu.edu/map.html. Accessed 2022-09-17..

CSSE at Johns Hopkins University. (2020). CSSE GIS and data COVID-19. https://github.com/CSSEGISandData/COVID-19.

Danielle Iuliano, A., Brunkard, J. M., Boehmer, T. K., Peterson, E., Adjei, S., Binder, A. M., Cobb, S., Graff, P., Hidalgo, P., Panaggio, M. J., et al. (2022). Trends in disease severity and health care utilization during the early Omicron variant period compared with previous SARS-CoV-2 high transmission periods United States, December 2020–January 2022. *Morbidity and Mortality Weekly Report, 71*(4), 146–152.

Darroch, G. (2021). The original coronavirus strain has almost disappeared in the US. One chart shows how variants took over. https://www.businessinsider.com/original-coronavirus-strain-replaced-by-variants-us-chart-2021-6. (Accessed 18 September 2023).

Diekmann, O., Heesterbeek, J. A. P., & Metz, J. A. J. (1990). On the definition and the computation of the basic reproduction ratio ${\mathcal{R}}_{0}$ in models for infectious diseases in heterogeneous populations. *Journal of Mathematical Biology, 28*(4), 365–382.

Djaharuddin, I., Munawwarah, S., Nurulita, A., Ilyas, M., Ahmad Tabri, N., & Lihawa, N. (2021). Comorbidities and mortality in COVID-19 patients. *Gaceta Sanitaria, 35*, S530–S532.

Duong, D. (2021). *Alpha, Beta, Delta, Gamma: What's important to know about SARS-CoV-2 variants of concern?*.

Eikenberry, S. E., Mancuso, M., Iboi, E., Phan, T., Eikenberry, K., Kuang, Y., Kostelich, E., & Gumel, A. B. (2020). To mask or not to mask: Modeling the potential for face mask use by the general public to curtail the COVID-19 pandemic. *Infectious Disease Modelling, 5*, 293–308.

Elamin H Elbasha and Abba B Gumel. (2021). Vaccination and herd immunity thresholds in heterogeneous populations. *medRxiv*.

Emilia Paladino, M., Riva, M. A., Belingheri, M., et al. (2021). COVID-19 vaccination and asymptomatic infection: Effect of BNT162b2 mRNA vaccine on the incidence of COVID-19 and duration of sick leave among healthcare workers. *Journal of Occupational and Environmental Medicine, 63*(12), e868.

Epstein, B., & Lofquist, D. (2021). US Census Bureau Today delivers state population totals for congressional apportionment. *US Census Bureau*. https://www.census.gov/library/stories/2021/04/2020-census-data-release.html.

Esteva, L., Gumel, A. B., & De LeóN, C. V. (2009). Qualitative study of transmission dynamics of drug-resistant malaria. *Mathematical and Computer Modelling, 50*(3–4), 611–630.

Esteva, L., & Vargas, C. (2000). Influence of vertical and mechanical transmission on the dynamics of dengue disease. *Mathematical Biosciences, 167*(1), 51–64.
Faes, C., Abrams, S., Van Beckhoven, D., Meyfroidt, G., Vlieghe, E., Hens, N., & Belgian Collaborative Group on COVID-19 Hospital Surveillance. (2020). Time between symptom onset, hospitalisation and recovery or death: Statistical analysis of Belgian COVID-19 patients. *International Journal of Environmental Research and Public Health, 17*(20), 7560.
FDA. (2022). COVID-19 pandemic planning scenarios. https://www.fda.gov/emergency-preparedness-and-response/coronavirus-disease-2019-covid-19/covid-19-vaccines. (Accessed 21 October 2022).
Ferguson, N. M., Laydon, D., Nedjati-Gilani, G., Imai, N., Ainslie, K., Baguelin, M., Bhatia, S., Boonyasiri, A., Cucunuba, Z., Cuomo-Dannenburg, G., Dighe, A., Dorigatti, I., Fu, H., Gaythorpe, K., Green, W., Hamlet, A., Hinsley, W., Okell, L. C., van Elsland, S., … Ghani, A. C. (2020b). *Report 9: Impact of non-pharmaceutical interventions (NPIs) to reduce COVID19 mortality and healthcare demand*. Imperial College London. Technical report.
Ferguson, N. M., Laydon, D., Nedjati-Gilani, G., Imai, N., Ainslie, K., Baguelin, M., Bhatia, S., Boonyasiri, A., Cucunubá, Z., Cuomo-Dannenburg, G., et al. (2020a). *Impact of non-pharmaceutical interventions (NPIs) to reduce COVID-19 mortality and healthcare demand*. Imperial College.
Flaxman, S., Mishra, S., Gandy, A., Unwin, H. J. T., Mellan, T. A., Coupland, H., Whittaker, C., Zhu, H., Berah, T., Eaton, J. W., et al. (2020). Estimating the effects of non-pharmaceutical interventions on COVID-19 in Europe. *Nature, 584*(7820), 257–261.
Freed, M., Cubanski, J., Neuman, T., Kates, J., & Michaud, J. (2021). *What share of people who have died of COVID-19 are 65 and older—and how does it vary by state?* Kaiser Family Foundation. https://www.kff.org/coronavirus-covid-19/issue-brief/what-share-of-people-who-have-died-of-covid-19-are-65-and-older-and-how-does-it-vary-by-state.
Freedman, H. I., & So, J. W.-H. (1985). Global stability and persistence of simple food chains. *Mathematical Biosciences, 76*(1), 69–86.
Gao, S., Pant, B., Williams Chukwu, C., Kwofie, T., Safdar, S., Newman, L., Choe, S., Datta, B. K., Attipoe, W. K., Zhang, W., et al. (2023). A mathematical model to assess the impact of testing and isolation compliance on the transmission of COVID-19. *Infectious Disease Modelling, 8*(2), 427–444.
Glasser, J., Feng, Z., Moylan, A., Valle, S. D., & Castillo-Chavez, C. (2012). Mixing in age-structured population models of infectious diseases. *Mathematical Biosciences, 235*(1), 1–7.
Gumel, A. B. (2009). Global dynamics of a two-strain avian influenza model. *International Journal of Computer Mathematics, 86*(1), 85–108.
Gumel, A. B. (2012). Causes of backward bifurcations in some epidemiological models. *Journal of Mathematical Analysis and Applications, 395*(1), 355–365.
Gumel, A. B., Iboi, E. A., Ngonghala, C. N., & Elbasha, E. H. (2021). A primer on using mathematics to understand COVID-19 dynamics: Modeling, analysis and simulations. *Infectious Disease Modelling, 6*, 148–168.
Gumel, A. B., Iboi, E. A., Ngonghala, C. N., & Ngwa, G. A. (2021). Toward achieving a vaccine-derived herd immunity threshold for COVID-19 in the US. *Frontiers in Public Health, 9*.
Gumel, A. B., McCluskey, C. C., & van den Driessche, P. (2006). Mathematical study of a staged-progression HIV model with imperfect vaccine. *Bulletin of Mathematical Biology, 68*(8), 2105–2128.
Guo, H., & Yi Li, M. (2006). Global dynamics of a staged progression model for infectious diseases. *Mathematical Biosciences and Engineering, 3*(3), 513.
Haischer, M. H., Beilfuss, R., Rose Hart, M., Opielinski, L., Wrucke, D., Zirgaitis, G., Uhrich, T. D., & Hunter, S. K. (2020). Who is wearing a mask? Gender-, age-, and location-related differences during the COVID-19 pandemic. *PLoS One, 15*(10), Article e0240785.
Hale, J. K. (1969). *Ordinary differential equations*. New York: John Wiley and Sons.
Hethcote, H. W. (2000). The mathematics of infectious diseases. *SIAM Review, 42*(4), 599–653.
Hethcote, H. W., & Thieme, H. R. (1985). Stability of the endemic equilibrium in epidemic models with subpopulations. *Mathematical Biosciences, 75*(2), 205–227.
Hinch, R., Probert, W. J. M., Nurtay, A., Kendall, M., Wymant, C., Hall, M., Lythgoe, K., Cruz, A. B., Zhao, L., Stewart, A., et al. (2021). OpenABM-COVID-19—an agent-based model for non-pharmaceutical interventions against COVID-19 including contact tracing. *PLoS Computational Biology, 17*(7), Article e1009146.
Hoertel, N., Blachier, M., Blanco, C., Olfson, M., Massetti, M., Sánchez Rico, M., Limosin, F., & Leleu, H. (2020). A stochastic agent-based model of the SARS-CoV-2 epidemic in France. *Nature Medicine, 26*(9), 1417–1421.
Horst, R. T. (1985). Local stability in epidemic models for heterogeneous populations. In *Mathematics in Biology and Medicine* (pp. 185–189). Springer.
Huang, C.-J., Chen, Y.-H., Ma, Y., & Kuo, P.-H. (2020). Multiple-input deep convolutional neural network model for COVID-19 forecasting in China. *medRxiv*.
Huff, H. V., & Singh, A. (2020). Asymptomatic transmission during the coronavirus disease 2019 pandemic and implications for public health strategies. *Clinical Infectious Diseases, 71*(10), 2752–2756.
Iboi, E. A., Ngonghala, C. N., & Gumel, A. B. (2020a). *Will an imperfect vaccine curtail the COVID-19 pandemic in the US? Infectious disease Modelling* (Vol. 5, pp. 510–524).
Iboi, E. A., Ngonghala, C. N., & Gumel, A. B. (2020b). *Will an imperfect vaccine curtail the COVID-19 pandemic in the U.S.? Infectious disease Modelling* (Vol. 5, pp. 510–524).
Improving public health policy in Europe through modelling and economic evaluation of interventions for the control of infectious diseases. https://cordis.europa.eu/project/id/502084/reporting. Accessed September 06, 2023..
Ing, E. B., Xu, Q., Salimi, A., & Torun, N. (2020). Physician deaths from corona virus (COVID-19) disease. *Occupational Medicine, 70*(5), 370–374.
Iyengar, K. P., Ish, P., Kumar Upadhyaya, G., Malhotra, N., Vaishya, R., & Jain, V. K. (2020). COVID-19 and mortality in doctors. *Diabetes & Metabolic Syndrome: Clinical Research Reviews, 14*(6), 1743–1746.
Jeffrey, V. L., Ratzan, S. C., Palayew, A., Gostin, L. O., Larson, H. J., Rabin, K., Kimball, S., & El-Mohandes, A. (2021). A global survey of potential acceptance of a COVID-19 vaccine. *Nature Medicine, 27*(2), 225–228.
Karaivanov, A. (2020). A social network model of COVID-19. *PLoS One, 15*(10), Article e0240878.
Katella, K. (2022). *Omicron, Delta, Alpha, and more: What to know about the coronavirus variants*. Yale Medicine, 28th February, available at: https://www.yalemedicine.org/news/covid-19-variants-of-concern-omicron (accessed 8th March, 2022).
Kenneth, D. K., Xu, J., & Arias, E. (2019). Mortality in the United States. https://www.cdc.gov/nchs/data/databriefs/db395-H.pdf.
Kerr, C. C., Stuart, R. M., Mistry, D., Abeysuriya, R. G., Rosenfeld, K., Hart, G. R., Núñez, R. C., Cohen, J. A., Selvaraj, P., Hagedorn, B., et al. (2021). Covasim: An agent-based model of COVID-19 dynamics and interventions. *PLoS Computational Biology, 17*(7), Article e1009149.
Khalife, J., & VanGennep, D. (2021). COVID-19 herd immunity in the absence of a vaccine: An irresponsible approach. *Epidemiology and Health, 43*.
Kim, Y. R., Choi, Y.-J., & Min, Y. (2022). A model of covid-19 pandemic with vaccines and mutant viruses. *PLoS One, 17*(10), Article e0275851.
Kissler, S. M., Tedijanto, C., Goldstein, E., Grad, Y. H., & Lipsitch, M. (2020). Projecting the transmission dynamics of SARS-CoV-2 through the postpandemic period. *Science, 368*(6493), 860–868. Publisher: American Association for the Advancement of Science Section: Report.
Kricorian, K., Civen, R., & Equils, O. (2022). COVID-19 vaccine hesitancy: Misinformation and perceptions of vaccine safety. *Human Vaccines & Immunotherapeutics, 18*(1), Article 1950504.
Kriss, J. L., Hung, M.-C., Srivastav, A., Black, C. L., Lindley, M. C., Lee, J. T., Koppaka, R., Tsai, Y., Lu, P.-J., Yankey, D., et al. (2022). COVID-19 vaccination coverage, by race and ethnicity—national immunization survey adult COVID module, United States, December 2020–November 2021. *Morbidity and Mortality Weekly Report, 71*(23), 757.
Lakshmikantham, V., Leela, S., & Martynyuk, A. A. (1989). *Stability analysis of nonlinear systems*. Springer.
Lauring, A. S., Tenforde, M. W., Chappell, J. D., Gaglani, M., Ginde, A. A., McNeal, T., Ghamande, S., Douin, D. J., Talbot, H. K., Casey, J. D., et al. (2022). Clinical severity of, and effectiveness of mRNA vaccines against, COVID-19 from Omicron, delta, and alpha SARS-CoV-2 variants in the United States: Prospective observational study. *BMJ, 376*.
Lisa Lockerd Maragakis. (2020). Coronavirus and COVID-19: Younger adults are at risk, too. https://www.hopkinsmedicine.org/health/conditions-and-diseases/coronavirus/coronavirus-and-covid-19-younger-adults-are-at-risk-too. (Accessed 18 September 2023).

Lopez Bernal, J., Andrews, N., Gower, C., Gallagher, E., Simmons, R., Thelwall, S., Stowe, J., Tessier, E., Groves, N., Dabrera, G., et al. (2021). Effectiveness of COVID-19 vaccines against the B. 1.617. 2 (Delta) variant. *New England Journal of Medicine, 385*(7), 585–594.
Lopez Bernal, J., Andrews, N., Gower, C., Robertson, C., Stowe, J., Tessier, E., Simmons, R., Cottrell, S., Roberts, R., O'Doherty, M., et al. (2021). Effectiveness of the Pfizer-BioNTech and Oxford-AstraZeneca vaccines on COVID-19 related symptoms, hospital admissions, and mortality in older adults in england: Test negative case-control study. *Bmj, 373*.
Ma, Q., Liu, J., Liu, Q., Kang, L., Liu, R., Jing, W., Wu, Y., & Liu, M. (2021). Global percentage of asymptomatic SARS-CoV-2 infections among the tested population and individuals with confirmed COVID-19 diagnosis: A systematic review and meta-analysis. *JAMA Network Open, 4*(12), Article e2137257–e2137257.
Mancuso, M., Eikenberry, S. E., & Gumel, A. B. (2021). Will vaccine-derived protective immunity curtail COVID-19 variants in the US? *Infectious Disease Modelling, 6*, 1110–1134.
Marino, S., Hogue, I. B., Ray, C. J., & Kirschner, D. E. (2008). A methodology for performing global uncertainty and sensitivity analysis in systems biology. *Journal of Theoretical Biology, 254*(1), 178–196.
Matz, M., Allemani, C., van Tongeren, M., Nafilyan, V., Rhodes, S., van Veldhoven, K., Pembrey, L., Coleman, M. P., & Pearce, N. (2022). Excess mortality among essential workers in england and wales during the COVID-19 pandemic. *Journal of Epidemiology & Community Health, 76*(7), 660–666.
McLeod, R. G., Brewster, J. F., Gumel, A. B., & Slonowsky, A. (2006). Sensitivity and uncertainty analyses for a SARS model with time-varying inputs and outputs. *Mathematical Biosciences and Engineering, 3*(3), 527.
Moline, H. L., Whitaker, M., Deng, L., Rhodes, J. C., Milucky, J., Pham, H., Patel, K., Anglin, O., Reingold, A., Chai, S. J., et al. (2021). Effectiveness of COVID-19 vaccines in preventing hospitalization among adults aged $\geq$ 65 years—COVID-NET, 13 states, February–April 2021. *Morbidity and Mortality Weekly Report, 70*(32), 1088.
Morens, D. M., & Fauci, A. S. (2007). The 1918 influenza pandemic: Insights for the 21st century. *The Journal of Infectious Diseases, 195*(7), 1018–1028.
Mossong, J., Hens, N., Jit, M., Beutels, P., Auranen, K., Mikolajczyk, R., Massari, M., Salmaso, S., Tomba, G. S., Wallinga, J., et al. (2008). Social contacts and mixing patterns relevant to the spread of infectious diseases. *PLoS Medicine, 5*(3), Article e74.
Mutambudzi, M., Niedzwiedz, C., Macdonald, E. B., Leyland, A., Mair, F., Anderson, J., Celis-Morales, C., Cleland, J., Forbes, J., Gill, J., et al. (2021). Occupation and risk of severe COVID-19: Prospective cohort study of 120075 UK Biobank participants. *Occupational and Environmental Medicine, 78*(5), 307–314.
Nasreen, S., Chung, H., He, S., Brown, K. A., Gubbay, J. B., Buchan, S. A., Fell, D. B., Austin, P. C., Schwartz, K. L., Sundaram, M. E., et al. (2022). Effectiveness of COVID-19 vaccines against symptomatic SARS-CoV-2 infection and severe outcomes with variants of concern in Ontario. *Nature Microbiology, 7*(3), 379–385.
NCIRD. (2022). COVID-19 vaccination and case trends by age group, United States. https://data.cdc.gov/Vaccinations/COVID-19-Vaccination-and-Case-Trends-by-Age-Group-/gxj9-t96f.
Neely, S. R., Eldredge, C., Ersing, R., & Remington, C. (2022). Vaccine hesitancy and exposure to misinformation: A survey analysis. *Journal of General Internal Medicine, 37*(1), 179–187.
Ngonghala, C. N., Iboi, E., Eikenberry, S., Scotch, M., Raina MacIntyre, C., Bonds, M. H., & Gumel, A. B. (2020). Mathematical assessment of the impact of non-pharmaceutical interventions on curtailing the 2019 novel coronavirus. *Mathematical Biosciences, 325*, Article 108364.
Ngonghala, C. N., Iboi, E. A., & Gumel, A. B. (2020). *Could masks curtail the post-lockdown resurgence of COVID-19 in the US? Mathematical Biosciences* (Vol. 329), Article 108452.
Ngonghala, C. N., Knitter, J. R., Marinacci, L., Bonds, M. H., & Gumel, A. B. (2021). Assessing the impact of widespread respirator use in curtailing COVID-19 transmission in the USA. *Royal Society Open Science, 8*(9), Article 210699.
Ngonghala, C. N., Taboe, H. B., & Gumel, A. B. (2022). Dynamics of the delta and Omicron variants of SARS-CoV-2 in the United States: The battle of supremacy in the presence of vaccination, mask usage and antiviral treatment. *medRxiv*.
NIH. NIH clinical trial shows Remdesivir accelerates recovery from advanced COVID-19. https://www.nih.gov/news-events/news-releases/nih-clinical-trial-shows-remdesivir-accelerates-recovery-advanced-covid-19, April 2020. Accessed August 28, 2023..
Nikolai, L. A., Meyer, C. G., Kremsner, P. G., & Velavan, T. P. (2020). Asymptomatic SARS coronavirus 2 infection: Invisible yet invincible. *International Journal of Infectious Diseases, 100*, 112–116.
Nishiura, H., & Chowell, G. (2009). The effective reproduction number as a prelude to statistical estimation of time-dependent epidemic trends. In *Mathematical and statistical estimation approaches in epidemiology* (pp. 103–121). Springer.
Oliver, S. E., Gargano, J. W., Scobie, H., Wallace, M., Hadler, S. C., Leung, J., Blain, A. E., McClung, N., Campos-Outcalt, D., Morgan, R. L., et al. (2021). The advisory committee on immunization practices' interim recommendation for use of Janssen COVID-19 vaccine—United States, February 2021. *Morbidity and Mortality Weekly Report, 70*(9), 329.
Omame, A., Sene, N., Nometa, I., Nwakanma, C. I., Nwafor, E. U., Iheonu, N. O., & Okuonghae, D. (2021). Analysis of COVID-19 and comorbidity co-infection model with optimal control. *Optimal Control Applications and Methods, 42*(6), 1568–1590.
Pant, B., Safdar, S., Santillana, M., & Gumel, A. (2024). Mathematical assessment of the role of human behavior changes on sars-cov-2 transmission dynamics. *medRxiv*, 2024–02.
Paul, P., Marie France, A., Aoki, Y., Batra, D., Biggerstaff, M., Dugan, V., Galloway, S., Hall, A. J., Johansson, M. A., Kondor, R. J., et al. (2021). Genomic surveillance for SARS-CoV-2 variants circulating in the United States, December 2020–May 2021. *Morbidity and Mortality Weekly Report, 70*(23), 846.
Peeling, R. W., Olliaro, P. L., Boeras, D. I., & Fongwen, N. (2021). Scaling up COVID-19 rapid antigen tests: Promises and challenges. *The Lancet Infectious Diseases, 21*(9), e290–e295.
Pfizer. (2020). Pfizer and BioNTech celebrate historic first authorization in the US of vaccine to prevent COVID-19. https://www.pfizer.com/news/press-release/press-release-detail/pfizer-and-biontech-celebrate-historic-first-authorization.
Powell, T., Bellin, E., & Ehrlich, A. R. (2020). Older adults and COVID-19: The most vulnerable, the hardest hit. *Hastings Center Report, 50*(3), 61–63.
Prem, K., Cook, A. R., & Jit, M. (2017). Projecting social contact matrices in 152 countries using contact surveys and demographic data. *PLoS Computational Biology, 13*(9), Article e1005697.
Rahimi, I., Chen, F., & Gandomi, A. H. (2021). A review on COVID-19 forecasting models. *Neural Computing & Applications*, 1–11.
Rahmani, K., Shavaleh, R., Forouhi, M., Disfani, H. F., Kamandi, M., Oskooi, R. K., Foogerdi, M., Soltani, M., Rahchamani, M., Mohaddespour, M., et al. (2022). The effectiveness of COVID-19 vaccines in reducing the incidence, hospitalization, and mortality from COVID-19: A systematic review and meta-analysis. *Frontiers in Public Health, 10*, 2738.
Richard, Q., Alizon, S., Choisy, M., Sofonea, M. T., & Djidjou-Demasse, R. (2021). Age-structured non-pharmaceutical interventions for optimal control of COVID-19 epidemic. *PLoS Computational Biology, 17*(3), Article e1008776.
Roy, M. A. (1992). The concept of herd immunity and the design of community-based immunization programmes. *Vaccine, 10*(13), 928–935.
Safdar, S., Ngonghala, C. N., & Gumel, A. (2022). Mathematical assessment of the role of waning and boosting immunity against the BA. 1 Omicron variant in the United States. *medRxiv*.
Safi, M. A., & Gumel, A. B. (2010). Global asymptotic dynamics of a model for quarantine and isolation. *Discrete Contin. Dyn. Syst. Ser. B, 14*(1), 209–231.
Sah, P., Fitzpatrick, M. C., Zimmer, C. F., Abdollahi, E., Juden-Kelly, L., Moghadas, S. M., Singer, B. H., & Galvani, A. P. (2021). Asymptomatic SARS-CoV-2 infection: A systematic review and meta-analysis. *Proceedings of the National Academy of Sciences, 118*(34), Article e2109229118.
Samuel Faust, J., Lin, Z., & Del Rio, C. (2020). Comparison of estimated excess deaths in New York City during the COVID-19 and 1918 influenza pandemics. *JAMA Network Open, 3*(8), Article e2017527–e2017527.
Sanyaolu, A., Okorie, C., Marinkovic, A., Patidar, R., Younis, K., Desai, P., Hosein, Z., Padda, I., Mangat, J., & Altaf, M. (2020). Comorbidity and its impact on patients with COVID-19. *SN Comprehensive Clinical Medicine, 2*(8), 1069–1076.
Singh, R., & Adhikari, R. (2020). Age-structured impact of social distancing on the COVID-19 epidemic in India. *arXiv preprint arXiv:2003.12055*.

Soures, N., Chambers, D., Carmichael, Z., Daram, A., Shah, D. P., Clark, K., Potter, L., & Kudithipudi, D. (2020). Sirnet: Understanding social distancing measures with hybrid neural network model for COVID-19 infectious spread. *arXiv preprint arXiv:2004.10376*.

The United States Census Bureau. Age and Sex Composition in the United States: 2019. https://www.census.gov/data/tables/2019/demo/age-and-sex/2019-age-sex-composition.html,20019. Accessed 12-Dec-2022..

US Food, Drug Administration. (2022). *Coronavirus (COVID-19) update: FDA authorizes emergency use of Novavax COVID-19 vaccine, adjuvanted*. et al. FDA News Release

Wang, B., Li, R., Zhong, L., & Huang, Y. (2020). Does comorbidity increase the risk of patients with COVID-19: Evidence from meta-analysis. *Aging (Albany NY), 12*(7), 6049.

Pauline van den Driessche, Watmough, J. (2002). Reproduction numbers and sub-threshold endemic equilibria for compartmental models of disease transmission. *Mathematical Biosciences, 180*(1–2), 29–48.

World Health Organization. WHO coronavirus disease (COVID-19) dashboard. https://covid19.who.int. Accessed September 17, 2023..

Wu, Y., Kang, L., Guo, Z., Liu, J., Liu, M., & Liang, W. (2022). Incubation period of COVID-19 caused by unique SARS-CoV-2 strains: A systematic review and meta-analysis. *JAMA Network Open, 5*(8), Article e2228008–e2228008.

Xin, H., Li, Y., Wu, P., Li, Z., Lau, E. H. Y., Qin, Y., Wang, L., Cowling, B. J., Tsang, T. K., & Li, Z. (2022). Estimating the latent period of coronavirus disease 2019 (COVID-19). *Clinical Infectious Diseases, 74*(9), 1678–1681.

Xue, L., Jing, S., Miller, J. C., Sun, W., Li, H., Estrada-Franco, J. G., Hyman, J. M., & Zhu, H. (2020). A data-driven network model for the emerging COVID-19 epidemics in Wuhan, Toronto and Italy. *Mathematical Biosciences, 326*, Article 108391.

Zhao, S., et al. (2020a). Estimating the time interval between transmission generations when negative values occur in the serial interval data: Using COVID-19 as an example. *Mathematical Biosciences and Engineering, 17*(4), 3512–3519.

Zhao, S., Musa, S. S., Hebert, J. T., Cao, P., Ran, J., Meng, J., He, D., & Qin, J. (2020). Modelling the effective reproduction number of vector-borne diseases: The yellow fever outbreak in luanda, Angola 2015–2016 as an example. *PeerJ, 8*, Article e8601.